Origin, characterization and fate of alpha smooth muscle actin-positive cells during lung development and disease

Inaugural Dissertation

submitted to the

Faculty of Medicine

in partial fulfillment of the requirements

for the PhD-Degree

of the Faculties of Veterinary Medicine and Medicine

of the Justus Liebig University Giessen

by

Alena Moiseenko

of

Novosibirsk, Russia

Giessen 2017

From the Department of Internal Medicine and

Excellence Cluster Cardio-Pulmonary System (ECCPS)

Director / Chairman: Prof. Dr. Werner Seeger

Faculty of Medicine of the Justus Liebig University Giessen

First Supervisor and Committee Member: Prof. Dr. Saverio Bellusci

Second Supervisor and Committee Member: Dr. Mohammad Hajihosseini

Committee Members (Chair):

Committee Member:

Date of Doctoral Defense:

Declaration

“I declare that I have completed this dissertation single-handedly without the unauthorized help of a second party and only with the assistance acknowledged therein. I have appropriately acknowledged and referenced all text passages that are derived literally from or are based on the content of published or unpublished work of others, and all information that relates to verbal communications. I have abided by the principles of good scientific conduct laid down in the charter of the Justus Liebig University of Giessen in carrying out the investigations described in the dissertation.”

_____

Alena Moiseenko

Giessen February 2017

Table of contents

List of figures

List of tables

Abbreviations and Acronyms

β-gal	beta galactosidase
ACTA2	smooth muscle actin
ADRP	adipose differentiation-related protein (adipophilin or ADFP)
AECI	alveolar epithelial cell type I
AECII	alveolar epithelial cell type II
ALK	aurora-like kinase
ANOVA	analysis of variance
APC	allophycocyanin
Apc	Adenomatosis polyposis coli
ASMC	airway smooth muscle cell
AXIN2	axis inhibition protein 2
BADJ	broncho-alveolar duct junction
BLM	bleomycin
BMP	bone morphogenetic protein
BPD	bronchopulmonary dysplasia
BSA	bovine serum albumin
cDNA	complementary DNA
COPD	chronic obstructive pulmonary disease
CPP	cardio-pulmonary progenitors
Cre-ERT2	fusion protein between Cyclization recombinase and triple mutated human estrogen receptor ligand binding domain
Crs	compliance
DMEM	Dulbecco's Modified Eagle Medium
DNA	deoxyribonucleic acid
DAPI	4',6-diamidino-2-phenylindole, dihydrochloride
DKK1	Dickkopf-1
E	embryonic stage
ECM	extra cellular matrix
EDTA	ethylenediaminetetraacetic acid
ELN	elastin
EMT	epithelial-mesenchymal transition

ER	endoplasmic reticulum
ERK	extracellular signal–regulated kinase
FACS	fluorescence-activated cell sorting
FBS	fetal bovine serum
FCS	fetal calf serum
FGF	fibroblast growth factor
FGFR	fibroblast growth factor receptor
FITC	fluorescein isothiocyanate
FSC	forward scatter
FZD	frizzled receptor
GEO	Gene Expression Omnibus database
GLI1	glioma-associated oncogene 1
H&E	hematoxylin and eosin stain
HBSS	Hank’s balanced salt solution
HPRT	hypoxanthine-guanine phosphoribosyltransferase
IF	immunofluorescence
INM	intermediate undifferentiated progenitors
IP	intraperitoneal
IPF	idiopathic pulmonary fibrosis
JUN	c-Jun kinase
KEGG	Kyoto Encyclopedia of Genes and Genomes
LacZ	bacterial β-galactosidase gene
LIF	lipofibroblasts
LEF	lymphoid enhancer binding factor
LRP	lipoprotein related protein receptor
MAPK	mitogen-activated protein kinase
MFB	matrix fibroblast
Mlc	myosin light chain
MYF	myofibroblast
MyoF	myofibroblast
P-value	probability
PBS	phospho-buffered saline
PCR	polymerase chain reaction
PDGF-A	platelet-derived growth factor A

PDGFR	platelet-derived growth factor receptor
PH	pulmonary hypertension
PLIN2	perilipin 2
PN	postnatal day
PFA	paraformaldehyde
PPARγ	peroxisome proliferation activator receptor gamma
PTC	patched receptor
qPCR	quantitative polymerase chain reaction
RA	retinoic acid
RFP	red fluorescent protein
RNA	ribonucleic acid
RT	room temperature
S.E.M.	standard error of mean
SAL	saline
SFTPA	surfactant protein A
SFTPC	surfactant protein C
SHH	sonic hedgehog
SMC	smooth muscle cell
SMO	smoothend protein
SSC	side scatter
TAE	tris-acetate-EDTA buffer
Tam	tamoxifen
TBS	tris-buffered saline
TCF	t-cell factor
tdTom	tdTomato
TGFβ	transforming growth factor beta
TUNEL	terminal deoxynucleotidyl transferase dUTP nick end labeling
VSMC	vascular smooth muscle cells
WT	wild type
WT1	Wilm’s tumor protein 1
X-Gal	5-Bromo-4chloro-indol-β-D-galactopyranoside

1. Introduction

1.1. Alpha smooth muscle actin–positive cells in lung development: overview, appearance and function

Murine lung development starts at embryonic day E9.5 (E9.5) with the formation of two buds, distal to the rudimentary trachea, on the ventral side of the primitive foregut endoderm. From E9.5 through E16, the epithelium undergoes a process of branching morphogenesis, which is regulated by epithelial/mesenchymal interactions and mechanical tension. As a result of this branching process, a tree-like tubular structure of the lung forms. At the same time as the lung branching process occurs, smooth muscle cells (SMCs) appear on the dorsal side of the trachea as well as around the bronchi and blood vessels through the differentiation of mesenchymal progenitor cells (Cardoso and Lu, 2006; Morrisey and Hogan, 2010). Distally, SMCs appear at the cleft site of the bud, prior to its branching, wrapping around the bifurcating bud. This process of smooth muscle cells wrapping the bifurcating bud, likely leading to the stabilization of the cleft, is very important since disruption of SMCs differentiation during this time leads to failure of branching (Kim et al., 2015). The appearance of smooth muscle cells around the bronchi begins several days before the appearance of smooth muscle cells around vessels (Li et al., 1996; McHugh, 1995). In the developing lung, SMCs defined as mesenchymal-derived $ACTA2^{+}$ cells, can be initially subdivided into vascular SMCs (VSMCs) and airway SMCs (ASMCs). Through their supportive/structural as well as contractile properties, they contribute to the stabilization as well as the homeostasis of the vascular system and the conducting airways. Both cell types are therefore extremely important, allowing normal respiratory function at birth and impaired formation or function of SMCs lead generally to organ failure.

The development of gas-exchange units called alveoli begins from E16.5 and continues after birth. Alveolarization includes thinning of the mesenchyme, enlargement of the distal airspaces and division by septation. Septation will result in formation of saccules containing a layer of double capillary network. The future alveoli are formed from saccules through the appearance of secondary septae that divides the saccules into airway sacs. The double capillary network inside the

alveolar walls remodel into a single-capillary layer. During the development of alveoli, the lung interstitium contains cells with smooth muscle cells characteristics. These cells are located at the tip of forming secondary septae and are called alveolar myofibroblasts (MYFs). During alveolarization alveolar MYFs express ACTA2 and form elongated cytoplasmic protrusions, establishing a continuous loop around the forming septal cup. These loops are interconnected to each other and form a "Fishnet"-like $ACTA2^{+}$ network with strings of the fishnet underlying future alveolar ridges (Branchfield et al., 2016). Alveolar MYFs deposit elastin and play a critical role in alveoli formation (Dickie et al., 2008). Absence of alveolar MYFs leads to failure of secondary septation and alveoli formation (Boström et al., 1996). Schematic representation of alveolarization is illustrated in Figure 1.

Thus, there are three types of alpha smooth muscle actin (ACTA2)–positive cells in the healthy lung: airway smooth muscle cell, vascular smooth muscle cell and alveolar myofibroblast. ASMCs and VSMCs are forming during early lung development, while alveolar MYFs are forming at late lung development, maturate postnatally and are not present in adult lung

The origin of lung ASMCs and VSMCs as well as alveolar MYFs is progressively emerging. There is a need for better understanding of the origin of SMCs that will lead to improvement of potential treatments against diseases associated with SMCs overproliferation such as asthma, broncho-pulmonary dysplasia and pulmonary fibrosis.

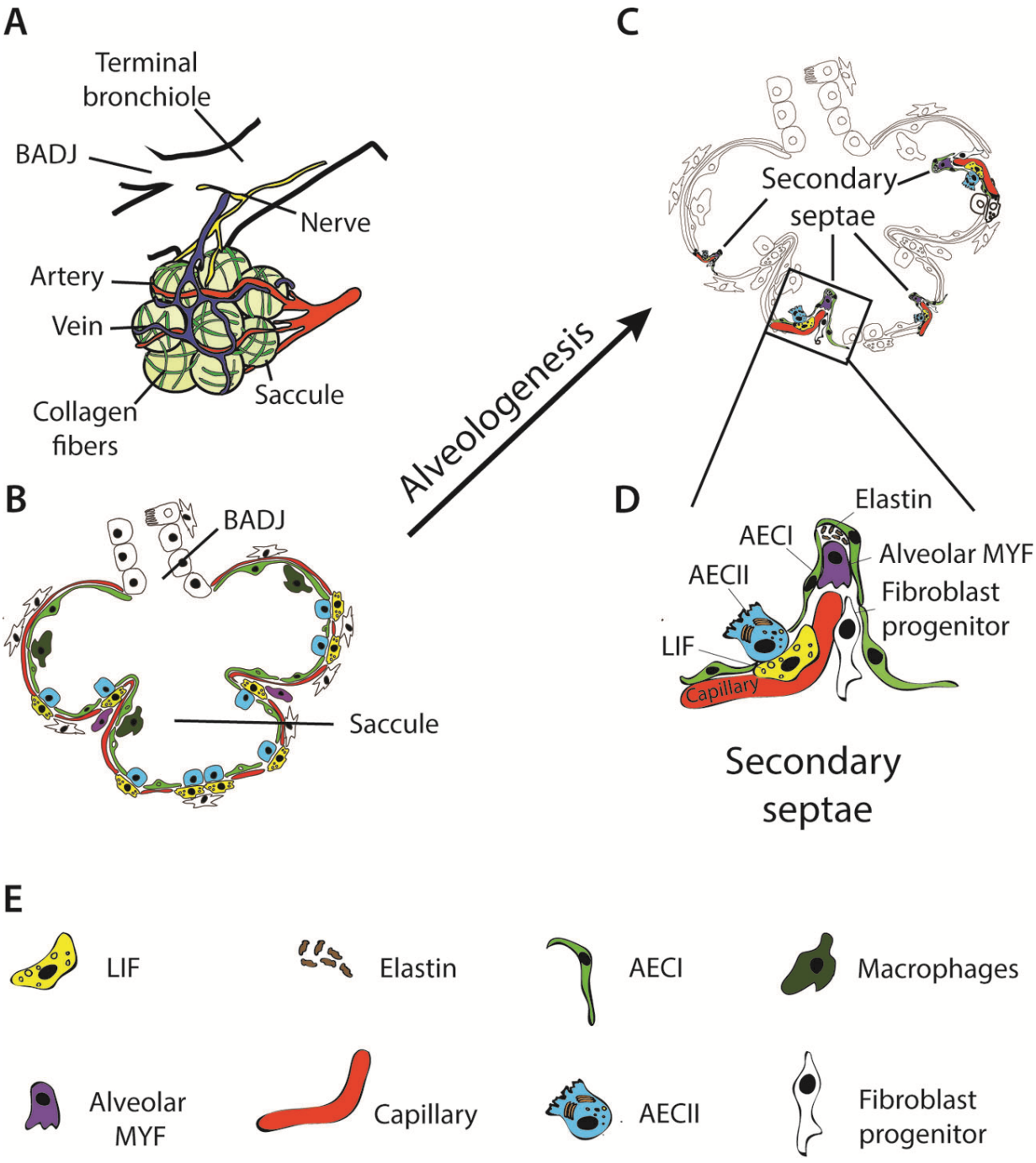

Figure 1. Schematic representation of alveolarization and cell types involved.
A. At the saccular stage of development, the lung forms primitive alveoli (saccule) surrounded by collagen fibers, nerves and blood vessels. B. The alveolar saccule is characterized by the presence of AECI/II, coating the walls of saccule, surfactant production, expansion of capillary tree, production of collagen and elastin by fibroblasts. C. During the alveolar stage, the sacs are subdivided by a process called “secondary septation”, which will give rise to mature alveoli. D. Secondary septae start to appear at the place of elastin deposition, which is produced by alveolar MYF.

The septae elongate toward the alveolar sac airspace. Double layer of capillaries become thinner giving rise to one layer of capillary network for more efficient gas exchange. AECI/II – alveolar epithelial cell type I/II; BADJ – broncho-alveolar duct junction; LIF – lipofibroblast; MYF – myofibroblast. Modified from Chao et al., 2016.

1.1.1. Airway and vascular SMCs and their progenitors

Several studies show that multiple progenitor cells participate to the smooth muscle cell pool during lung development. Mesenchymal progenitors expressing fibroblast growth factor 10 *(Fgf10)*, Wilm's tumor 1 *(Wt1)* or glioma-associated oncogene 1 *(Gli1)* contribute to SMC formation from early stages of lung development.

1.1.1.1. Fibroblast growth factor 10^{+} progenitors

FGF10 is a key signaling pathway that is required for the branching process (Bellusci et al., 1997b; Sekine et al., 1999; Weaver et al., 2000). *Fgf10* null mutation as well as expression of dominant negative FGF receptor completely prevent the branching process in mice (Peters et al., 1994; Sekine et al., 1999). *Fgf10* is expressed in the distal lung mesenchyme during early lung development and acts via the Fibroblast growth factor receptor 2-IIIb (FGFR2b) on the adjacent epithelium to induce branching. The distal lung mesenchyme, expressing FGF10 stimulates the epithelial bud to grow into the distal mesenchyme (Bellusci et al., 1997b; Lü et al., 2005; Park et al., 1998). Apart from lung branching, FGF10 also plays role in ASMC development. Using $Fgf10^{LacZ}$ enhancer trap line, in which expression of LacZ recapitulates endogenous *Fgf10* expression, we previously showed that *Fgf10*-expressing progenitor cells during the early pseudoglandular stage massively contribute to the ASMC pool (Mailleux et al., 2005). However, our recent lineage tracing data using the $Fgf10^{CreERT2}$ knock in line (El Agha et al., 2012) showed that only around 3-18% of the *Fgf10*-expressing cells labeled before E13.5 contribute to the SMCs (both vascular and airway). In addition, after E14.5, these progenitor cells are no longer committed to the SMC lineage (El Agha et al., 2014). The discrepancy between the two approaches ($Fgf10^{LacZ}$ versus $Fgf10^{CreERT2}$) is still unresolved.

1.1.1.2. Mesothelial WT1$^+$ progenitors

The role of the mesoderm derived-mesothelium, a monolayer of flattened squamous-like epithelial cells forming the external lining of the lung remains controversial. Mesothelial cells, positive for the Wilm's tumor marker 1 (WT1), were initially described as a source of VSMCs. Using the *Wt1-Cre* driver line, where a non-inducible Cre is expressed under the control of the *Wt1* promoter, it was proposed that WT1$^+$ cells migrate and invade the mesenchyme of the developing lung, consequently giving rise to VSMCs, but not ASMCs (Que et al., 2008). Contrasting follow-up results were reported using the *Wt1^{CreERT2}* line (a better lineage-tracing tool) where it was shown that mesothelial cells do not significantly contribute to the VSMC lineage when labeled at E9.5 (Greif et al., 2012). A more recent study suggested that mesothelial cells, labeled at E10.5 and E11.5, contribute to ASMCs and VSMCs, as well as DESMIN$^+$ fibroblasts (Dixit et al., 2013). Beyond the difference in the time of labeling, the extent of the mesothelium's contribution to the SMC lineage is so far unclear.

1.1.1.3. Sonic hedgehog-responding GLI1$^+$ progenitors

Sonic hedgehog (SHH) signaling has been also known as a key regulator of lung epithelial branching and ASMC development (Bellusci et al., 1997b). SHH signaling is activated by the binding of SHH ligand to the receptor Patched (PTC), which stops PTC-mediated inhibition of Smoothend (SMO) protein. Relieved SMO induces GLI-proteins to translocate to the nucleus and bind to SHH-responsive elements (McMahon, 2000). Upregulation of glioma-associated oncogene 1 *(Gli1)*, a main transcription factor operating downstream of SHH (Bai et al., 2004; Grindley et al., 1997; Hynes et al., 1997; Lee et al., 1997; Méthot and Basler, 2001; Miller et al., 2004) but likely also downstream of other signaling pathways such as FGF9 (del Moral et al., 2006), appears to be important for the differentiation of mesothelial cells along the SMC lineage (Dixit et al., 2013). This is in line with the phenotype of *Shh* knock out lungs showing complete absence of SMC (Miller et al., 2004; Pepicelli et al., 1998). Using the *Gli1^{CreERT2}* driver line, it was shown that E10.5 GLI1$^+$ cells and their descendants give rise to ASMCs and VSMCs as well as other parenchymal cells at E18.5 (Li et al., 2015). For this reason, it was proposed that the *Gli1^{CreERT2}* driver line could be useful to target the SMC lineage with a certain level of specificity. Using the same driver line, a multipotent population of cardio-pulmonary progenitors

(CPPs), which are marked by the expression of *Gli1* as well as *Wnt2* and *Isl1,* was identified. GLI1$^+$ CPPs, labeled at E8.5, give rise to different mesenchymal lineages, including pulmonary ASMCs and VSMCs. CPPs are regulated by SHH that is expressed by the foregut endoderm (Peng et al., 2013). The above-mentioned ASMCs progenitors are summarized in figure 2.

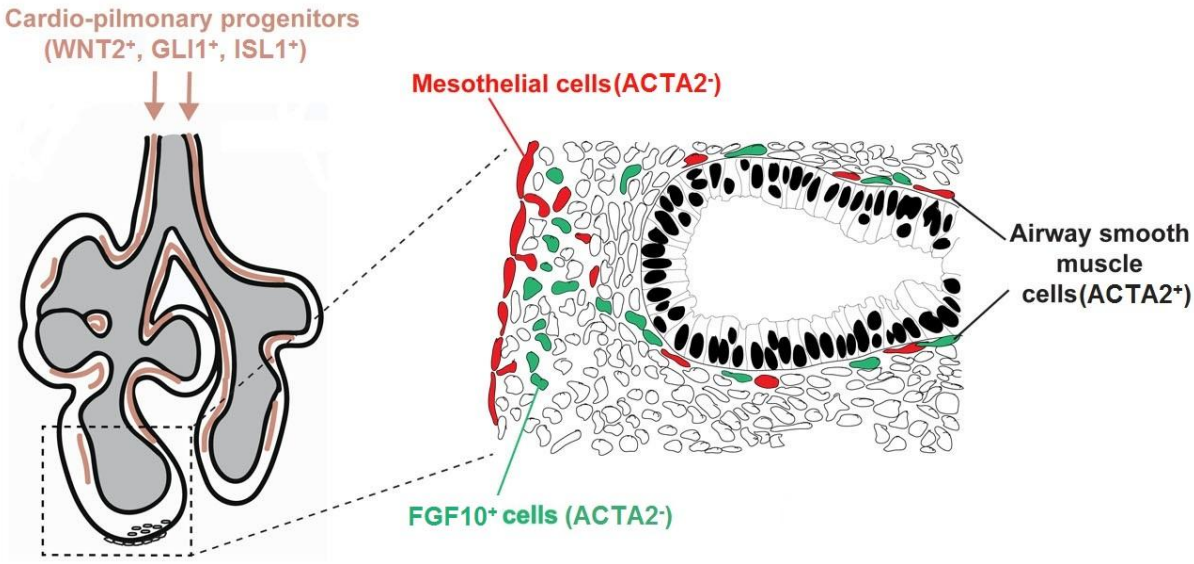

Figure 2. Airway smooth muscle cell progenitors. WNT2$^+$, GLI1$^+$ and ISLI1$^+$ cardio-pulmonary progenitors labeled at E8.5 give rise to proximal ASMC. Distally ASMCs are coming from mesothelial WT1$^+$ cells and FGF10$^+$ cells (both initially ACTA2$^-$).

1.1.1.4. Progenitors with active WNT signaling

The WNT family consists of 19 secreted WNT ligands interacting with 10 Frizzled (FZD) receptors and 2 low-density lipoprotein related protein receptors LRP5 and LRP6. WNT signaling is divided into canonical and non-canonical pathway. The canonical pathway includes Wnt ligand binding to FZD receptor that leads to hypophosphorilation of β-catenin, translocation of β-catenin to nucleus and activation of lymphoid enhancer binding factor/t-cell factor (LEF/TCF) transcription factors to induce target gene expression. The non-canonical pathway includes activation of c-Jun kinase (JNK) (Wang et al., 2005). Mice expressing β-galactosidase under the control of a LEF/TCF and β-catenin inducible promoter showed that in the E10.5 and E12.5 lung WNT signaling is active in airway epithelium and ASMCs. After E13.5 β-

galactosidase activity is absent in mesenchyme and is reduced in epithelium, correlating with the onset of *Dickkopf-1* (*Dkk1*) expression, a gene encoding an inhibitor of WNT signaling. It was shown that lung explants treated with DKK1 display impaired branching and reduced ASMC and VSMC formation (De Langhe et al., 2005). This suggests that WNT signaling may be involved in SMCs formation. It was also shown that WNT/β-catenin signaling in mesenchyme is crucial for the amplification but not differentiation of *Fgf10*-expressing cells that give rise to SMCs (De Langhe et al., 2008). Some of the WNT ligands have been also shown to play a role in pulmonary SMCs development. For example loss of *Wnt7b* resulted in loss of VSMCs integrity and lung hypoplasia (Shu et al., 2002). WNT7b ligand is secreted by epithelium and acts via FZD1 receptor on the mesenchyme, including VSMCs (Wang et al., 2005). Another WNT ligand seems to be important for lung SMCs formation – WNT2. As it was described before, cardio-pulmonary progenitors that give rise to ASMCs and VSMCs express *Wnt2* (Peng et al., 2013). It was also shown that specific inactivation of *β-catenin* (*Ctnnb1)* in SMCs using the *SM22α-Cre* driver line leads to decreased ASMC and VSMC formation in the lung (Cohen et al., 2009). This study again underscores the importance of WNT signaling in seemingly differentiated SMCs and/or their intermediate SM22α^+ progenitors for SMC formation. The role of WNT signaling in SMCs formation remains unclear. There is a need for lineage-tracing studies to monitor cells with active WNT signaling.

1.1.1.5. Progenitors coming from pre-existing ACTA2$^+$ cells

It remains unclear whether differentiated SMCs serve as progenitors for newly forming SMCs, particularly due to their limited proliferation capacity during developmental stages (El Agha et al., 2014).

It has been proposed that SMC progenitors are located proximally, near the lung hilum. This is the site found on the medial part of each lung, where the bronchi, blood vessels and nerves enter and exit the lung. These progenitor cells are believed to expand towards the distal/peripheral part of the lung, while giving rise to ASMCs (Shan et al., 2008). A more recent study has shown that pulmonary arterial SMCs (PASMCs) derive from progenitor cells located in the mesenchyme immediately surrounding the arteries at E13.5 (Greif et al., 2012). It was shown that PASMCs proliferate, migrate radially and give rise to the outer SMC layer. A more recent study showed that under hypoxic conditions, most distal PASMCs derive from pre-existing

SMCs in the adult lung. These pre-existing distal SMCs dedifferentiate, migrate more distally, proliferate and re-differentiate to new SMCs (Sheikh et al., 2014). However, this does not apply to ASMC formation, as it appears that the mesenchyme located immediately close to bronchi (stalk mesenchyme) does not contribute to ASMCs, at least not at E13.5. ASMC progenitors are proposed to be located exclusively at the tips of the budding bronchi, and migration of these progenitors to the site of differentiation seems to be WNT-dependent (Kumar et al., 2014; Mailleux et al., 2005).

1.1.2. Alveolar myofibroblasts and their progenitors

Alveolar myofibroblasts (MYFs) are $ACTA2^{+}$ mesenchymal cells that transiently populate the lung during the alveolar stage of lung development. During lung development, alveolar MYFs are believed to be present mostly in a progenitor state (based on low levels or even absence of *Acta2* expression in the lung parenchyma). Alveolar MYFs are believed to be critical for the formation of secondary septa during alveologenesis, thereby allowing the subdivision of the respiratory saccules into smaller units, the alveoli.

Apart from the expression of ACTA2, alveolar MYFs are producing extracellular matrix fibers, such as elastin and collagen. Elastin deposition is critical for the normal alveoli, maintaining the alveolar integrity and allowing alveoli to stretch during inhalation (Dickie et al., 2008). During alveolarization, elastin forms a matrix that serves as a scaffold on which alveolar MYFs adhere and mark future secondary septae sites. In *Elastin*-knock-out lungs, secondary septae failed to form and lungs exhibited an emphysematous-like phenotype. Mutant mice die within a few days after birth before alveologenesis began (Wendel et al., 2000).

Alveolar MYFs are abundant in the postnatal lung but they disappear after alveolarization process and are absent in adult lung (Kapanci et al., 1995; Yamada et al., 2005). Dysregulated behavior of MYFs are involved in several lung diseases such as fibrosis and BPD thus disappearance of alveolar MYFs from the lung is important, since they might be involved in disease process. The disappearance of alveolar MYFs from the lung is poorly understood and requires further investigation.

The origin of alveolar MYFs is still not understood. The use of specific driver lines directly targeting alveolar MYF progenitors is needed to follow the fate of these cells postnatally, as well as during repair after injury.

1.1.2.1. PDGFA signaling in alveolar MYF formation

It was proposed that alveolar MYFs are derived from platelet derived growth factor receptor alpha^{+} (PDGFRa^{+}) cells. At the end of the saccular stage and at the beginning of secondary septae formation (PN0-PN3) PDGFRa^{+} cells migrate to future sites of septae formation. PDGFA-mediated activation of PDGFRA is neded for proliferation and spreading of alveolar MYF progenitors (Lindahl et al., 1997). In newborn *Pdgfa*-null mice, this migration is absent and lungs display complete absence of alveolar MYFs and elastin deposition as well as failure of alveolar septation (Boström et al., 1996; Lindahl et al., 1997; McGowan et al., 2008). Interestingly, *Pdgfra* mutants did not show any failure of alveolar MYFs migration (Boström et al., 2002; McGowan and McCoy, 2014, 2013a). More recent study proposed that PDGFRa^{+} cells give rise to alveloar MYFs and later differentiate into lipofibroblasts (LIF) (Branchfield et al., 2016). Altogether these data suggest that alveolar MYFs undergo PDGFA/PDGFRa signaling (Boström et al., 1996; Lindahl et al., 1997; McGowan et al., 2008), but the exact role of this signaling pathway, in terms of proliferation and/or differentiation, remains unclear. To demonstrate that PDGFRa^{+} cells present at pseudoglandular stage are indeed progenitors for alveolar MYF lineage tracing experiments of PDGFRa^{+} cells must be performed.

1.1.2.2. FGF signaling in alveolar MYF formation

FGF signaling has also been shown to play an important role in alveolar MYF formation. Lungs of the Fgf10 hypomorph mice, expressing around 20% of normal *Fgf10* expression, display complete absence of alveolar MYFs and respiratory airways are significantly enlarged (Ramasamy et al., 2007). Inhibition of all FGFR2b ligands, including FGF10, by using dominant negative approach overexpressing soluble form of FGFR2b *(Spc-rtTA/+; tet(O)solFgfr2b/+)* during lung development (E14.5-E18.5) led to disrupted alveologenesis. Treatment with retinoic acid (RA), a vitamin A derivative, can partially restore the process – secondary septa will form with presence of alveolar MYFs. But this regenerative effect of RA can be blocked by re-expression of sFGFR2b, suggesting that FGFR2b ligands are critical for secondary septa formation not only during development but also postnatally (Perl and Gale, 2009). Another study showed that FGFR2b ligands are important during alveolar regeneration process after pneumonectomy (Chen et al., 2012). The same study proposed that PDGFRa^{+} LIFs give rise to alveolar MYFs and this process

involves FGFR2b ligands (likely FGF10). Clearly FGFR2b ligands (particularly FGF10) are involved in alveolar MYF formation, but it is still unclear whether this effect is direct effect of FGF10 on alveolar MYF progenitors or indirect effect via alveolar epithelial type II cells (AECII), while AECII are the major epithelial component of forming alveoli. Interestingly, forced activation of FGF in lung mesenchyme during lung development also led to absence of alveolar MYFs and reduced elastin expression (De Langhe et al., 2006). This result suggests that FGF10 might act in different ways – it might prevent alveolar MYF differentiation allowing their proliferation or induce alveolar MYF differentiation. These different effects of FGF10 might be possible when FGF10 acts via different receptors – either via FGFR2b or FGFR2c.

1.1.2.3. SHH and WNT signaling in alveolar MYF formation

It has been demonstrated that migration of alveolar MYFs to the sites of secondary septation is dependent on SHH signaling (McGowan and McCoy, 2013b). Downstream target of SHH signaling GLI1 that has been shown to be involved in ASMC and VSMC formation is also involved in alveolar MYF formation. Using *Gli1*^{CreERT2} driver line to specifically target cells undergoing SHH signaling it was shown that GLI1^{+} cells labeled at E10.5 give rise to alveolar MYFs at PN14 and this process depends on WNT signaling. Ectopic activation of WNT signaling by targeted inactivation of *Adenomatosis polyposis coli* (*Apc*) led to significant increase in alveolar MYFs which subsequently led to formation of multiple fibrotic masses in the perinatal lungs (Li et al., 2015).

1.2. Smooth muscle cells in lung disease

Abnormal behavior of ACTA2^{+} cells is known to be involved in numerous pathological conditions such as asthma, pulmonary hypertension (PH), broncho-pulmonary dysplasia (BPD) and fibrosis. ASMCs in the lungs of asthmatic patients have features of hyperplasia and hypertrophy, airways are hyper responsive and the airflow is reduced (Halayko and Stephens, 1994; Jeffery, 2004). Pulmonary hypertension is associated with excessive VSMC proliferation, which involves alteration in all three layers (intima, media and adventitia) of the vascular wall, often with the interplay of inflammatory cells (Tuder, 2016). BPD is a lung disease of prematurely born infants

that are being treated with mechanical ventilation. Among the features of BPD is overproliferation of ASMCs (Bland, 2005). Some of lung diseases such as pulmonary fibrosis and BPD are characterized by the presence of another $ACTA2^+$ cell type – the activated MYF. In pulmonary fibrosis overproliferation of activated MYFs result in scarring of lung tissue, deposition of collagen and extracellular matrix (Thannickal et al., 2004; Zhang et al., 1996). The origin of the over-proliferative SMCs and MYFs in pathological conditions is very poorly understood. There is a great need to expand this knowledge. Additionally, SMCs by themselves serve as an important intermediate source of signaling molecules during the repair process in different diseases. For example, it was shown that ASMCs secret FGF10 to induce repair process after naphthalene-induced epithelial injury in mice (an established model to deplete airway epithelial Clara cells or Club cells) (Volckaert et al., 2011). Understanding the role and impact of SMCs on repair process is another interesting issue that needs to be investigated.

1.2.1. Smooth muscle cells and activated myofibroblasts in bleomycin-induced lung fibrosis

Idiopathic pulmonary fibrosis (IPF) is a fatal lung disease characterized by scarring of lung tissue and progressive decline in lung function. One of the primary effector cells in IPF lungs are $ACTA2^+$ activated MYFs, cells that are responsible for extracellular matrix production (ECM) such as collagen and leading to scarring of the tissue. Progressive scarring prevents gas exchange, ultimately leading to respiratory failure and death.

The pathogenesis and treatment of IPF, however, remains unclear (du Bois et al., 2011). It has been speculated that repetitive injury to alveolar type II cells (AECII) may be the prime event that initiates mesenchymal cells recruitment and ECM deposition (Günther et al., 2012). Injury to alveolar epithelial cells will lead to the emergence of spindle-shaped fibroblasts located in fibrotic foci. These foci will be the sites of activated MYF accumulation and tissue remodeling. Additionally, misfolding of surfactant proteins A and C (SFTPA and C) leads to endoplasmic reticulum stress and reactive oxygen species production by AECII, which contributes to lung remodeling. TGFβ pathway, particularly TGFβ1 is believed to drive the fibrotic response in IPF lungs. It has been shown that TGF-β1 Requires SMO/GLI Pathway activity to trigger and sustain MYF differentiation. Inhibition of GLI partially reverts MYF phenotype (Cigna et al., 2012). Another study shows that $GLI1^+$ cells proliferate

after kidney, lung, liver, or heart injury to generate MYFs (Kramann et al., 2015).

The cellular origin of activated MYFs in IPF has been a topic of high interest but still remains understudied. There are several hypotheses suggesting some cell types that can give rise to activated MYFs. It has been proposed that activated MYFs originate from resident fibroblasts expressing high affinity type II TGFb receptor. These resident fibroblasts proliferate and start to express ACTA2 (Hoyles et al., 2011). Another hypothesis is that activated MYFs originate from circulating bone-marrow-derived fibrocytes (Hashimoto et al., 2004; Phillips et al., 2004). Pericytes, $ACTA2^+$ contractile cells that wrap around the endothelial cells of capillaries and venules, were also suggested as a source for activated MYFs in lung fibrosis (Hung et al., 2013; Rock et al., 2011; Wong et al., 2015). Additionally, many studies suggest that activated MYFs derive from epithelial cells of the lung, including AECII, undergoing TGFβ1-driven epithelial-mesenchymal transition (EMT) (Corvol et al., 2009; Degryse et al., 2010; Felton et al., 2009; Tanjore et al., 2011; Willis et al., 2006). However, there was no evidence for EMT when AECII were lineage-traced during bleomycin-induced lung fibrosis (Rock et al., 2011). The potential cell types giving rise to activated MYFs are illustrated in Figure 3. It is still unclear whether pre-existing $ACTA2^+$ airway and vascular SMCs can give rise to activated MYFs in lung fibrosis.

It is widely accepted that the pathogenesis of IPF starts in the alveolar region of the lung. Alveolar region of the lung harbors lipid droplet-containing cells – lipofibroblasts (LIFs) that are located in close proximity to AECII. LIF are involved in alveolar maturation and surfactant production (Rehan and Torday, 2014) and contribute to the epithelial stem-cell niche in adult mouse lungs (Barkauskas et al., 2013; McQualter et al., 2013). Our group has shown that LIFs trace back to at least one embryonic mesenchymal cell population expressing *Fgf10* (El Agha et al., 2014). The involvement of LIFs in alveolar repair after injury has not been investigated.

An in-vivo bleomycin-induced model for IPF in mice is commonly used (Degryse and Lawson, 2011). In this model, the anti-cancer drug bleomycin is administered intratracheally or systemically which leads to the development of fibrotic lesions. In contrast to IPF in humans, where fibrosis induces irreversible pathological remodeling, bleomycin-induced fibrosis in mice is followed by repair with complete recovery. After fibrosis resolution activated MYFs have been thought to undergo apoptosis (Hinz et al., 2007; Issa et al., 2001). Recent data indicate that during fibrosis resolution activated MYFs dedifferentiate and this dedifferentiation is

controlled by ERK and MAPK pathways. In contrast, during fibrosis onset, myofibroblast formation is driven by TGFb1, MyoD and ALK5 (Hecker et al., 2011). This study hypothesized that activated MYF descendants dedifferentiate to LIFs that are associated with alveolar repair.

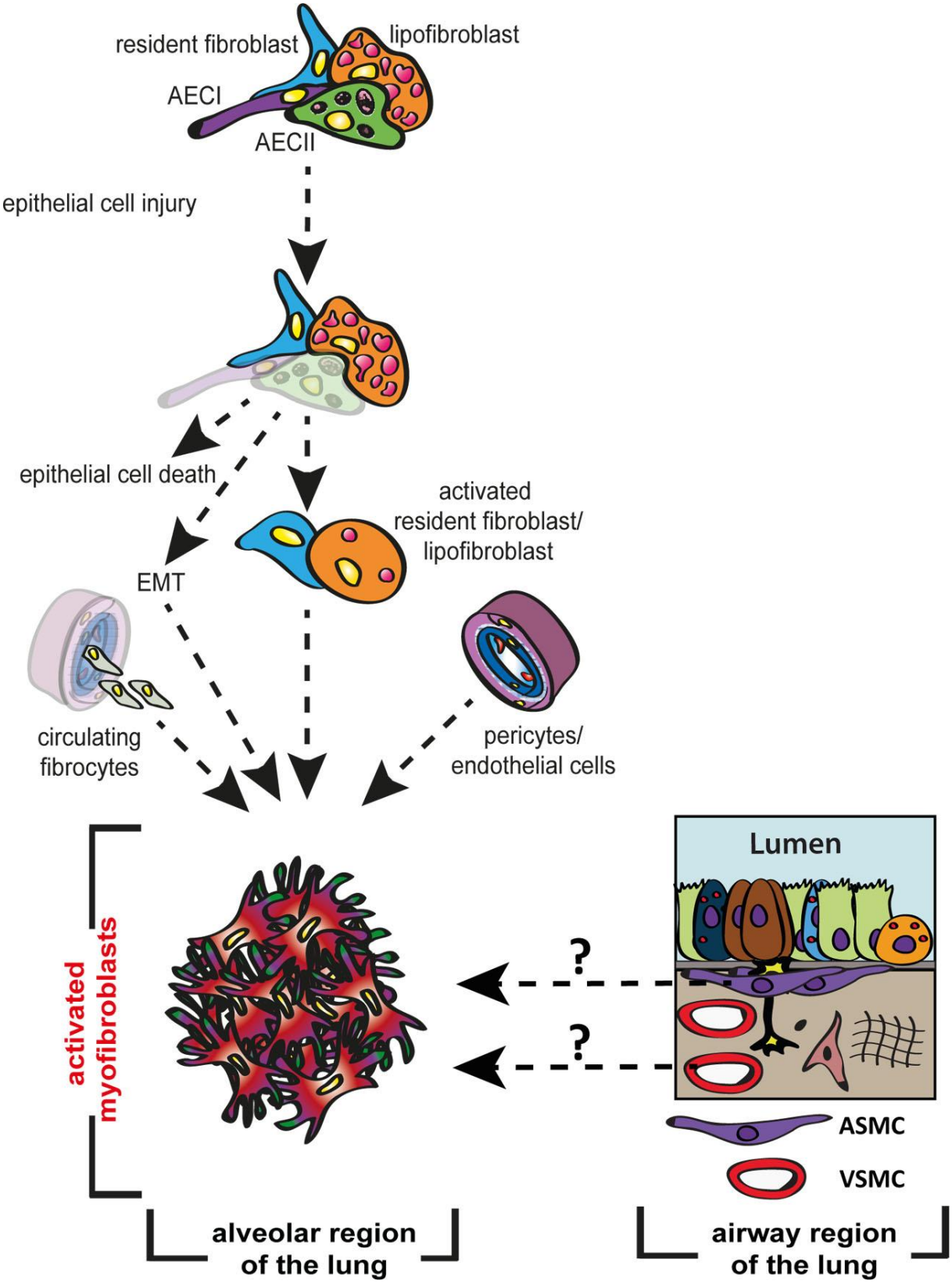

Figure 3. Putative cell types giving rise to activated myofibroblasts. Resident fibroblast/lipofibroblast, AECII, pericytes and circulating fibrocytes are potential precursor cells giving rise to activated MYFs. It remains unknown whether ASMC and VSMC can give rise to activated MYFs. AECI/II – alveolar epithelial type I/II cells, EMT – epithelial-mesenchymal transition.

2. Objectives

The lung mesenchyme, in comparison to the lung epithelium remains understudied. Among the mesenchymal cells that are poorly characterized are airway and vascular SMCs in addition to alveolar MYFs. Although conventional SMCs and alveolar MYFs share ACTA2 expression, little is known about the differences in terms of cellular origin and gene expression between these cell types. $ACTA2^+$ cells play crucial roles during development to establish mature lungs and also during the repair process after injury. More detailed understanding of the origin and fate of SMCs and alveolar MYFs during development and repair will definitely bring new ideas for the potential treatments against proliferative diseases such as asthma, BPD, PH and pulmonary fibrosis.

This study provides a more balanced view on the origin, fate and role of $ACTA2^+$ cells during embryonic lung development and lung regeneration. In vivo lineage tracing followed by fluorescence-activated cell sorting, gene expression analysis and histological examination were used to address our scientific questions. Our side-by-side analyses will be instrumental to design new experiments addressing the function of signaling pathways in various ACTA2-derived subpopulations.

This study is divided into two parts, emphasizing the following topics:

1. **The origin of SMCs and alveolar MYFs during murine lung development.**
   Using *in vivo* lineage tracing of different mesenchymal progenitors that were reported to target SMCs the impact of different progenitor cells to SMCs and alveolar MYFs was measured. The driver lines used for this study included $Fgf10^{CreERT2}$ to target $FGF10^+$ cells, $Wt1^{CreERT2}$ to target mesothelial cells, $Gli1^{CreERT2}$ to target SHH-responding cells, $Axin2^{CreERT2}$ to target cells with activated WNT signaling and *Acta2-CreERT2* to target differentiated SMCs. $Tomato^{flox}$ line was used to label cells with tdTomato signal. Specific cell populations were labeled at different time points of development and were lineage-traced and analyzed at later time points.

2. **The origin and fate of activated MYFs in bleomycin-induced lung fibrosis in mice**

   One of the proposed origin for the activated MYFs are pre-existing ACTA2^{+} cells (Sheikh et al., 2014). Using the *Acta2-CreERT2; Tomato^{flox}* line we tested the hypothesis whether pre-existing ASMCs and VSMCs give rise to activated MYFs. For that reason ACTA2^{+} SMCs were labeled before bleomycin injury to induce lung fibrosis. At the peak of fibrosis the presence of labeled ACTA2^{+} cells was measured. To study the fate of activated MYFs, the same *Acta2-CreERT2; Tomato^{flox}* line was used. ACTA2^{+} activated MYFs were labeled during the fibrotic phase and the fate of these cells were studied, particularly whether these activated MYFs persist in the lung and transition to a lipofibroblast-like phenotype during fibrosis resolution.

The objectives of this study are summarized below:

1. Identifying the relative contribution of various mesenchymal progenitors to airway and vascular SMC formation during embryonic lung development
2. Identifying alveolar MYF progenitors during late lung development
3. Establishing transcriptomic signatures for various ACTA2^{+} cell populations during late lung development
4. Investigating the contribution of pre-existing SMCs to activated MYFs in lung fibrosis postnatally
5. Targeting activated MYFs during fibrosis formation and tracing their fate during the resolution phase in adult mice

3. Materials and Methods

3.1. Mice and animal experiment approval

The *Fgf10-LacZ* (*Fgf10*$^{Tg(Mlc1v\text{-}nLacZ)}$) mouse line was described previously (Kelly et al., 2001; Mailleux et al., 2005). *Fgf10*^{CreERT2} (*B6-Fgf10*$^{tm1.1(cre/ERT2)Sbel}$) mice were generated previously by our group (El Agha et al., 2012). Mouse strains *Axin2*^{LacZ} (*B6.129P2-Axin2*^{tm1Wbm}*/J*, stock number 009120), *Gli1*^{LacZ} (*STOCK_Gli1*^{tm2Alj}*/J*, stock number 008211), *Wt1*^{CreERT2} (*STOCK_Wt1*$^{tm2(cre/ERT2)Wtp}$*/J,* stock number 010912), *Gli1*^{CreERT2} (*STOCK_Gli1*$^{tm3(cre/ERT2)Alj}$, stock number 007913), *Axin2*^{CreERT2} (*B6.129(Cg)-Axin2*$^{tm1(cre/ERT2)Rnu}$*/J*, stock number 018867) and *tdTomato*^{flox} (*B6;129S6-Gt(ROSA)26Sor*$^{tm9(CAG\text{-}tdTomato)Hze}$*/J,* stock number 007905) were purchased from Jackson laboratory. *Acta2-CreERT2 (STOCK_Tg(Acta2-cre/ERT2)12Pcn)* mice (Wendling et al., 2009) were kindly provided by Dr. Pierre Chambon.

Animal experiments were approved by Regierungspraesidium Giessen (117/2012, 55/2015 and 613_M).

3.2. Mice Genotyping

Tissues from the distal tip of the tails were digested in 200 µl Viagen including 1 µl proteinase K in 55°C on a shaker overnight, then reaction was stopped in 85°C for 40 min. Genotyping were done by PCR. For protocol and primer sequences please see Table 1. PCR products were analyzed using a 1,5 % agarose gel containing TAE buffer with Sybrsafe (50 µl Sybrsafe + 500 ml 1x TAE buffer). 10 µl of PCR samples were loaded with 2 µl loading dye (Biorad Nucleic Acid Sample loading buffer, 5x), and then gel was run with 120V for 30-45 min. A molecular ladder (QX Size Marker, 100bp-2.5kb, Qiagen) was used to detect the expected band sizes (Table 2).

Table 1. Primer sequences and protocols for genotyping.

Mouse line	Primer sequence	PCR protocol		
		Step	**Temp. (°C)**	**Time**
Fgf10-LacZ	Run separately LacZ/WT: 1) LacZ: TTC ACT GGC CGT CGT TTT ACA ACG TCG TGA 2) LacZ: ATG TGA GCG AGT AAC AAC CCG TCG GAT TCT 3) WT: CGA GTG GAG CAT GTA CTT CCG TGT CCT GAA 4) WT: TCC CTA CCC AGT CAC AGT CAC AGC TGC ATA	1	94	1/2 min
		2	94	30 sec
		3	55/59.5	30 sec
		4 (repeat Step 2-4 31 times total)	72	1 min
		5	72	5 min
		6	4	Hold
Fgf10^{CreERT2}	1) ATT TGC CTG CAT TAC CGG TC 2) ATC AAC GTT TTG TTT TCG GA	1	94	3 min
		2	94	30 sec
		3	51.7	1 min
		4 (repeat Step 2-4 35 times total)	72	1 min
		5	72	2 min
		6	4	Hold
Axin2^{LacZ}	1) AAG CTG CGT CGG ATA CTT GAG A 2) AGT CCA TCT TCA TTC CGC CTA GC 3) WT: TGG TAA TGC TGC AGT GGC TTG	1	94	3 min
		2	94	30 sec
		3	67	30 sec
		4 (repeat Step 2-4 35 times total)	72	30 sec
		5	72	2 min
		6	4	Hold
Gli1^{LacZ}	1) GGG ATC TGT GCC TGA AAC TG 2) TCT GCC AGT TTG AGG GGA	1	94	3 min
		2	94	30 sec
		3	65	1 min
		4 (repeat	72	45 sec

Mouse line	Primer sequence	PCR protocol		
		Step	**Temp. (°C)**	**Time**
	CGA C 3) WT: AGG TGA GAC GAC TGC CAA GT	Step 2-4 35 times total)		
		5	72	2 min
		6	10	Hold
Wt1^{CreERT2}	Run separately Cre/WT: 1) Cre: TGA AAC AGG GGC AAT GGT GCG 2) Cre: CGG AAT AGA GTA TGG GGG GCT CAG 3) WT: GCG ATC CTG GAC TTC CTC CT 4) WT: GGA CCG CCC AGC GAC CCG TA	1	94	3 min
		2	94	30 sec
		3	65/61	45 sec
		4 (repeat Step 2-4 30/35 times total)	72	45 sec
		5	72	2 min
		6	10	Hold
Gli1^{CreERT2}	1) GGG ATC TGT GCC TGA AAC TG 2) CTT GTG GTG GAG TCA TTG GA 3) WT: CAG GTT CTT GCG AAC CTC AT	1	94	5 min
		2	94	30 sec
		3	64.6	1 min
		4 (repeat Step 2-4 35 times total)	72	1 min
		5	10	Hold
Axin2^{CreERT2}	1) AAA GCT GCG TCG GAT ACT TG 2) ACA TGT CCA TCA GGT TCT TGC 3) WT: CTT GCC CAC ACT AGG CTG AC	1	94	2 min
		2	94	20 sec
		3	65	15 sec
		4 (repeat Step 2-4 11 times total)	68	10 sec
		5	94	15 sec
		6	60	15 sec
		7 (repeat Step 5-7 29 times total)	72	10 sec
		8	72	1 min
		9	4	Hold

Mouse line	Primer sequence	PCR protocol		
		Step	**Temp. (°C)**	**Time**
Acta2-CreERT2	1) ATT TGC CTG CAT TAC CGG TC 2) ATC AAC GTT TTG TTT TCG GA	1	94	30 sec
		2	94	30 sec
		3	55	30 sec
		4 (repeat Step 2-4 30 times total)	72	1 min
		5	4	Hold
tdTomato^{flox}	1) CTG TTC CTG TAC GGC ATG G 2) GGC ATT AAA GCA GCG TAT CC 3) CCG AAA ATC TGT GGG AAG TC 4) AAG GGA GCT GCA GTG GAG TA	1	94	3 min
		2	94	20 sec
		3	61	30 sec
		4 (repeat Step 2-4 35 times total)	72	30 sec
		5	72	2 min
		6	4	Hold

Table 2. Expected band size of genotyping products.

Mouse line	Expected band size for WT	Expected band size for mutant
Fgf10$^{Lacz/-}$	500bp	370bp
Fgf10^{CreERT2}	-	349bp
Axin2^{LacZ}	493 bp	400 bp
Gli1^{LacZ}	261 bp	480 bp
Wt1^{CreERT2}	374 bp	194 bp
Gli1^{CreERT2}	136 bp	204 bp
Axin2^{CreERT2}	493 bp	520 bp
Acta2-CreERT2	-	349bp
tdTomato^{flox}	297 bp	196 bp

3.3. Tamoxifen administration

Tamoxifen stock solution was prepared by dissolving tamoxifen powder (T5648, Sigma) in corn oil at a concentration of 20 mg/mL. Pregnant mice received a single intraperitoneal (IP) injection of 0.1 mg of tamoxifen per gram of body weight. For continuous tamoxifen exposure, mice were fed tamoxifen-containing food (0.4 g of tamoxifen per kg of food) (Altromin).

3.4. Bleomycin injury

Acta2-CreERT2, tdTomato^{flox} mice received an intratracheal installation of either saline or bleomycin (3.5 U/kg of body weight) at the Ludwig Boltzmann Institute in Graz, Austria (protocol number BMWFW-66.010/0043-WF/V/3b/2016) and National Jewish Health (Denver, USA) according to recommendations in the Guide for the Care and Use of Laboratory Animals of the National Institute of Health (IACUC number AS2774-05-16).

3.5. Lung function measurements

Mice were anesthetized with Ketamine (1.2 μl/g), Domitor (0.6 l/g) and 1:4 parts of Heparin (Ratiopharm) mixed in saline solution. Then mice were tracheotomized and intubated with a 20G catheter connected to a FlexiVent^{TM} plesythmograph (Scireq). Lungs were mechanically ventilated at a rate of 150 breaths/min with a tidal volume of 10 μl/g of body weight. Lung compliance was measured. After plesythmography, animals were euthanized and lungs were isolated for further processing.

3.6. Fluorescence microscopy and time-lapse microscopy

Dissected lungs were examined using a fluorescent stereoscope M205FA (Leica) equipped with DFC360FX camera (Leica). For time-lapse microscopy, E12.5 lungs were cultured on Whatman Nucleopore membrane filters (GE Healthcare) placed on 500 μl of Dulbecco's modified Eagle medium (DMEM) with 10% fetal bovine serum (FBS) and 1% penicillin/streptomycin. Culture dishes with embryonic lungs were placed in the chamber (37°C, 5% CO_2) of the live imaging microscope DMI6000B (Leica) with DFC365FX camera (Leica), where live imaging was performed.

For thick vibratome sections Z-stack and de-convolution was used.

3.7. Immunofluorescence and immunohistochemistry

Isolated lungs were fixed with 4% paraformaldehyde (postnatal lungs were perfused with PBS prior to fixation, embryonic lungs were not perfused). Then, tissues were embedded in paraffin and sectioned at 5 µm thickness. Slides were deparaffinized and then blocked with 3% BSA and 0.4% Triton-X (in TBS) at RT for 1 h. If antigen retrieval was necessary it was performed prior blocking by placing slides in a staining container and steaming in a pressure cooker with 10mM citrate buffer, 0.05% Tween 20, pH 6 for 15 min following 30 min cooling on ice and washing three times in TBST (TBS buffer + 0.1% Tween20) for 5 min. Then, slides were incubated with primary antibodies at RT for 1 h or at 4°C overnight. After incubation with antibodies, slides were washed three times in TBST for 5 min and stained with secondary antibodies at RT for 1 h. Slides were then washed three times in TBST for 5 min and mounted with Prolong Gold Anti-fade Reagent with DAPI (Invitrogen). Immunofluorescent (IF) stainings were performed using monoclonal anti-ACTA2 (Sigma, 1:200), polyclonal anti-ADRP (PLIN2) (Abcam, 1:50), monoclonal anti-Elastin (ELN) antibodies (Santa Cruz Biotechnology, 1:200), polyclonal anti-SFTPC (Santa Cruz, 1/1000), polyclonal anti-beta Galactosidase (β-gal) (Abcam, 1:200), polyclonal anti-collagen type 1 (Rockland Immunochemicals, 1:200) and monoclonal anti-Ki67 (Cell Signaling, 1:200). The endogenous tdTomato signal was detected without the use of antibodies. When antigen retrieval was required for double staining, polyclonal anti-tdTomato (anti-RFP) antibodies (Rockland Immunochemicals, 1:250) were used. Apoptosis was detected using DeadEnd Fluorometric TUNEL assay according to manufacturer's instructions (Promega). For quantitative analysis, multiple images were used (n > 8). For each experiment, sections from at least 3 independent lungs were analyzed.

Hematoxylin/Eosin staining was performed according to standard procedures.

To get thick sections isolated lungs were filled with 1.5% low melting agarose (Invitrogen) and then vibratome sections were cut at 100 µm. After cutting lungs were kept overnight in PBS to get rid of agarose and then fixed in 4% paraformaldehyde and stained with antibodies.

3.8. X-Gal staining

X-Gal staining of *Fgf10-LacZ* and *Gli1-LacZ* lungs was performed as previously described (Volckaert et al., 2011). Briefly, lungs were dissected in Hank's Balanced Solution (HBSS) (Invitrogen), shortly fixed in 4% Paraformaldehyde (PFA), washed in PBS and incubated with LacZ buffer solution for 10 min. Then, they were incubated with LacZ buffer solution containing 40 mg/mL X-Gal at 37°C overnight.

3.9. Flow cytometry analysis and cell sorting

Individual embryonic lungs at E18.5 were isolated in Hank's balanced salt solution (HBSS), cut into small pieces with a sharp blade and treated with 0.5% Collagenase Type IV in HBSS (Life technologies, Invitrogen) at 37°C for 45 minutes. Lung homogenates were passed through 18, 21 and 24G needles and then through 70 and 40 µm cell strainers (BD Biosciences) to obtain single cell suspensions. Cells were centrifuged at 4°C at 1200 rpm for 5 minutes and then resuspended in staining solution (0,1% sodium azide, 5% FCS, 0,05% Triton X-100 in PBS) containing anti-ACTA2 (FITC-conjugated, Sigma, 1:100) and anti-PDGFRa antibodies (APC-conjugated, Biolegend, 1:100) for 30 minutes on ice in the dark. Then, cells were washed with 0.1 % sodium azide in PBS. LipidTOX staining was performed according to manufacturer's protocol (Invitrogen). Flow cytometry measurements of labeled cells and cell sorting were done using a FACSAriaIII cell sorter (BD Biosciences).

3.10. Quantitative Real-time PCR

Extraction of RNA from sorted cells was performed using RNeasy Micro kit (Qiagen). Primers were designed using the Universal Probe Library Assay Design center program available online (Roche Applied Science). More details about the used primers can be found in table 3. Quantitative real-time PCR was performed using Light Cycler 480 II (Roche Applied Science). Data were obtained using hypoxanthine-guanine phosphoribosyltransferase (*Hprt*) as a reference gene. Data were presented as expression relative to *Hprt.*

Table 3. Mouse primers used for qPCR

Gene	Forward Primer 5'-3'	Reverse Primer 5'-3'
Adrp	cctcagctctcctgttaggc	cactactgctgctgccattt
Acta2	actctcttccagccatctttca	ataggtggtttcgtggatgc
Elastin	ccacctctttgtgtttcgct	ccaaagagcacaccaacaatca
Fgf10	atgactgttgacatcagactcctt	cactgttcagccttttgagga
HPRT	gctgacctggattac	ttggggctgtactgctta
Pdgfra	tgcaaattgacatagaaggagaag	gccctgtgaggagacagc
PPAR gamma	gaaagacaacggacaaatcacc	gggggtgatatgtttgaacttg

3.11. Gene array

Purified total RNA from FACS-isolated cells was amplified using the Ovation PicoSL WTA System V2 kit (NuGEN Technologies). Per sample, 2 µg amplified cDNA was Cy3-labeled using the SureTag DNA labeling kit (Agilent). Hybridization to 8x60K 60mer oligonucleotide spotted microarray slides (Agilent catalog gene expression microarray for Mouse, v2 8x60K, design ID 074809) and subsequent washing and drying of the slides was performed following the Agilent hybridization protocol in Agilent hybridization chambers, with the following modifications: 2 µg of the labeled cDNA were hybridized for 22h at 65°C. The cDNA was not fragmented before hybridization. The dried slides were scanned at 2 µm/pixel resolution using the InnoScan is900 (Innopsys). Image analysis was performed with Mapix 6.5.0 software, and calculated values for all spots were saved as GenePix results files. Stored data were evaluated using the R software ("R: The R Project for Statistical Computing," n.d.) and the limma package (Smyth, 2005) from BioConductor (Gentleman et al., 2004). Log2 mean spot signals were taken for further analysis. Data was background corrected using the NormExp procedure on the negative control spots and quantile-normalized (Smyth, 2005; Smyth and Speed, 2003) before averaging. Log2 signals of replicate spots were averaged, and from several different probes addressing the same gene only the probe with the highest average signal was used. Genes were ranked for differential expression using a moderated t-statistic (Smyth, 2005). Pathway analyses were done using gene set tests on the ranks of the t-values (Smyth, 2005, 2004). Pathways were taken from the KEGG database

(http://www.genome.jp/kegg/pathway.html). Heatmaps were generated from the normalized log2 spot intensities (I) and show the gene-wise z-values (where $z_j = \left(I_j - mean(I)\right) / SD(I)$ for $j = 1 \ldots n$). The microarray data are available in GEO (GSE87683).

3.12. Statistical analysis and figure assembly

Quantitative data were assembled using GraphPad Prism software (GraphPad Software) and presented as average values +/- S.E.M. Statistical analyses were performed using Student's t-test for comparing 2 groups or One-way ANOVA for comparing 3 or more groups. Results were considered significant if $P<0.05$. Figures were assembled using Adobe Photoshop CS5 or Adobe Illustrator Ai6.

4. Results

4.1. PART I. Origin and fate of ACTA2$^+$ cells during lung development

4.1.1. FGF10$^+$ cells contribute, to a limited extent, to ASMC formation

The relatively stable β-galactosidase expression in the *Fgf10-LacZ* enhancer-trap line allows following the distribution of FGF10$^+$ cells and their immediate progenitors in the embryonic lung. Whole-mount LacZ staining revealed FGF10$^+$ (LacZ$^+$) cells in the distal mesenchyme as well as around the bronchi in E12.5 and E15.5 lungs (Fig. 4A-E), as previously reported (Mailleux et al., 2005). These observations previously led to the conclusion that FGF10$^+$ cells, which are originally found only in the distal mesenchyme (Bellusci et al., 1997a), migrate proximally and significantly differentiate along the ASMC lineage. Indeed, most of the ASMC regions were covered with LacZ$^+$ cells. Using the *Fgf10^{CreERT2}; tdTomato^{flox}* lineage-tracing tool, we also reported that FGF10$^+$ cells, labeled at E11.5 via a single intraperitoneal injection of tamoxifen (Tam IP), give rise to ASMCs and VSMCs at E13.5 and E15.5, but to a lesser extent than observed with the *Fgf10-LacZ* line (El Agha et al., 2014) (Fig. 4F-J). In the absence of tamoxifen, tdTomato$^+$ cells could not be observed in *Fgf10^{CreERT2}; tdTomato^{flox}* lungs (Fig. S1A-B). Quantification of the IF showed that the proportion of SMCs arising from FGF10$^+$ cells labeled at E11.5 was around 2±1%, indicating a minor contribution of FGF10$^+$ cells to ASMC and VSMC lineages. A reason for this discrepancy in the relative contribution of FGF10$^+$ cells to the ASMC lineage between the enhancer-trap line and the knock-in line could be the nature of the *Fgf10-LacZ* line. This transgenic line contains a minimal promoter for myosin light chain 1v (*Mlc1v)* upstream of the *LacZ* cassette but at the same time, it was found that the *LacZ* expression pattern mimicked *Fgf10* expression in many organs. The *Mlc1v-LacZ* transgene was found to be integrated 120 kb upstream of the *Fgf10* gene and likely due to a positional effect, *LacZ* expression was found to mimic *Fgf10* expression (Kelly et al., 2001; Mailleux et al., 2005). In spite of all the *in vivo* and *in vitro* evidence to rule out the activation of the *Mlc1v-LacZ* cassette in the *Fgf10-LacZ* enhancer trap (see (Mailleux et al., 2005) for details), residual expression of *Mlc1v-LacZ* can not be excluded with certainty.

Therefore, the *LacZ* expression pattern in the *Fgf10-LacZ* reporter line reflects the expression of *Fgf10* (mostly distally) and likely to some extent the *Mlc1v* (mostly proximally). Altogether, our data show that FGF10^{+} cells are progenitors for ASMCs and VSMCs in the distal lung at early embryonic development. However, this contribution to the SMC lineage is minor (El Agha et al., 2014).

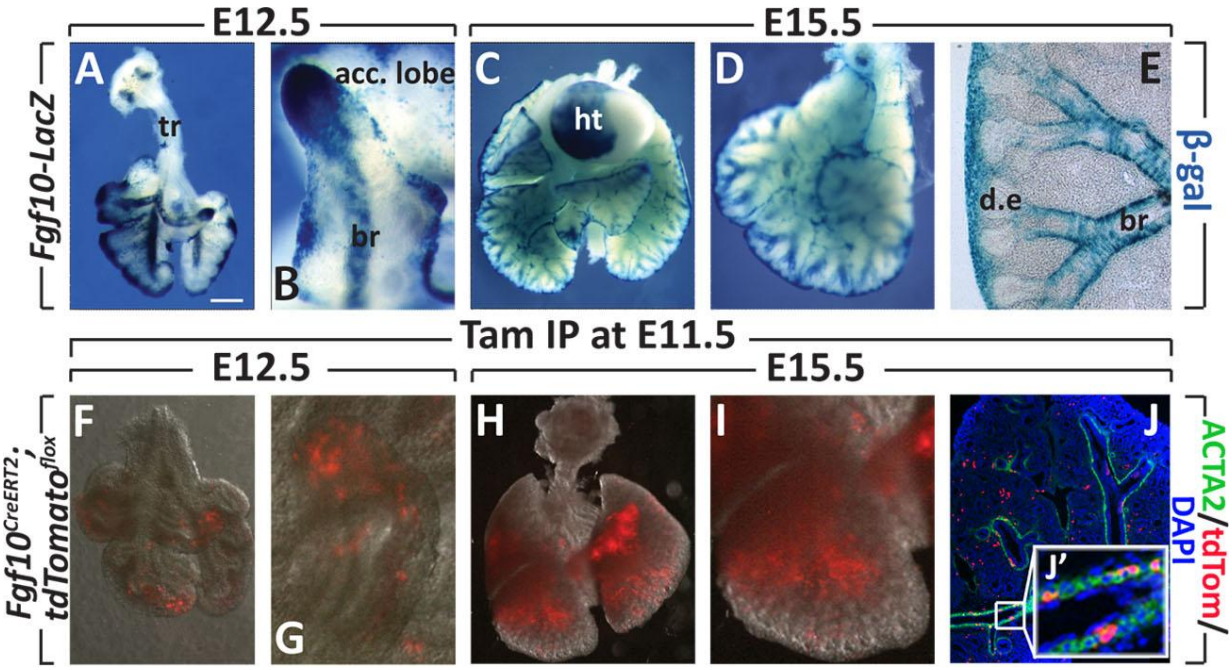

Figure 4: Contribution of FGF10^{+} cells to the SMC lineage. (A-E) *Fgf10 (LacZ)* expression in *Fgf10-LacZ* lungs at E12.5 (A,B) and E15.5 (C,D). (E) Vibratome section of the lung shown in D. **(F-J)** *Fgf10^{CreERT2}; tdTomato^{flox}* lungs induced with Tam IP at E11.5 and collected at E12.5 (F, G) and E15.5 (H,I). (J) Immunofluorescence for ACTA2 and tdTomato on the lung shown in (H). **(J')** High magnification of an airway showing tdTomato^{+} ACTA2^{+} cells. Tr – trachea, acc.lobe – accessory lobe, br. – bronchus, ht – heart, d.e. – distal epithelium, β-gal – β-galactosidase, Tam IP – tamoxifen intraperitoneal injection, ACTA2 – alpha smooth muscle actin. N = 3 for all experiments. Scale bars: 200 µm in A; 170 µm in F; 60 µm in B, G; 450 µm in C, H; 220 µm in D, I; 50 µm in E; 130 µm in J. (Moiseenko et al., 2017, Stem Cells, manuscript accepted for publication)

4.1.2. FGF10^{+} and GLI1^{+} domains are for the most part mutually exclusive at E12.5

SHH signaling is critical for SMC formation as *Shh* KO lungs show complete absence of ACTA2^{+} cells (Miller et al., 2004; Pepicelli et al., 1998). SHH, expressed at high levels in the distal lung epithelium, acts on the mesenchyme and inhibits *Fgf10* expression (Bellusci et al., 1997a, 1996). In order to validate this finding, the expression pattern of *LacZ* in *Fgf10-LacZ* and *Gli1^{LacZ}* lungs (Gli1 is a reporter for the activation of SHH signaling) at E12.5 was examined (Fig. 5). FGF10^{+} cells were observed mostly in the submesothelial mesenchyme whereas GLI1^{+} cells were mostly abundant in the subepithelial mesenchyme, and to a lower extent in the submesothelial mesenchyme. Both lines showed LacZ^{+} cells in the mesothelium.

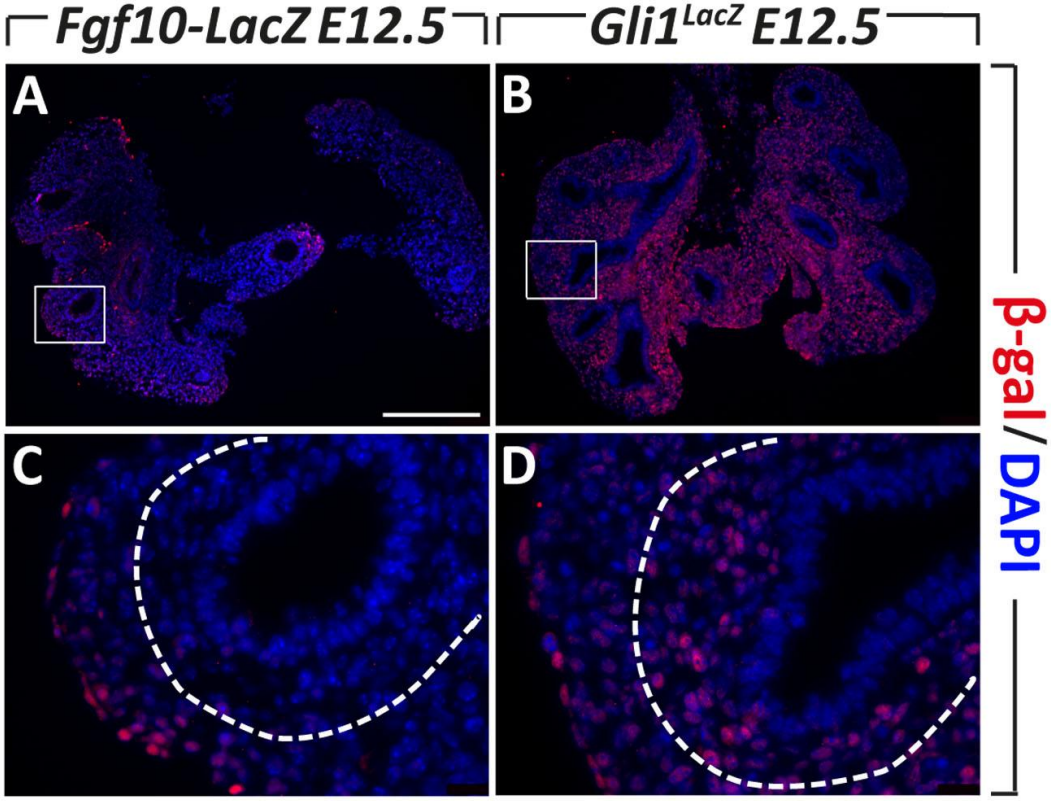

Figure 5: *Fgf10-LacZ* and *Gli1^{LacZ}* are expressed in different mesenchymal areas. (A-D) Immunofluorescence for β-galactosidase on lungs at E12.5 of *Fgf10-LacZ* (A,C) and *Gli1^{LacZ}* (B,D). Dashed line divides sub-mesothelial mesenchyme and sub-epithelial mesenchyme. N = 3 for both experiments. Scale bar: 150 µm in A, B; 35 µm in C; 40 µm in D.

4.1.3. GLI1$^+$ cells give rise to most SMCs but do not exclusively differentiate along the SMC lineage

In order to verify whether SMCs express GLI1 at E11.5, we analyzed *Gli1*^{LacZ} lungs and we could not identify LacZ$^+$ cells in the SMC layer at this time point (Fig. 6A,B).

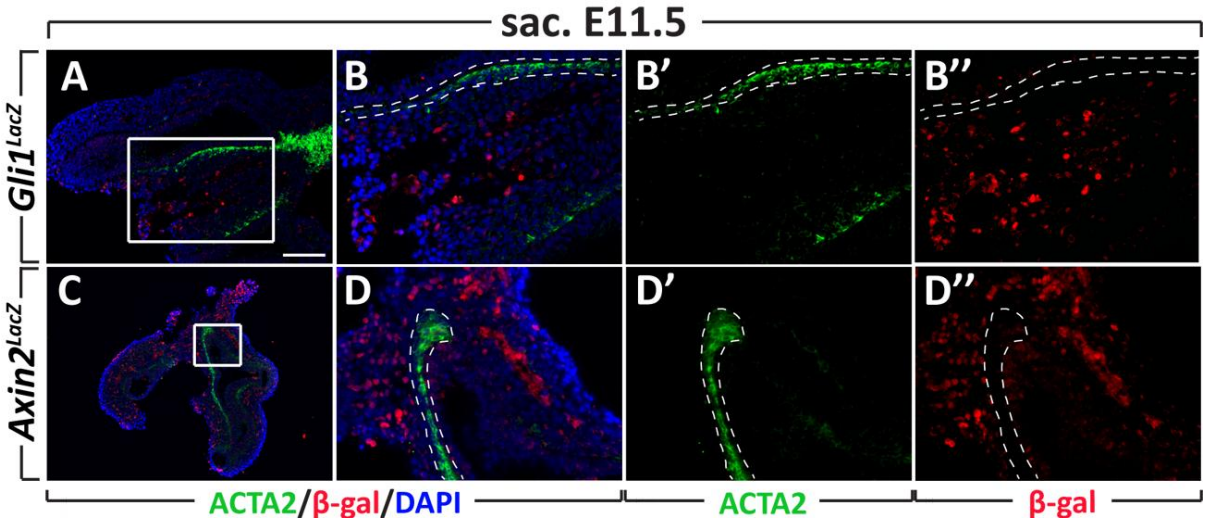

Figure 6: GLI1$^+$ and AXIN2$^+$ cells are not present in the SMC layer at E11.5. (A) Immunofluorescence for β-galactosidase on *Gli1*^{LacZ} lungs at E11.5. High magnification of ASMCs is shown in **(B-B')**. **(C)** Immunofluorescence for β-galactosidase on *Axin2*^{LacZ} lungs at E11.5. High magnification of ASMCs is shown in **(D-D")** Note the absence of β-galactosidase signal in ACTA2$^+$ cells. N = 3. Scale bar: 100 µm in A; 80 µm in C; 50 µm in B, D. (Moiseenko et al., 2017, Stem Cells, manuscript accepted for publication)

We then set out to test the specificity of the GLI1$^+$ lineage in terms of differentiation into SMCs, pregnant mice carrying *Gli1*^{CreERT2}*; tdTomato*^{flox} embryos received a Tam-IP injection at E11.5 and lungs were harvested at E12.5 and placed on nucleopore filters for live imaging for 3 days. The tdTomato signal expanded and labeled ring-like structures around the trachea and main bronchi. In addition, many tdTomato$^+$ cells were observed throughout the lung mesenchyme (Fig. 7A-D). Similar imaging using *Acta2-CreERT2; tdTomato*^{flox} lungs showed that most tdTomato$^+$ SMCs were located in proximal regions and expanded distally along the bronchi (Fig. 7E-H). Interestingly, few tdTomato$^+$ cells were found in the distal mesenchyme. The differences in terms of localization and behavior of tdTomato$^+$ cells between the *Gli1* and *Acta2* driver lines suggest that the GLI1$^+$ lineage does not only contain SMC progenitors.

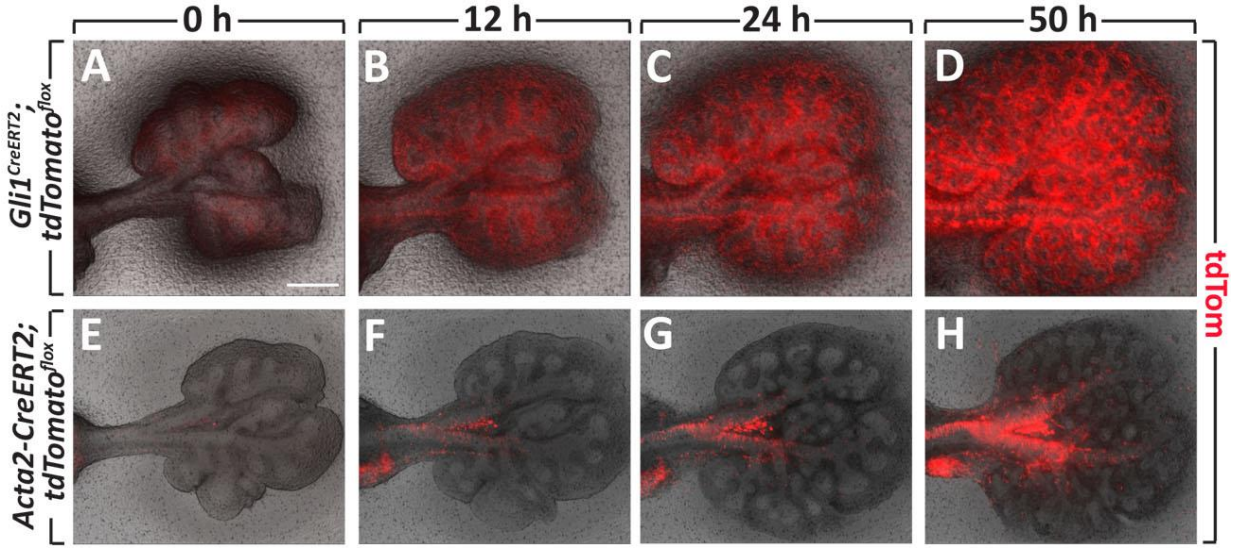

Figure 7: Distribution of GLI1$^+$ and ACTA2$^+$ cells labeled at E11.5 in the E12.5 developing lung. (A-D) Single images from live imaging with Gli1^{CreERT2}; tdTomato^{flox} tdTomato^{flox} lungs at E12.5 + 12, 24 and 50 hours. Note the intensity of tdTomato signal and appearance of ring like structures around trachea and main bronchi displaying contribution of GLI1$^+$ cells to SMC lineage. Also note the presence of tdTomato$^+$ cells in the mesenchyme throughout the lung. **(E-H)** Single images from live imaging with Acta2-CreERT2; tdTomato^{flox} lungs at E12.5 + 12, 24 and 50 hours. Note how tdTomato signal expands from proximal labeled SMCs distally along the bronchi. Note the presence of few tdTomato$^+$ cells in distal mesenchyme. h – hours. N = 3 for both experiments. Scale bar: 500 μm in A-H. (Moiseenko et al., 2017, Stem Cells, manuscript accepted for publication)

The *Gli1^{CreERT2}; tdTomato^{flox}* line was also used to label GLI1$^+$ cells at E11.5 and the lungs were harvested at E18.5. IF for ACTA2 was carried out and the contribution of GLI1$^+$ cells to the SMC lineage was quantified (N=3). No tdTomato signal was observed in *Gli1^{CreERT2};Tomato^{flox}* lungs not treated with tamoxifen (Fig. S1E,F). The results showed that the majority of ACTA2$^+$ cells were also tdTomato$^+$ (72±3% for VSMCs and 97±2% for ASMCs) (Fig. 8A-C,E,F). Interestingly, most tdTomato$^+$ cells in the quantified areas were ACTA2$^-$ parenchymal cells (71±2%) (Fig. 8D,G). Flow cytometry was also used and the initial gating for all experiments was set up to select live cells based on forward/side scatter profiles and exclude cell debris and highly granulated cells (Fig. S2). The analysis revealed that out of the total tdTomato$^+$ cells in the lung (representing 13±2% of the total cell suspension at E18.5), only 9±1% were ACTA2$^+$. In comparison, out of the total ACTA2$^+$ cells (representing 4±1% of the

total cell suspension at E18.5), only 28±4% were tdTomato^{+} (Fig. 8H). The difference in the results between IF and flow cytometry might reflect the difference in sensitivity between the two approaches.

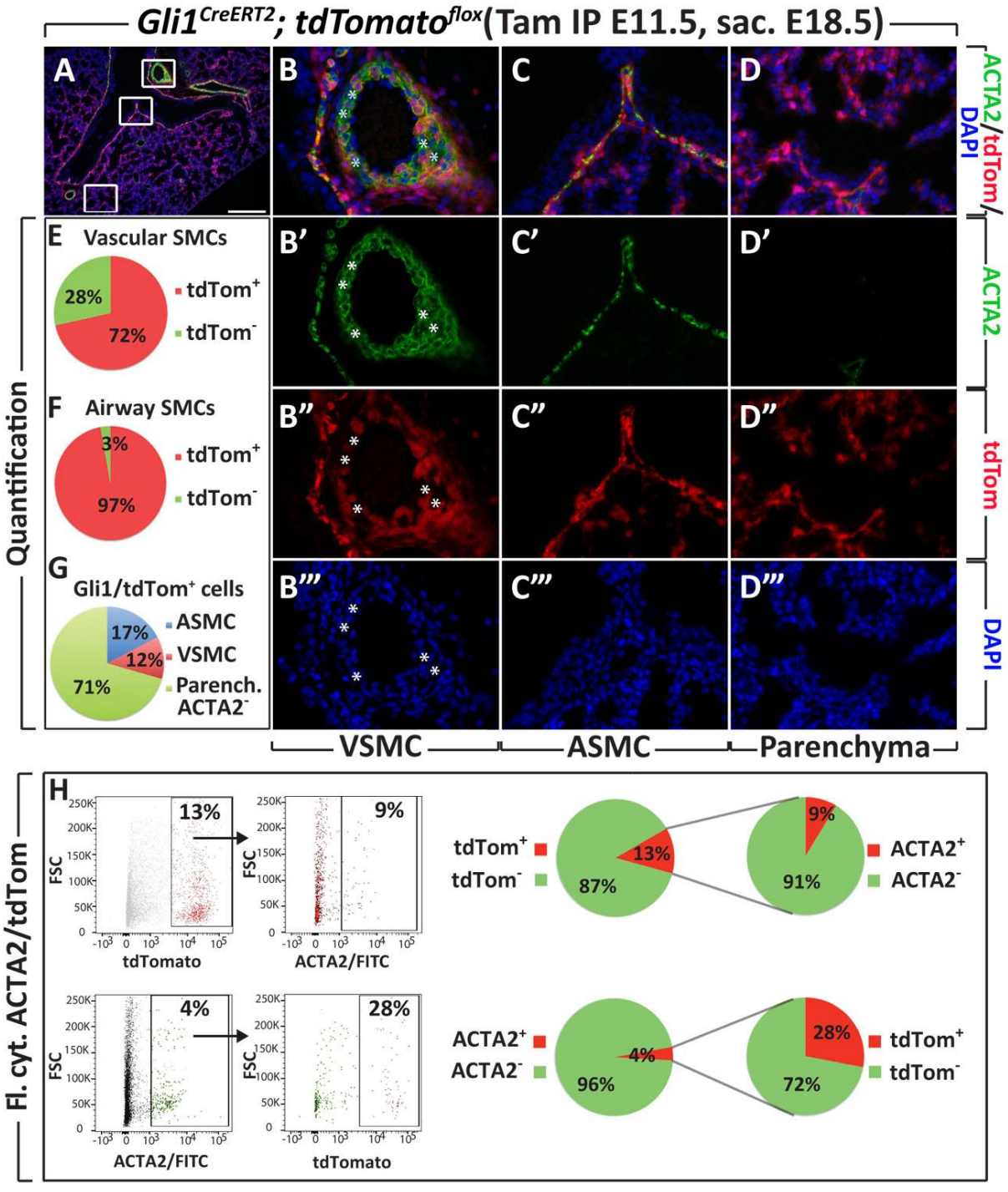

Figure 8: Contribution of GLI1^{+} cells labeled at E11.5 to the SMC lineage. (A-D) Immunofluorescence for ACTA2 on *Gli1^{CreERT2}; tdTomato^{flox}* lungs induced at E11.5 and analyzed at E18.5. Merged and single-channel images of the boxes shown in (A) are shown for VSMCs (B-B''), ASMCs (C-C''') and parenchymal cells (D-D''). **(E-G)**

Quantification of tdTomato$^+$ cell contribution to VSMCs (E) and ASMCs (F). Note that most of the tdTomato$^+$ are in parenchymal areas (G). **(H)** Flow cytometry analysis of E18.5 *Gli1^{CreERT2}; tdTomato^{flox}* lungs labeled at E11.5. Fl.Cyt. – Flow cytometry, FSC – forward scatter. N = 3. Scale bar: 200 μm in A; 36 μm in B-D. (Moiseenko et al., 2017, Stem Cells, manuscript accepted for publication)

In a previous study it was shown that GLI1$^+$ cells labeled at E10.5 and E11.5 give rise exclusively to SMCs and alveolar MYF, and do not give rise to other mesenchymal lineages such as lipofibroblasts (Li et al., 2015). In our work, staining for PLIN2 (ADRP), a lipofibroblast marker, showed that a proportion of tdTomato$^+$ cells were indeed ADRP$^+$. Flow cytometry analysis using the neutral lipid stain, LipidTOX, revealed that out of the total tdTomato$^+$ cells in the lung (representing 13±2% of the total cell suspension at E18.5), 46±3% were LipidTOX$^+$ (Fig. 9). On the other hand, out of the total LipidTOX $^+$ cells (representing 26±3% of the total cell suspension at E18.5), 18±1% were tdTomato$^+$. Altogether, the data revealed that the GLI1$^+$ lineage not only contributes to the ASMC and VSMC lineages, but also to lipofibroblasts, in addition to other undetermined lineages.

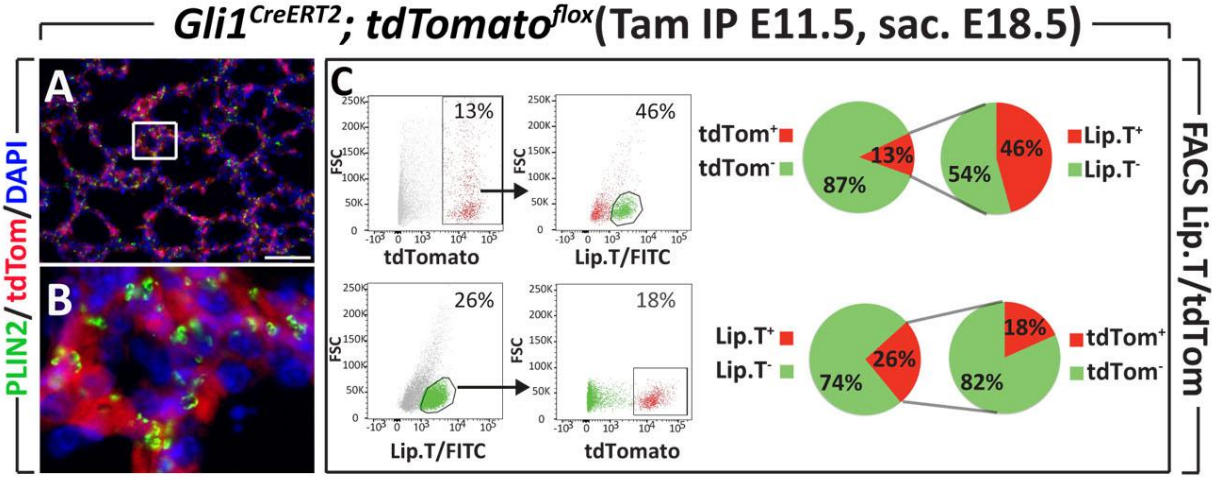

Figure 9: GLI1$^+$ cells partially give rise to lipofibroblasts. (A-B) Immunofluorescence for PLIN2 on *Gli1^{CreERT2}; tdTomato^{flox}* lungs induced at E11.5 and analyzed at E18.5. (B) High magnification image of parenchymal cells. **(C)** Flow cytometry analysis of E18.5 *Gli1^{CreERT2}; tdTomato^{flox}* lungs labeled at E11.5. PLIN2 – perilipin 2 (adipose differentiation-related protein). N = 3. Scale bar: 70 μm in A; 35 μm in B. (Moiseenko et al., 2017, Stem Cells, manuscript accepted for publication)

4.1.4. GLI1$^+$ cells significantly contribute to the alveolar MYF lineage during the alveolar stage of lung development

In another set of experiments, GLI1$^+$ cells were labeled during the end of the saccular stage (between PN2 and PN5 via tamoxifen-containing food) and lungs were analyzed (N=3) during the process of alveolarization at PN15. Elastin-secreting ACTA2$^+$ alveolar MYFs are critical players during this developmental stage. The results showed that most tdTomato$^+$ cells were located in secondary septa and were ACTA2$^+$ (Fig. 10A,C,F). Quantification of IF showed that under these experimental conditions, around 50±3% of alveolar MYFs in secondary septa were tdTomato$^+$ (Fig. 10E). By contrast, continuous labeling between PN2 and PN14 revealed almost all the alveolar MYFs in secondary septa were tdTomato$^+$ (Fig. 10B,D,E). Moreover, ASMCs were also significantly labeled in both experimental conditions (Fig. 10G), with only minor labeling of VSMCs (Fig. 10H).

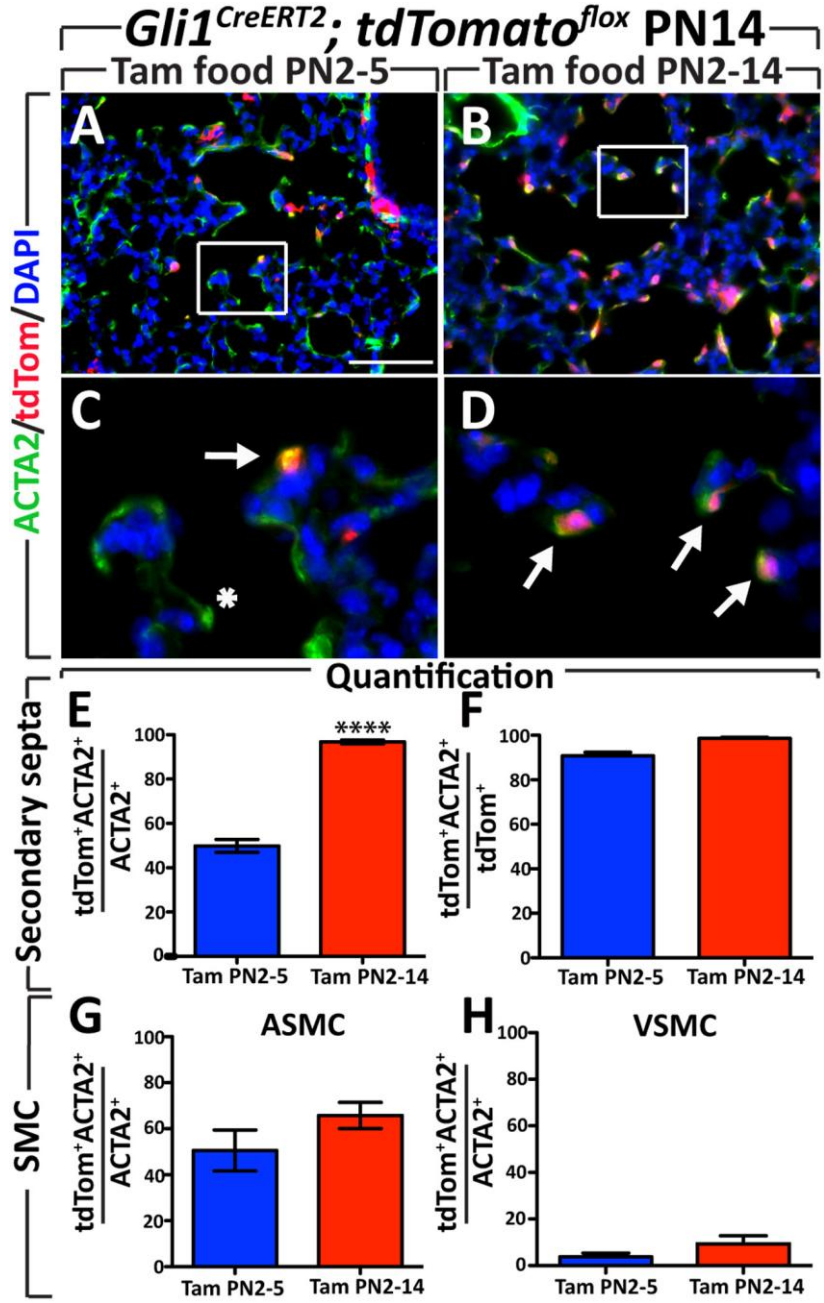

Figure 10: Contribution of GLI1^{+} cells labeled at PN2-PN5 or PN2-PN14 to the ACTA2^{+} lineage. (A-D) Immunofluorescence for ACTA2 on *Gli1^{CreERT2}; tdTomato^{flox}* lungs at PN14. (C,D) High-magnification images of the boxes shown in (A) and (B) showing ACTA2^{+} tdTomato^{+} alveolar MYFs marked by arrows and an ACTA2^{+} tdTomato^{-} cell marked by an asterisk. Note that when induced at PN2-PN14 (B,D) tdTomato^{+} cells significantly give rise to ACTA2^{+} cells as compared to labeling at PN2-PN5 (A,C). **(E)** Quantification of immunofluorescence showing that the majority of alveolar MYFs are tdTomato^{+} when cells are labeled between PN2 and PN14. Less alveolar MYFs are tdTomato^{+} when cells are labeled between PN2 and PN5. **(F)** Under both labeling conditions, the majority of tdTomato^{+} cells are ACTA2^{+} in

secondary septa. **(G, H)** A significant proportion of ASMCs and a minor proportion of VSMCs are labeled in both approaches. N = 3 for both experiments. PN – postnatal. Scale bar: 70 µm in A, B; 18 µm in C, D. **** *P*<0.0001. (Moiseenko et al., 2017, Stem Cells, manuscript accepted for publication)

4.1.5. WT1$^+$ cells contribute to the SMC lineage in a minor fashion

The *Wt1^{CreERT2}; tdTomato^{flox}* line was used to label WT1$^+$ cells at E11.5 and lungs were analyzed by IF at E18.5 (N=3). As expected, the mesothelium was abundantly labeled as well as individual cells in the parenchyma (Fig. 11A-D). However, quantification of tdTomato$^+$ ACTA2$^+$ cells in the vascular compartment indicated no contribution of these cells to VSMCs proximally, and only 1±1% of these cells contributed to VSMCs distally (Fig. 11E). A similar observation was made for ASMCs (1±1% proximally and 7±5% distally) (Fig. 11F). Finally, 72±3% of tdTomato$^+$ cells were ACTA2$^-$, and located in the parenchyma (Fig. 11G).

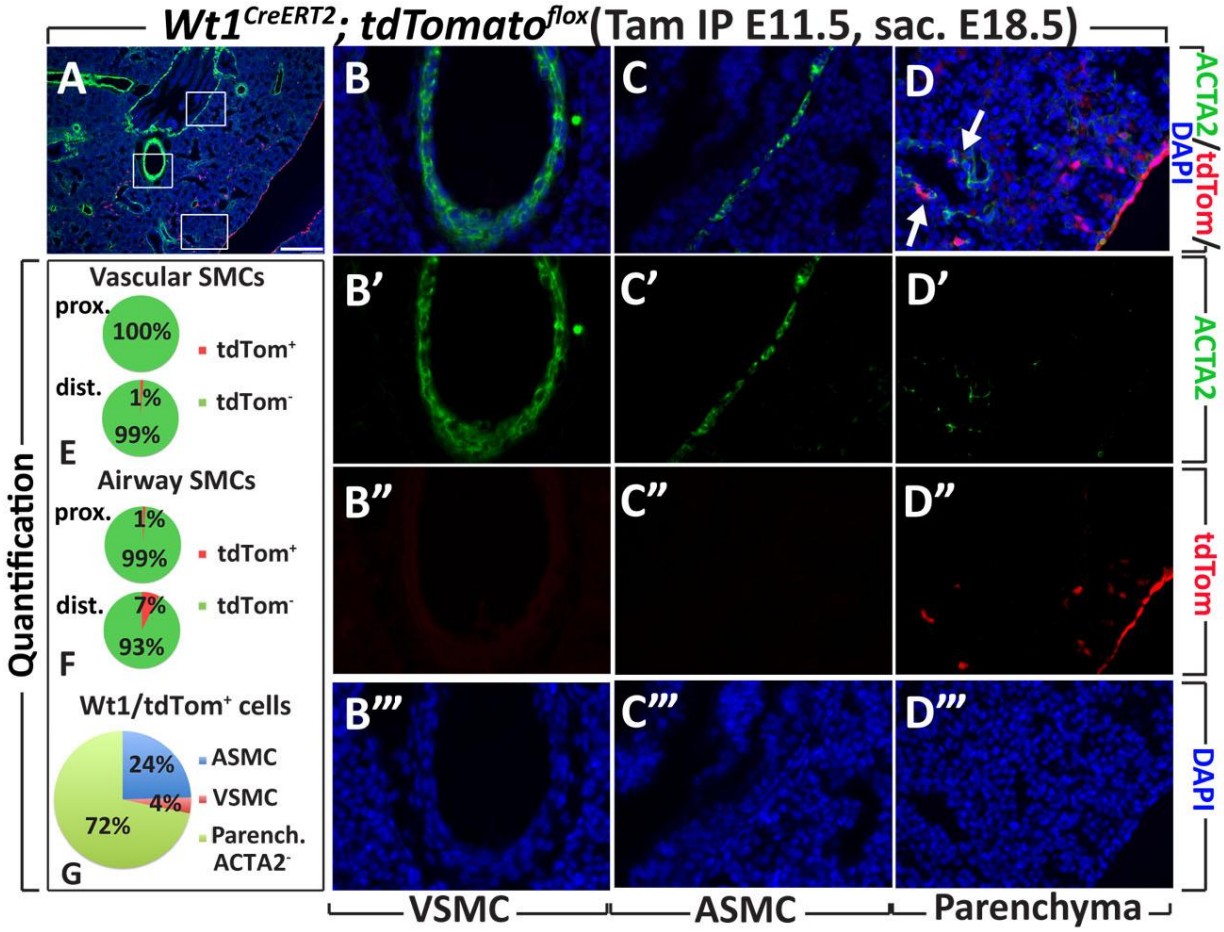

Figure 11: Contribution of WT1$^+$ cells labeled at E11.5 to the SMC lineage. (A-D) Immunofluorescence for ACTA2 on *Wt1^{CreERT2}; tdTomato^{flox}* lungs at induced at E11.5 and analyzed at E18.5. Merged and single-channel images of the boxes shown in (A) are shown for VSMCs (B-B''), ASMCs (C-C''') and parenchymal cells (D-D''). **(E-G)** Quantification of tdTomato$^+$ cell contribution to proximal and distal VSMCs (E) and ASMCs (F). Note that most of the tdTomato$^+$ are in parenchymal areas (G). N = 3. Scale bar: 200 µm in A; 20 µm in B-D. (Moiseenko et al., 2017, Stem Cells, manuscript accepted for publication)

4.1.6. AXIN2$^+$ cells give rise to most SMCs but do not exclusively differentiate along the SMC lineage

Considering the proposed role of WNT signaling in SMC formation (Cohen et al., 2009; Li et al., 2015), we decided to analyze the contribution of AXIN2$^+$ cells to this lineage. In order to verify whether ASMCs express AXIN2 at E11.5, the *Axin2^{LacZ}* reporter line was used and ACTA2/β-galactosidase double staining showed that ASMCs do not express AXIN2 at this time point (Fig. 6C,D). The *Axin2^{CreERT2}* line was then used to determine the fate of cells undergoing active WNT signaling during development. No tdTomato signal was observed in *Axin2^{CreERT2}; tdTomato^{flox}* lungs not treated with tamoxifen (Fig. S1I,J). AXIN2$^+$ cells were labeled at E11.5 and lungs were analyzed at E18.5 (N=3). TdTomato$^+$ cells showed a high level of contribution to the VSMC and ASMC lineages, similarly to GLI1$^+$ cells (Fig. 8). IF showed that most of ACTA2$^+$ SMCs were also tdTomato$^+$ (77±8% for VSMCs and 97±3% for ASMCs) (Fig. 12A-C,E,F). Similar to the results obtained with the GLI1$^+$ lineage, most of tdTomato$^+$ cells in the quantified areas were ACTA2$^-$ parenchymal cells (70±1%) (Fig. 12D,G).

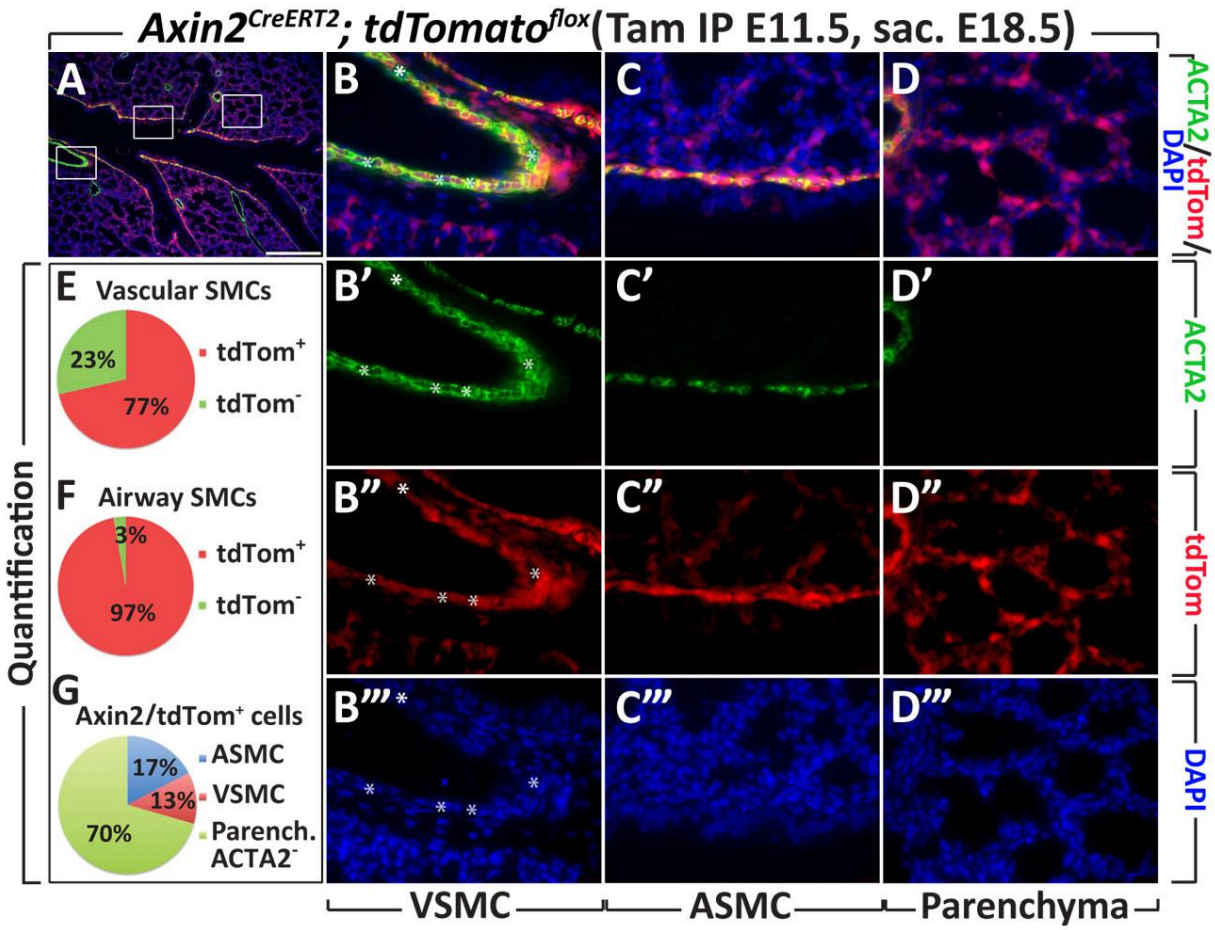

Figure 12: Contribution of AXIN2^{+} cells labeled at E11.5 to the SMC lineage. (A-D) Immunofluorescence for ACTA2 on *Axin2^{CreERT2}; tdTomato^{flox}* lungs at E18.5. Merged and single-channel images of the boxes shown in (A) are shown for VSMCs (B-B''), ASMCs (C-C''') and parenchymal cells (D-D''). **(E-G)** Quantification of tdTomato^{+} cell contribution to VSMCs (E) and ASMCs (F). Note that most of the tdTomato^{+} are in parenchymal areas (G). High magnification images of (B) VSMCs, (C) ASMCs, (D) parenchymal cells. N = 3. Scale bar: 200 µm in A; 40 µm in B-D. (Moiseenko et al., 2017, Stem Cells, manuscript accepted for publication)

4.1.7. Proximal ACTA2^{+} cells labeled at E11.5 do not give rise to SMCs distally

The *Acta2-CreERT2* line was used to investigate whether differentiated SMCs can serve as progenitors for newly forming SMCs. No tdTomato signal was observed in *Acta2-CreERT2; tdTomato^{flox}* lungs not treated with tamoxifen (Fig. S1M,N). SMCs were labeled at E11.5 and lungs were analyzed at E18.5 (N=3). The results showed that most of the labeled cells were present proximally rather than distally for both

ASMCs (94±3% vs. 24±4%; proximal vs. distal, respectively) and VSMCs (95±2% vs. 32±5%; proximal vs. distal, respectively) (Fig. 13A,B,D,F,G). This suggests that differentiated SMCs have very limited progenitor-like characteristics and therefore do not massively give rise to distal SMCs. Interestingly, tdTomato^{+} cells were also observed in the parenchyma throughout the lung (2-4 cells per section at 63X magnification) (Fig. 13C, E, H).

When ACTA2^{+} cells were labeled at E15.5 and lungs were analyzed at E18.5 (N=3), an increase in the number of tdTomato^{+} ACTA2^{+} cells was observed throughout the lung (Fig. 13I-P). By contrast to labeling at E11.5, ASMCs and VSMCs were labeled in both proximal and distal regions of the lung - ASMCs (97±1% vs. 87±5%; proximal vs. distal, respectively) and VSMCs (96±1% vs. 85±4%; proximal vs. distal, respectively) (Fig. 13J,L,N,O). In addition, an increase in the number of parenchymal tdTomato^{+} cells was observed (8-10 cells per section when induced at E15.5 vs. 2-4 cells per section when induced at E11.5) (Fig. 13P).

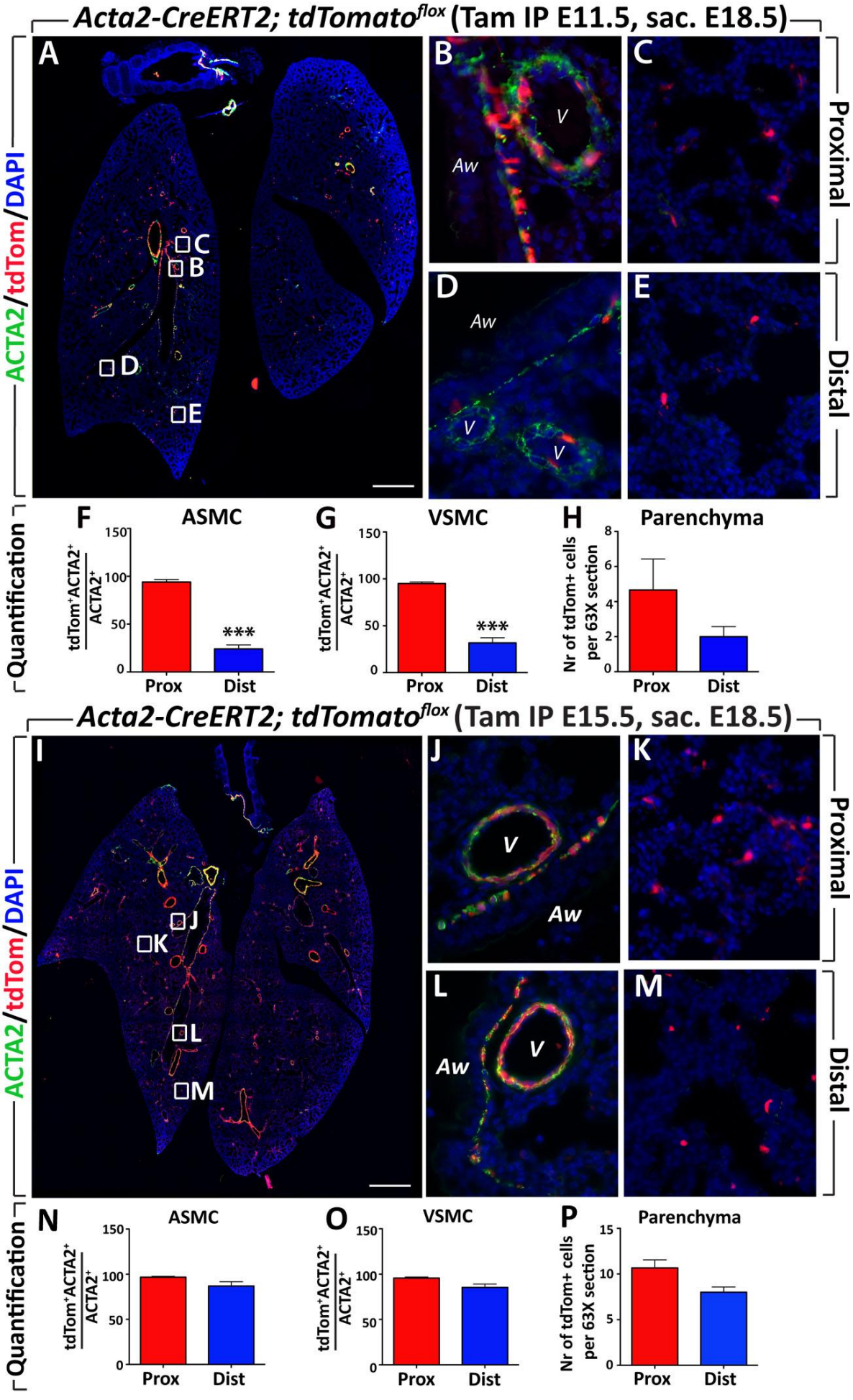
Acta2-CreERT2; tdTomato^flox (Tam IP E11.5, sac. E18.5)
ACTA2/tdTom/DAPI
A
B
C
D
E
Aw
V
Proximal
Distal
Quantification
F
ASMC
tdTom+ACTA2+ / ACTA2+
***
Prox
Dist
G
VSMC
H
Parenchyma
Nr of tdTom+ cells per 63X section
Acta2-CreERT2; tdTomato^flox (Tam IP E15.5, sac. E18.5)
I
J
K
L
M
N
O
P

Figure 13: Contribution of ACTA2$^+$ cells labeled at E11.5 and E15.5 to the SMC lineage. (A-E). Immunofluorescence for ACTA2 on *Acta2-CreERT2; tdTomato^{flox}* lungs labeled at E11.5 and sacrificed at E18.5. (B-E) High-magnification images of proximal and distal ACTA2$^+$ tdTomato$^+$ ASMCs and VSMCs as well as ACTA2$^-$ tdTomato$^+$ parenchymal cells. Note that labeled tdTomato$^+$ cells are located more proximally, but not distally. **(F)** Quantification of ASMC coverage by tdTomato signal. **(G)** Quantification of VSMCs coverage by tdTomato signal. **(H)** Quantification of parenchymal tdTomato$^+$ cells. **(I-M)** Immunofluorescence for ACTA2 on *Acta2-CreERT2; tdTomato^{flox}* lungs labeled at E15.5 and sacrificed at E18.5. (J-M) High-magnification images of proximal and distal ACTA2$^+$ tdTomato$^+$ ASMCs and VSMCs as well as ACTA2$^-$ tdTomato$^+$ parenchymal cells. Note the significant colocalization of an ACTA2 stain and tdTomato signal both proximally and distally. **(N)** Quantification of ASMC coverage by tdTomato signal. **(O)** Quantification of VSMC coverage by tdTomato signal. **(P)** Quantification of parenchymal tdTomato$^+$ cells. Aw – airway, V - blood vessel, prox. – proximal, dist. – distal. N=3 for both experiments. Scale bar: 400 μm in A, I; 20 μm in B-E, J-M. *** P<0.001. (Moiseenko et al., 2017, Stem Cells, manuscript accepted for publication)

4.1.8. Parenchymal ACTA2^{low} lineage contains progenitors for alveolar myofibroblasts that appear postnatally

Next, we tested whether parenchymal ACTA2^{low} tdTomato$^+$ cells at E18.5, which trace back to E11.5 and more significantly to E15.5, are progenitors for alveolar MYFs. To test this hypothesis, the *Acta2-CreERT2; tdTomato^{flox}* line was used to label ACTA2$^+$ cells at E15.5 and lungs were harvested at PN14 (N=6). Alveolar MYFs are known to produce elastin (ELN), deposition of which is critical for maintaining the alveolar integrity and allowing alveoli to stretch during inhalation (Dickie et al., 2008). Our results showed the presence of tdTomato$^+$ ACTA2$^+$ ELN$^+$ cells at PN14 (Fig. 14B,E). Out of the total tdTomato$^+$ cells that are not located around airways and within vessels, 90±2% were alveolar MYFs at PN14, based on two criteria: expression of ACTA2/ELN and location at the tip of secondary septa (Fig. 14D). 9±2% of tdTomato$^+$ cells were ACTA2$^-$ at PN14 (Fig. 14D). In addition, out of the total alveolar MYFs, 36±3% were tdTomato$^+$ (Fig. 14C). Additionally, flow cytometry

revealed that 24±3% of tdTomato^{+} cells labeled at E15.5 were PDGFRα^{+} at PN14 (Fig. 14F).

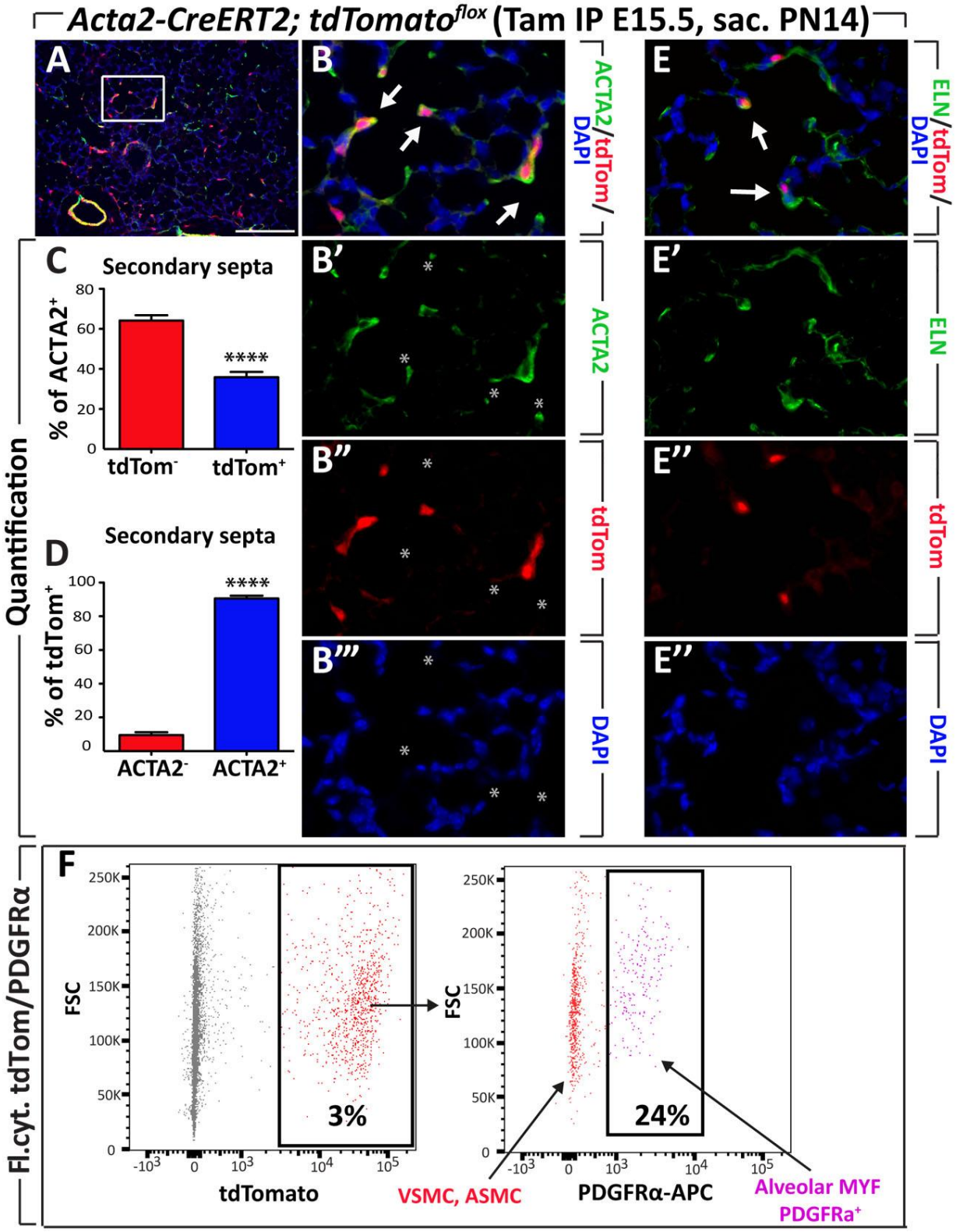

Figure 14: Parenchymal ACTA2^{low} cells labeled at E15.5 give rise to PDGFRα^{+} alveolar MYFs at PN14. (A) Immunofluorescence for ACTA2 on *Acta2-CreERT2;*

tdTomato^{flox} lungs at PN14. **(B-B''')** Merged and single-channel high magnification images of the box shown in (A) showing ACTA2^{+} tdTomato^{+} alveolar MYFs marked by arrows, ACTA2^{+} tdTomato^{-} cells are marked with asterisks. **(C,D)** Quantification of ACTA2^{+} and tdTomato^{+} cells in the tips of secondary septa. **(E)** Merged and single-channel images of immunofluorescence for elastin (ELN) on *Acta2-CreERT2; tdTomato*^{flox} lungs at PN14. tdTomato^{+} ELN^{+} cells are marked by arrows. **(F)** Flow cytometry analysis of *Acta2-CreERT2; tdTomato*^{flox} lungs (Tam IP E15.5) at PN14 based on tdTomato expression and PDGFRα staining. ELN – elastin, PDGFRα – platelet-derived growth factor receptor alpha. N = 6. Scale bar: 150 μm in A; 35 μm in B; 40 μm in E. **** P<0.0001. (Moiseenko et al., 2017, Stem Cells, manuscript accepted for publication)

Since PDGFRα is believed to be a marker for alveolar MYFs and/or their progenitors, FACS was used to sort various tdTomato^{+} cell populations based on ACTA2 and PDGFRα expression at E18.5. TdTomato^{+} cells labeled at 15.5 and collected at E18.5 represented 2±0.3% of total lung cells (Fig. 15A). Further analysis based on PDGFRα and ACTA2 expression revealed the presence of three distinct cell populations (N=9). In particular, the AMCS and VSMCs (tdTomato^{+} ACTA2^{high} PDGFRα^{-}) represented around 15±1% of total tdTomato^{+} cells, while alveolar MYF progenitors (tdTomato^{+} ACTA2^{low} PDGFRα^{+}) represented around 21±4% of total tdTomato^{+} cells. QPCR-based validation of these two pools of lineage-traced cells confirmed that alveolar MYF progenitors expressed high levels of *Pdgfra* and *Eln,* while ASMCs and VSMCs expressed high levels of *Acta2*. Note that *Eln* was upregulated by 400 fold in alveolar MYF progenitors compared to ASMCs and VSMCs (Fig. 15B).

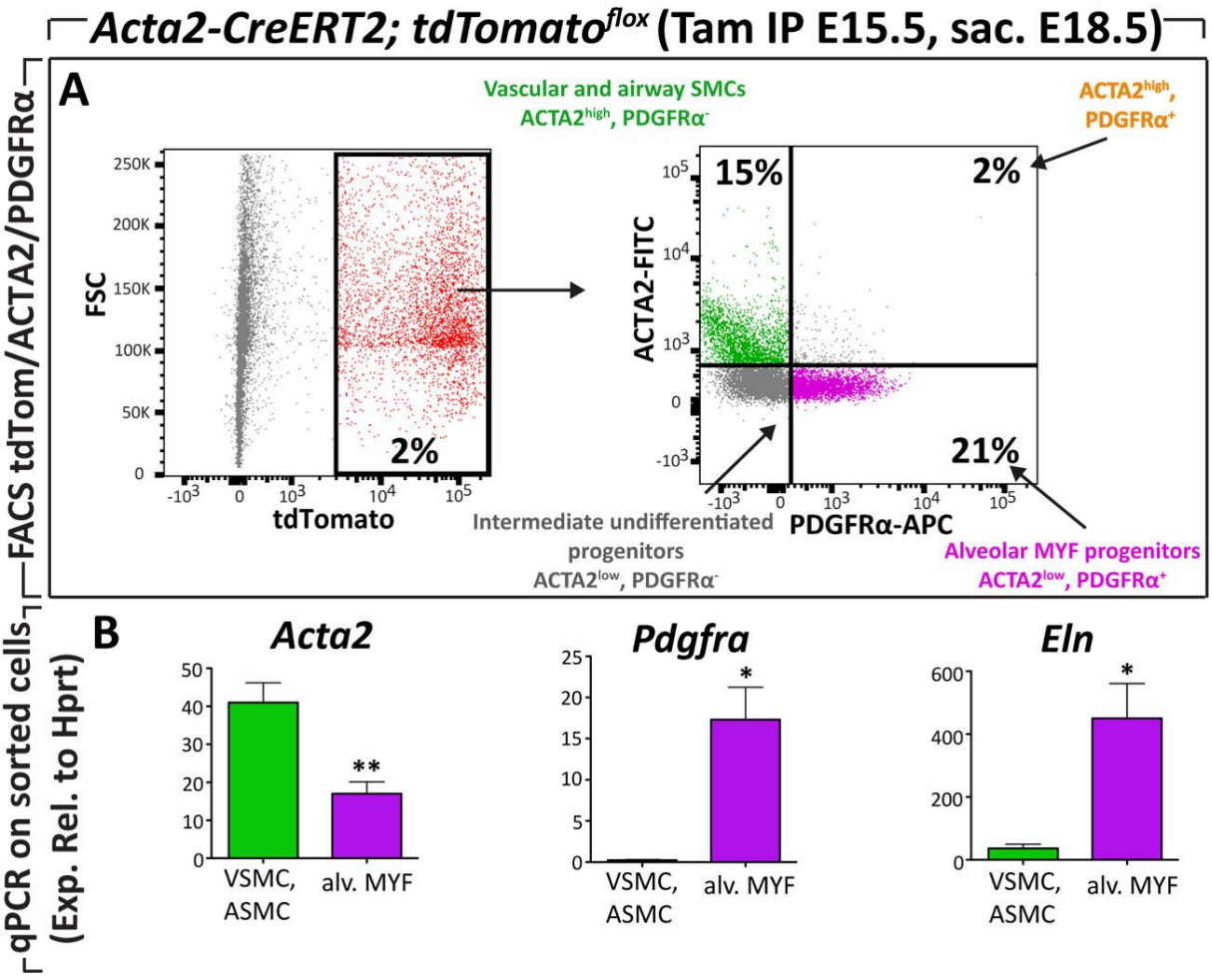

Figure 15: Analysis of different ACTA2$^+$ cell populations labeled at E15.5 and collected at E18.5. (A) Gating strategy for isolating various tdTomato$^+$ cell populations (induced at E15.5 and collected at E18.5) based on ACTA2 and PDGFRα expression. **(B)** Gene expression analysis of sorted cells. ELN – elastin, PDGFRα – platelet-derived growth factor receptor alpha. N=9. * *P*<0.05, ** *P*<0.01. (Moiseenko et al., 2017, Stem Cells, manuscript accepted for publication)

Next, gene arrays were carried out on isolated lineage-labeled cells (3 independent experiments, 3 lungs used per pool): ASMCs and VSMCs (ACTA2^{high} PDGFRα$^-$), alveolar MYF progenitors (ACTA2^{low} PDGFRα$^+$) and ACTA2^{low} PDGFRα$^-$ cells (called intermediate undifferentiated progenitors or INMs). Note that the minor ACTA2^{high} PDGFRα$^+$ pool, which represented around 2±1% of the overall tdTomato$^+$ population, was not considered for further analysis. Most changes in gene expression levels occurred between SMCs and alveolar MYF progenitors. The INM pool was very similar to the SMC pool in regards to gene expression levels (Fig. 16A). The top 100 up/downregulated genes according to fold-change values are represented in the heat

maps (Fig. 16A). KEGG analysis revealed that in contrast to SMCs, alveolar MYF progenitors display an upregulation of the genes related to sonic hedgehog, WNT and FGF signaling pathways – the known regulators of smooth muscle cell differentiation (Fig 16B,C; Table 4). Transcriptomic signatures of different ACTA2-derived populations were identified and the results showed genes enriched either in ASMCs and VSMCs or in alveolar MYF progenitors at E18.5 (Supplementary Table 1 and 2). Among the highly upregulated genes in alveolar MYF progenitors are members of the WNT signaling pathway, such as WNT inhibitory factor 1 (*Wif1*), Lymphoid enhancer binding factor 1 (*Lef1)*, Transcription factor 7 (T cell specific) (*Tcf7)*, and WNT family member 5a (*Wnt5a)*. Members of the Transforming growth factor β (TGFβ) pathway were also enriched in alveolar MYF progenitors, such as Transforming growth factor β receptor 3 (*Tgfbr3)* and Bone morphogenetic protein 4 *(Bmp4*), confirming the importance of this pathway in alveolar MYF differentiation. Genes enriched in SMCs were mostly structural proteins – actinin, myosin, troponin, and proteins regulating muscle contraction. Signaling pathways such SHH, WNT, FGF and TGFβ were downregulated, suggesting that these pathways mostly regulate the fate of progenitor cells and are significantly inactive in fully differentiated SMCs, the main function of which is contraction.

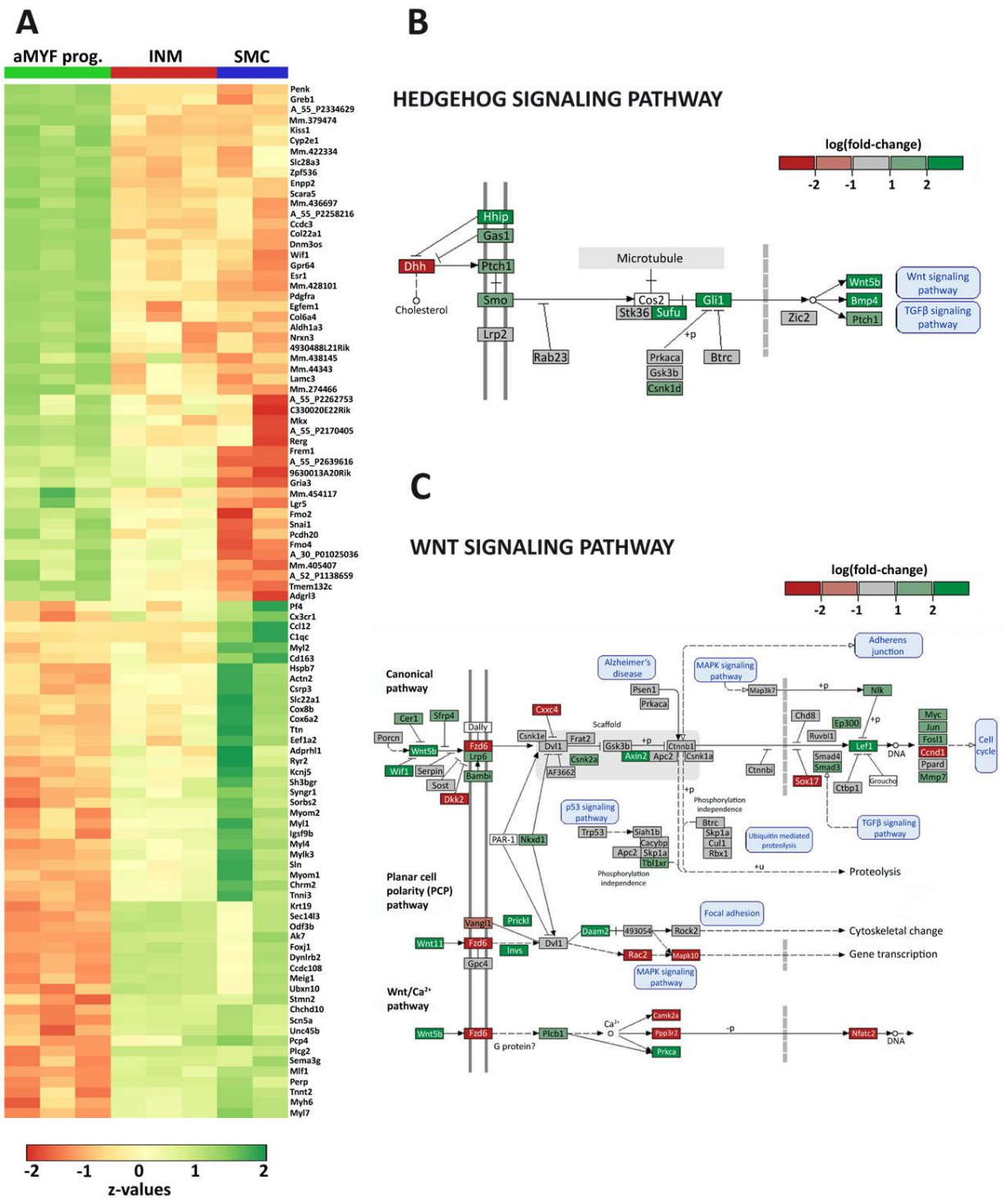

Figure 16: Genes and pathways regulated in ACTA2-derived cell populations. (A) Top 50 genes specifically upregulated and top 50 genes downregulated in alveolar MYF progenitors (aMYF prog.) in comparison to airway and vascular SMCs (SMC) and intermediate undifferentiated progenitors (INM). (B, C) KEGG analysis of specific signaling pathways – (B) Hedgehog and (C) WNT, showing that the majority of the genes in these pathways are upregulated in alveolar MYF progenitors versus SMCs. (Moiseenko et al., 2017, Stem Cells, manuscript accepted for publication)

Table 4. Genes related to SHH, WNT and FGF signaling pathways upregulated in alveolar MYF progenitors in contrast to SMCs.

Genes upregulated in alveolar MYF progenitors vs. SMCs	
Sonic hedgehog signaling	**WNT signaling**
Gli1 (GLI-Kruppel family member GLI1) FC=7.26, p<0.0001	*Wif1 (Wnt inhibitory factor 1)* FC=235.57, p<0.0001
Bmp4 (*bone morphogenetic protein 4*) FC=5.34, p<0.001	*Lef1 (lymphoid enhancer binding factor 1)* FC=32, p<0.0001
Hhip (*Hedgehog-interacting protein*) FC=5.03, p<0.005	*Tcf7 (transcription factor 7, T cell specific)* FC=16.56, p<0.0001
Bmp2 (bone morphogenetic protein 2) FC=5.1, p<0.01	*Wnt5a (wingless-type MMTV integration site family, member 5A)* FC=11.47, p<0.0001
Sufu (suppressor of fused homolog (Drosophila)) FC=4.69, p<0.05	*Fzd1 (frizzled homolog 1 (Drosophila)* FC=9.45, p<0.0001
Gli3 (GLI-Kruppel family member GLI3) FC=3.86, p<0.01	*Invs (Inversin)* FC=9.25, p<0.0001
Ptch1 (patched homolog 1) FC=3.81, p<0.001	*Daam2 (dishevelled associated activator of morphogenesis 2)* FC=7.94, p=0.09
Gas1 (growth arrest specific 1) FC=3.14, p<0.01	*Wnt5b (wingless-type MMTV integration site family, member 5B)* FC=6.68, p<0.001
Smo (smoothened homolog (Drosophila) FC=2.81, p<0.01	*Wnt9a (wingless-type MMTV integration site family, member 9A)* FC=5.81, p<0.01
Csnk1d (casein kinase 1, delta) FC=2.23, p<0.01	*Nfatc4 (nuclear factor of activated T cells, cytoplasmic, calcineurin dependent 4)* FC=5.73, p<0.001
	Tle1 (transducin-like enhancer of split 1, homolog of Drosophila E(spl)) FC=5.62, p<0.001
Fibroblast growth factor signaling	*Lrp1 (low density lipoprotein receptor-related protein 1))* FC=4.89, p<0.0001

Fgf10 (fibroblast growth factor 10) FC=29.04, p<0.0001	*Axin2* FC=4.79, p<0.001
Fgf7 (fibroblast growth factor 7) FC=20.82, p<0.01	*Fzd10 (frizzled homolog 10 (Drosophila)* FC=4.59, p<0.05
Map3k6 (mitogen-activated protein kinase 6) FC=9.19, p<0.01	*Prickle2 (prickle homolog 2 (Drosophila)* FC=4.5, p<0.05
Fgf11 (fibroblast growth factor 11) FC=8.22, p=0.08	*Dkk3 (dickkopf homolog 3 (Xenopus laevis)* FC=4.2, p<0.01
Fgf2 (fibroblast growth factor 2) FC=7.36, p<0.05	*Wnt11 (wingless-type MMTV integration site family, member 11)* FC=4.17, p<0.01
Fgf18 (fibroblast growth factor 18) FC=7.41, p<0.01	*Prkca (protein kinase C, alpha)* FC=4.03, p<0.001
Fgf5 (fibroblast growth factor 5) FC=4.86, p=0.13	*Tbl1xr1 (transducin (beta)-like 1X-linked receptor 1)* FC=3.14, p<0.01
Ptpn5 (protein tyrosine phosphatase, non-receptor type 5) FC=4.14, p<0.05	*Bambi (BMP and activin membrane-bound inhibitor)* FC=3.12, p=0.05
Prkca (protein kinase C, alpha) FC=4.03, p<0.001	*Ep300 (E1A binding protein p300)* FC=2.73, p<0.05
Fgfr4 (fibroblast growth factor receptor 4) FC=3.84, p<0.05	*Nlk (nemo like kinase)* FC=2.67, p<0.01
Ngf (nerve growth factor) FC=2.91, p<0.05	*Plcb1 (phospholipase C, beta 1)* FC=2.64, p<0.05
Fgf17 (fibroblast growth factor 17) FC=2.83, p<0.05	*Nkd1 (naked cuticle 1 homolog (Drosophila)* FC=2.57, p<0.005
Fgfbp3 (fibroblast growth factor binding protein 3)) FC=2.62, p<0.05	*Mmp7 (matrix metallopeptidase 7)* FC=2.55, p=0.12
Fgfr1 (fibroblast growth factor receptor 1) FC=2.46, p<0.01	*Fosl1 (fos-like antigen 1)* FC=2.53, p=0.36
Fgf12 (fibroblast growth factor 12) FC=2.03, p=0.44	*Smad3 (SMAD family member 3)* FC=2.34, p<0.05
	Myc (myelocytomatosis oncogene) FC=2.03, p=0.06

4.1.9. Differentiated SMCs as well as progenitors for alveolar MYFs and mature alveolar MYFs do not proliferate

To assess the proliferation status of different ACTA2^{+} populations lungs were stained for Ki67, a cellular marker for proliferation. No proliferation were observed in ASMCs when labeled at E15.5 and analyzed at E18.5 and PN14 (Fig 17A,C). No proliferation was also observed for alveolar MYF progenitors as well as mature alveolar MYFs (Fig 17B,D).

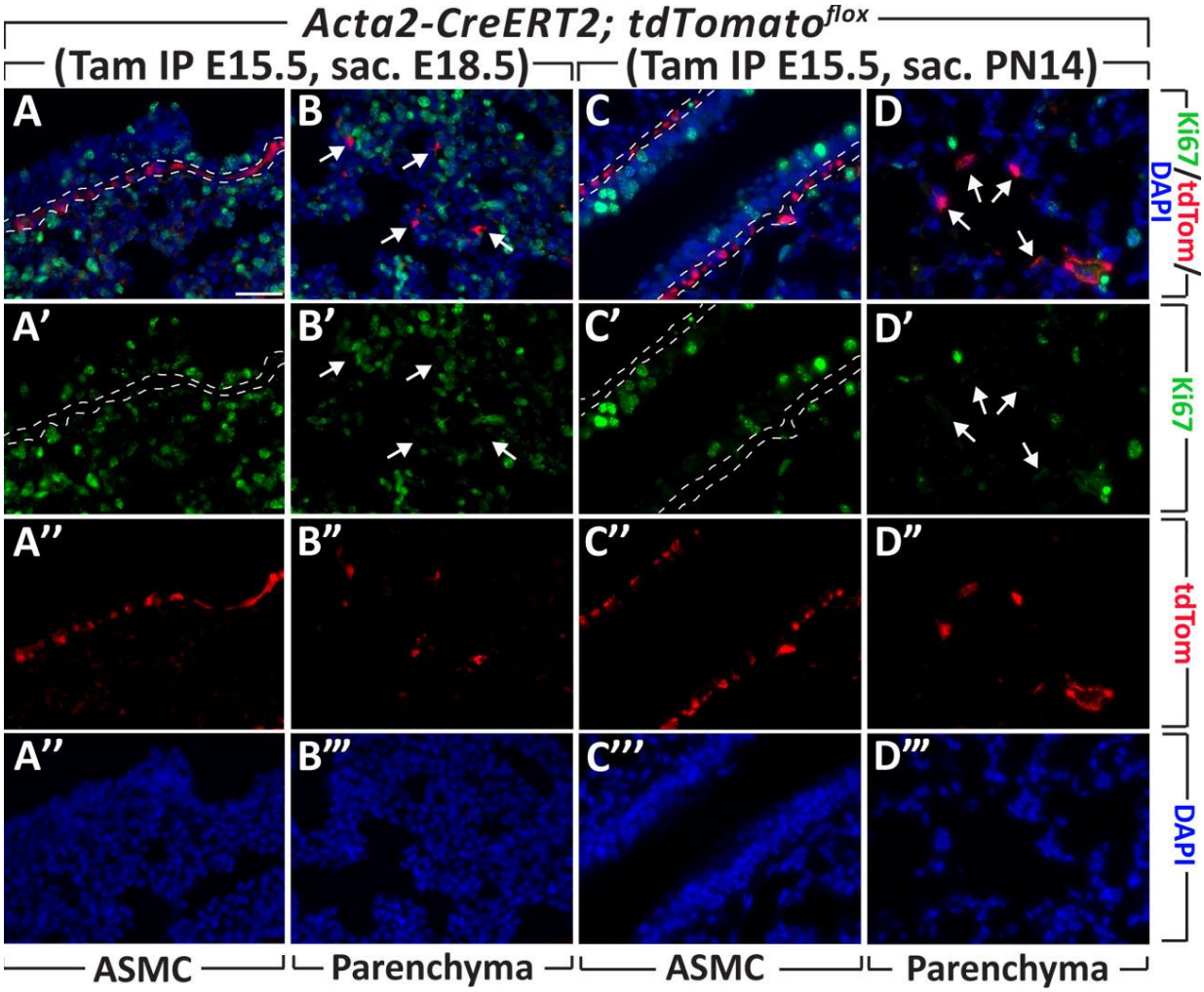

Figure 17: Parenchymal ACTA2^{+} cells labeled at E15.5 do not proliferate at E18.5 or at PN14. (A-D) Merged and single channel images of immunofluorescence for tdTomato and KI67 on *Acta2-CreERT2; tdTomato^{flox}* lungs labeled at E15.5 and sacrificed at (A, B) E18.5 and (C, D) PN14 showing no proliferation in both (A, C) ASMCs and (B, D) parenchymal cells for both time points. N = 3 for both experiments. Scale bar: 40 µm in all panels. (Moiseenko et al., 2017, Stem Cells, manuscript accepted for publication)

4.1.10. Alveolar MYFs do not disappear from the lung after alveolarization

Alveolar MYFs play an important role in creating alveoli. But after the process of alveolarization is finished alveolar MYFs were believed to disappear from the lung (Kapanci et al., 1995; Yamada et al., 2005). However, when labeling at PN2-5, $ACTA2^{+}$ MYFs that are present with high number in parenchyma and show high ACTA2 expression at PN14 (Fig. 18A) are still present in lung parenchyma at PN30 and PN60 (Fig. 18B,C) but with lower number and with lower ACTA2 expression (Fig. 18D,E).

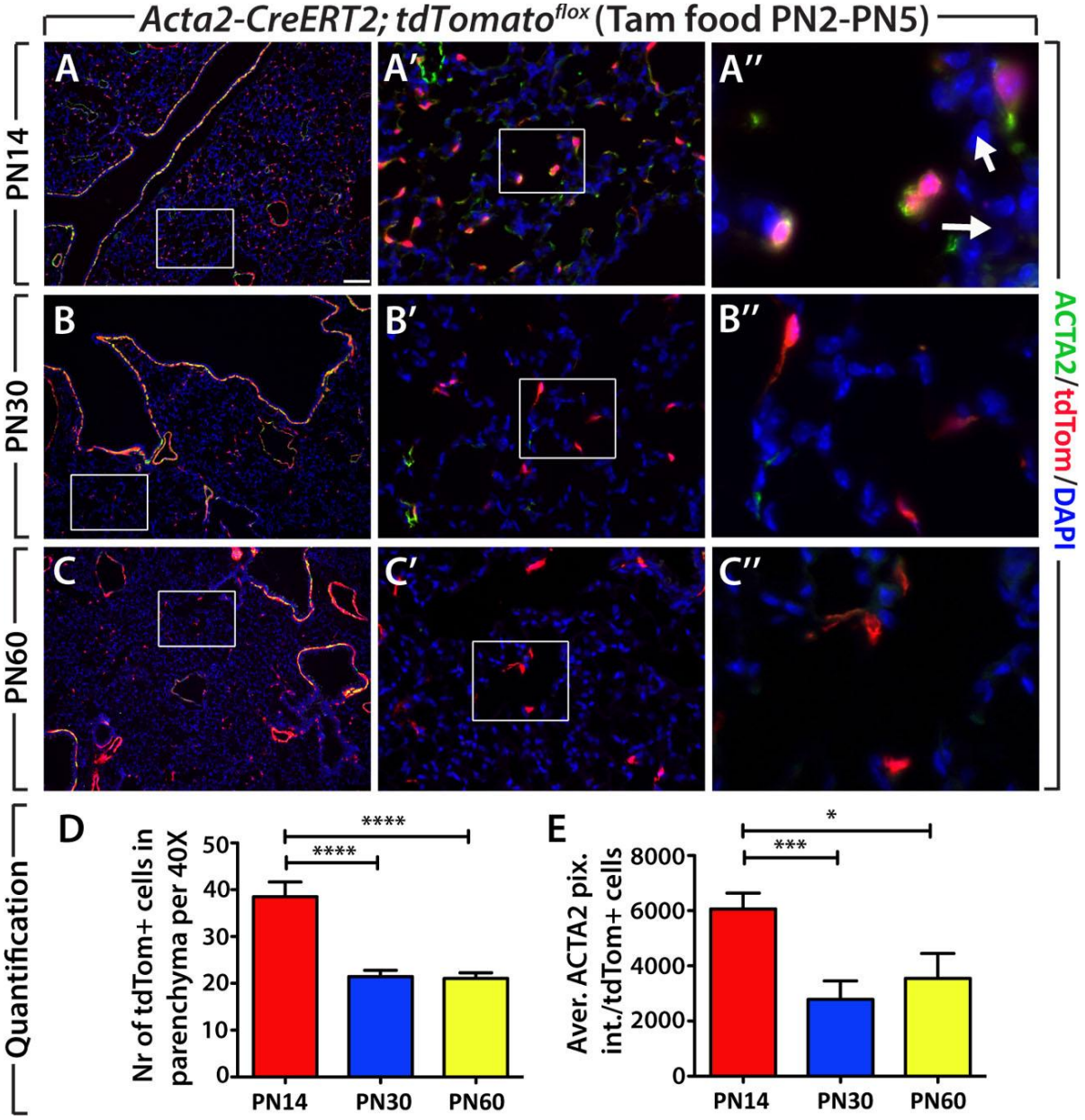

Figure 18: $ACTA2^{+}$ alveolar MYFs labeled at PN2-PN5 are present in lung at PN30 and PN60 but with less number and lower ACTA2 expression than at

PN14. (A-C) Immunofluorescence for ACTA2 (green) in lungs of *Acta2-CreERT2; tdTomato^{flox}* labeled at PN2-PN5 and sacrificed at (A) PN14, (B) PN30 and (C) PN60 showing the presence of tdTomato^{+} cells in parenchyma, but with lower number and lower ACTA2 expression. A'- higher magnification shown in A, A''- higher magnification shown in A'. (D) Quantification of tdTomato^{+} cells in parenchyma. (E) Quantification of ACTA2 signal intensity in tdTomato^{+} cells. PN2 – postnatal day 2, Tam – tamoxifen, aver. – average, pix. – pixel, int. - intensity, tdTom - tdTomato. N = 3 for all experiments. Scale bar: 100 μm in A, 25 μm in B, 7 μm in C. * P<0.05, *** P<0.001, **** P<0.0001.

4.2. PART II. Origin and fate of activated MYFs in bleomycin-induced lung fibrosis

4.2.1. Pre-existing SMCs do not give rise to activated MYFs in bleomycin induced lung fibrosis

In some diseases pre-existing SMCs were shown to give rise to pathological remodeled structures. It was shown that in hypoxia-induced pulmonary hypertension SMCs in the remodeled vessels originate from pre-existing SMCs (Sheikh et al., 2014). In our work we were interested to investigate whether pre-existing ASMCs and VSMCs give rise to activated MYFs in lung fibrosis. Using *Acta2-CreERT2; tdTomato^{flox}* mice pre-existing SMCs were labeled before they were treated either with saline or bleomycin to induce lung fibrosis (Fig. 20A,C). Before the intratracheal installation of bleomycin, mice were fed tamoxifen-containing food for two weeks following two weeks of feeding with normal food to ensure enough time for tamoxifen clearance (Fig. 20C). The peak of fibrosis is happening at day 14 after bleomycin treatment, at this time point the number of fibroblasts and severity of fibrosis are usually the highest. At day 14 after bleomycin treatment lung fibrosis was confirmed using forced oscillation plethysmography, which revealed decreased lung compliance in bleomycin-treated mice in comparison to saline-treated mice, hematoxylin and eosin (H&E) staining also confirmed the presence of fibrotic tissue in the lung (Fig. 19).

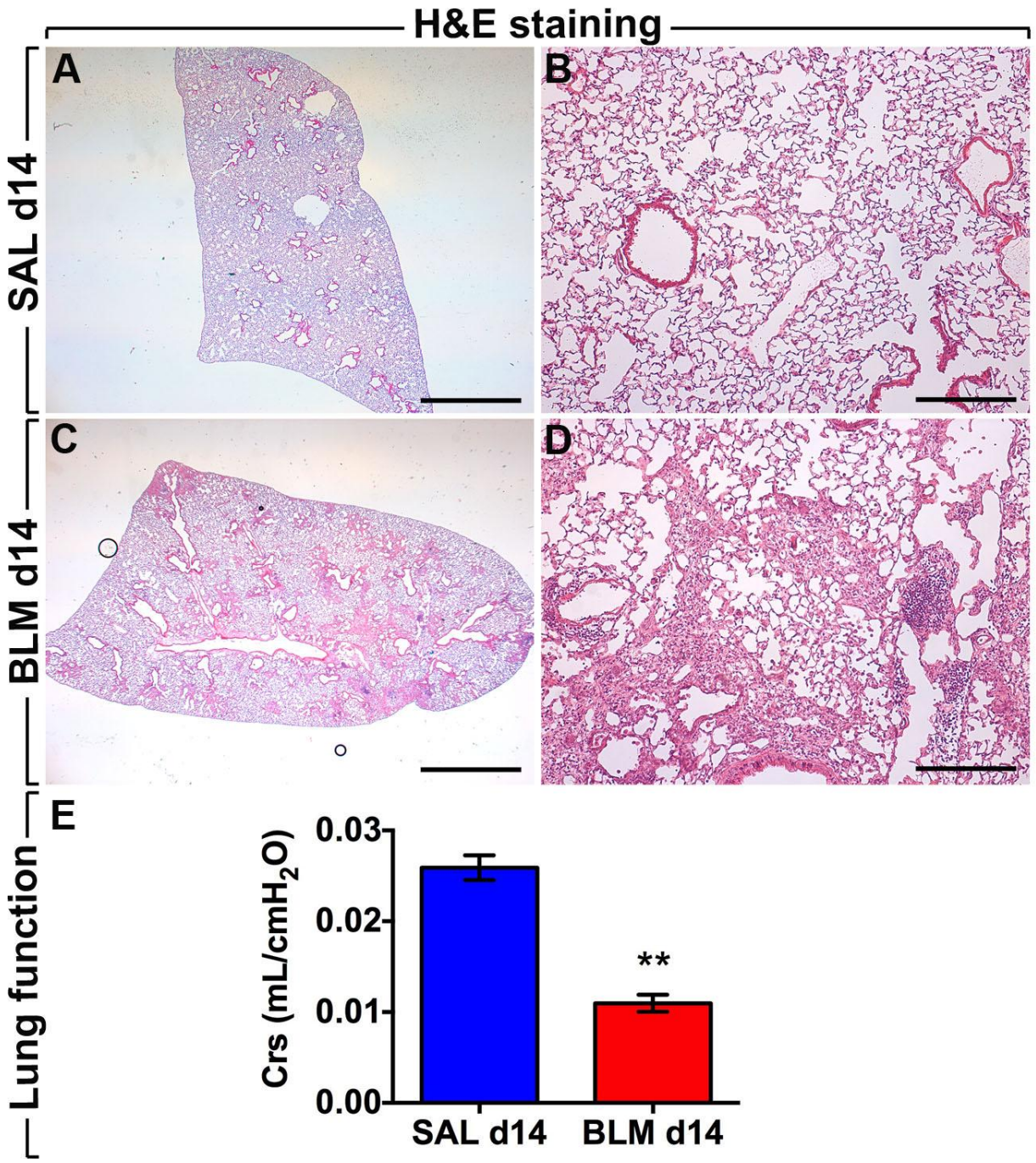

Figure 19: Fibrosis validation in *Acta2-CreERT2; tdTomato^{flox}* mice at day 14 after saline or bleomycin treatment. (A) H&E staining of saline treated lungs at day 14 after the treatment. A higher magnification is show in (B). **(C)** H&E staining of bleomycin treated lungs (3.5 U/kg) at day 14 after the treatment. A higher magnification is show in (D). **(E)** Lung function measurement demonstrating decreased compliance in bleomycin treated group in comparison to control group. BLM – bleomycin, SAL – saline, Crs - compliance. N = 4 for SAL, N = 7 for BLM. Scale bar: 2 mm in A and C, 200 µm in B and D. ** *P*<0.01. (El Agha et al., 2017)

Lungs from day 14 after bleomycin treatment were immunostained for ACTA2 (a marker for SMCs and activated MYFs). Efficiency of the labeling of $ACTA2^+$ cells using *Acta2-CreERT2; tdTomato^{flox}* was 83.5% in saline treated lungs (Fig. 20I). The pre-existing ASMCs and VSMCs were found to express the lineage label tdTomato in both saline (Fig. 20B) and bleomycin-treated groups (Fig. 20D). A different result was observed for activated MYFs. $ACTA2^+$ activated MYFs located in dense fibrotic areas did not express the lineage label tdTomato in bleomycin-treated lungs (Fig. 20E). This result suggests that pre-existing SMCs do not give rise to activated MYFs in lung fibrosis. FACS-based quantification supported the histological observation showing the increase in the number of ACTA2+ cells in bleomycin-treated lungs (1.8% out of total lung suspension), compared to saline-treated lungs (0.6%) (Fig. 20F). There was no significant change in number of lineage-labeled $tdTomato^+$ cells between two groups, showing that pre-existing SMCs do not significantly amplify after bleomycin treatment (Fig. 20G), and lineage-labeled $tdTomato^+$ cells were mostly $ACTA2^+$ (81.6-92.2%) (Fig. 20H). However, while 83% of $ACTA2^+$ cells (SMCs) were lineage-labeled (tdTomato+) in the saline-treated group, only 52.7% of $ACTA2^+$ cells (SMCs and activated MYFs) were lineage-labeled in the bleomycin-treated group (Fig. 20I), showing that activated MYFs do not originate from pre-existing $ACTA2^+$ cells (SMCs).

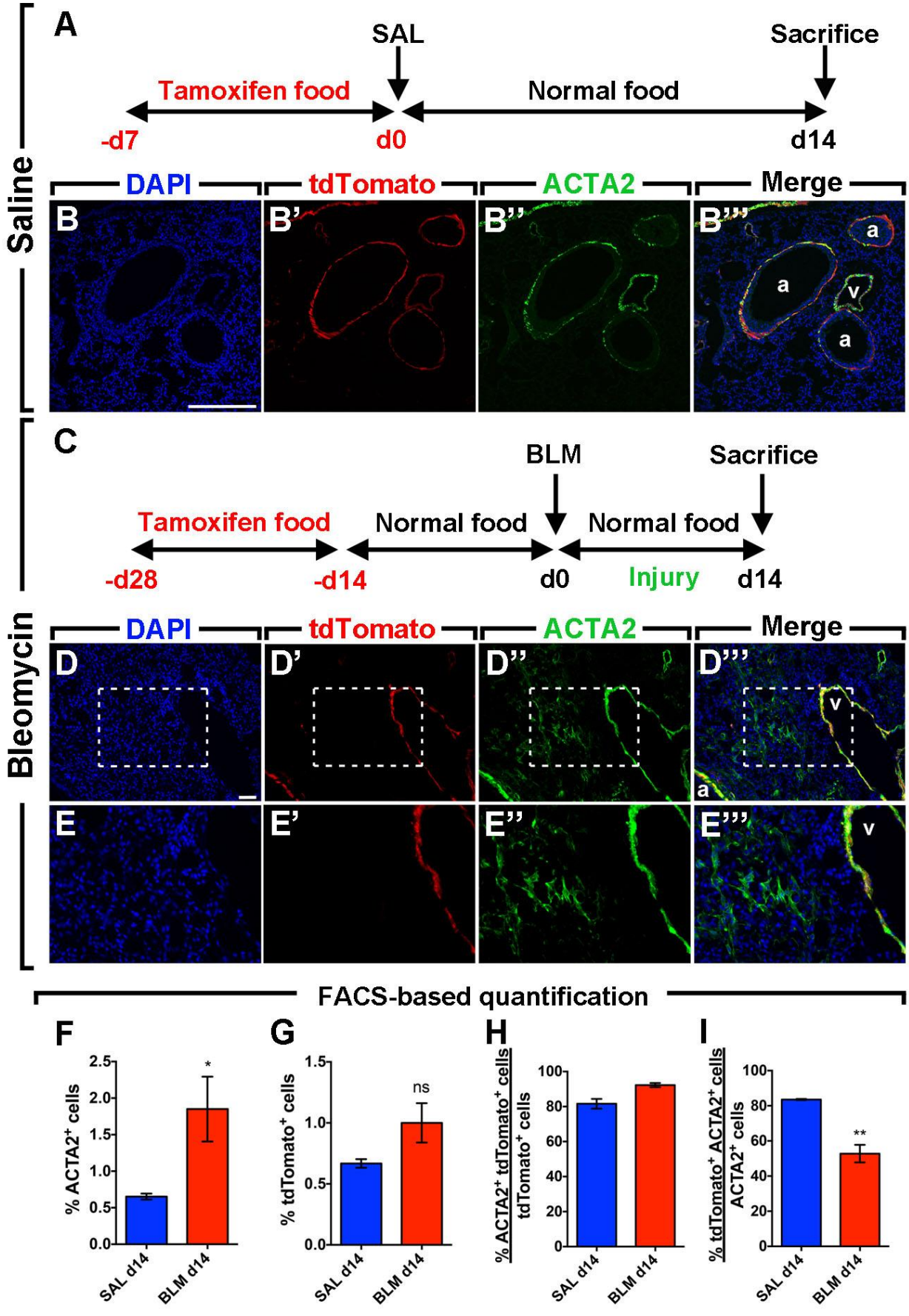

Figure 20: Labeled pre-existing SMCs do not give rise to activated MYFs in lung fibrosis in *Acta2-CreERT2; tdTomato^{flox}* mice. (A) Schematic timeline of

tamoxifen and saline treatment. Mice received tamoxifen-containing food before saline was administered intra-tracheally. Lungs were harvested at day 14 after saline treatment **(B)** Immunofluorescence for ACTA2 in lungs treated with saline. DAPI, tdTomato and ACTA2 single channels are shown in addition to merged image. **(C)** Schematic timeline of tamoxifen and bleomycin treatment. Mice received tamoxifen-containing food before bleomycin was administered intra-tracheally. Lungs were harvested at day 14 after saline treatment. **(D-E)** Immunofluorescence for ACTA2 in lungs treated with bleomycin. DAPI, tdTomato and ACTA2 single channels are shown in addition to merged image. High magnification images of the boxes in (D) are shown in (E). **(F-I)** FACS-based quantification of $ACTA2^+$ and $tdTomato^+$ populations in saline and bleomycin treated lungs at day 14 after treatment. BLM – bleomycin, SAL – saline, a – airway, v – vessel, ns – not significant. N = 4 for SAL, N = 6 for BLM. Scale bar: 250 μm in B and D, 50 μm in E. *P<0.05, ** *P*<0.01. (El Agha et al., 2017)

4.2.2. Activated MYFs persist in the lung after fibrosis resolution and lose ACTA2 expression

Since activated MYFs express ACTA2 it is possible to label and lineage-trace them using *Acta2-CreERT2; tdTomato^{flox}* mouse line. To validate this, *Acta2-CreERT2; tdTomato^{flox}* mice were treated with bleomycin and then fed tamoxifen-containing food between day 5 and 14 after bleomycin treatment (Fig. 21A). At day 14 lungs were harvested and stained for ACTA2. Activated MYFs were labeled as demonstrated by co-localization of the ACTA2 and the tdTomato lineage label in fibrotic areas of bleomycin-treated lungs (Fig. 21B). Quantification of the immunofluorescence showed that 79.2% of lineage-labeled $tdTomato^+$ cells were $ACTA2^+$ at day 14 after bleomycin treatment (Fig. 21C). Such quantification was challenging since ACTA2 is not uniformly expressed in fibrotic regions and it was not easy to detect cell boundaries and co-localize nuclear and cytoplasmic tdTomato signal with cytoskeletal ACTA2. To strengthen these data, FACS-based quantification was made and results showed that labeling efficiency of SMCs and activated MYFs was 93.2% at day 14 after bleomycin treatment (Fig. 21M). FACS-based quantification also revealed that 92.2% of lineage-labeled $tdTomato^+$ cells

were ACTA2^{+} at day 14 after bleomycin treatment (Fig. 21L) (compared to 79.2% based on quantification of immunofluorescence).

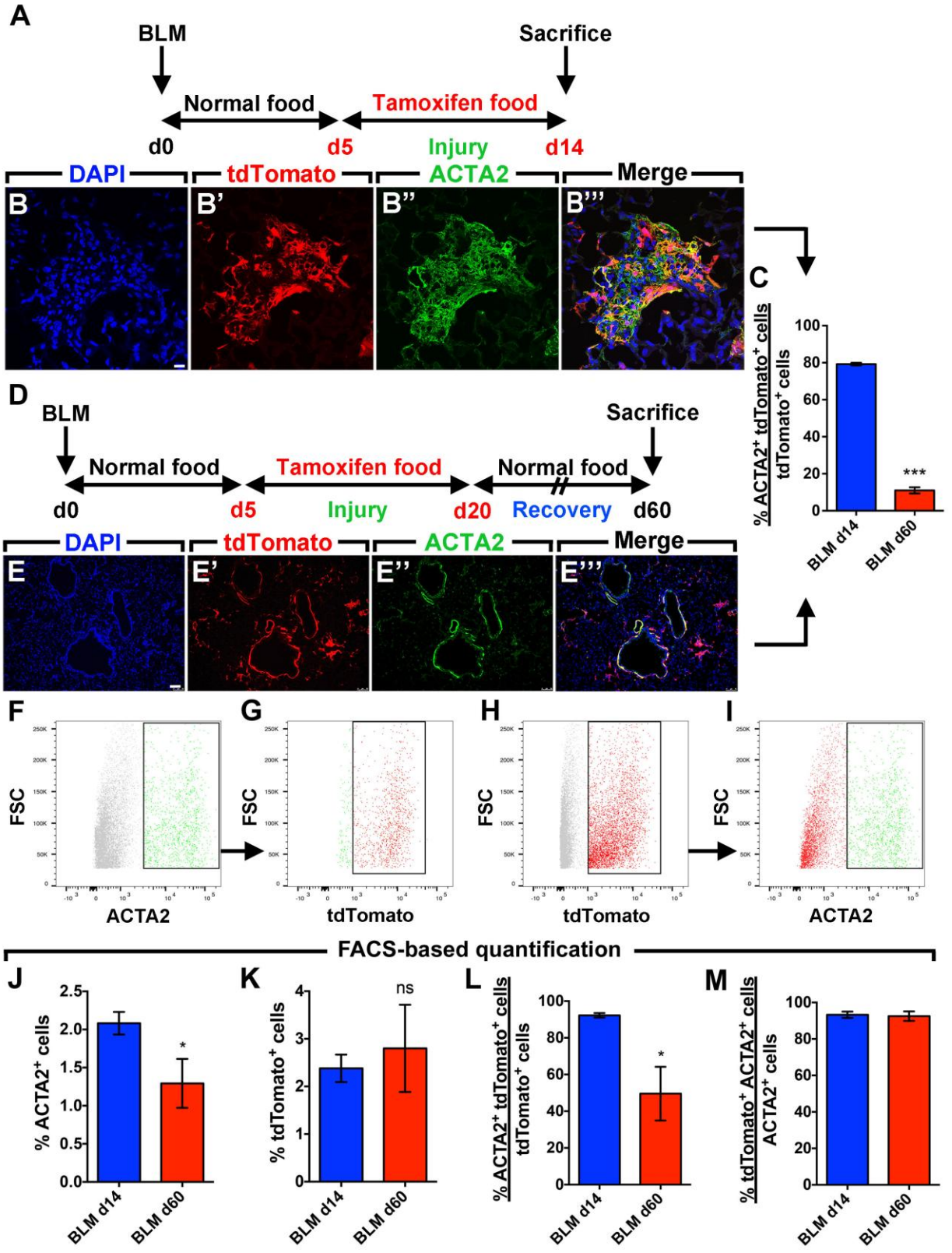

Figure 21: Labeled activated MYFs lose their myogenic phenotype during resolution of fibrosis. (A) Schematic timeline of bleomycin and tamoxifen treatment. Mice were treated with bleomycin and then received tamoxifen-containing

food between day 5 and 14 after bleomycin treatment. Lungs were harvested at day 14 after bleomycin treatment. **(B)** Immunofluorescence for ACTA2 in lungs at day 14 after bleomycin treatment. DAPI, tdTomato and ACTA2 single channels are shown in addition to merged image. **(C)** Quantification of the immunofluorescence shown in B and E. **(D)** Schematic timeline of bleomycin and tamoxifen treatment. Mice were treated with bleomycin and then received tamoxifen-containing food between day 5 and 20 after bleomycin treatment. Lungs were harvested at day 60 after bleomycin treatment. **(E)** Immunofluorescence for ACTA2 in lungs at day 60 after bleomycin treatment. DAPI, tdTomato and ACTA2 single channels are shown in addition to merged image. **(F-I)** Gating strategy for FACS-based quantification of $ACTA2^+$ and $tdTomato^+$ cell populations. **(J-M)** FACS-based quantification of $ACTA2^+$ and $tdTomato^+$ cell populations in lung suspensions at day 14 and 60 after bleomycin treatment. BLM – bleomycin, FSC – forward scatter. N = 6-8 for BLM d14, N = 3 for BLM d60. Scale bar: 10 μm in B, 75 μm in E. *P<0.05, *** *P*<0.001. (El Agha et al., 2017)

To investigate the fate of activated MYFs after fibrosis resolution the time point of 60 day after bleomycin treatment was chosen to ensure that lung fibrosis was adequately resolved (Fig. 21D). Resolution of fibrosis was confirmed by lung function measurements and H&E staining (Fig. 22). Interestingly, activated MYF descendants (lineage labeled activated MYFs) were observed in the lung after fibrosis resolution. Immunofluorescent staining and quantification of the immunofluorescent signal showed that only 11% of these cells were $ACTA2^+$ (Fig. 21E,C). FACS-based quantification (Fig. 21F-I) supported histological findings, showing a decrease in the number of $ACTA2^+$ cells at day 60 compared to day 14 (2% vs. 1.2%) after bleomycin treatment (Fig. 21J). The total number of $tdTomato^+$ cells was unchanged between the two time points (2.3%-2.8%) (Fig. 21K), showing that these cells are not cleared from the lung after fibrosis resolution. Interestingly, only 49.6% of these lineage-labeled $tdTomato^+$ cells were $ACTA2^+$ at day 60, in contrast to 92.2% at day 14 after bleomycin treatment (Fig. 21L), indicating that MYF descendants lose *Acta2* expression significantly. The majority of $ACTA2^+$ cells at both day 14 (SMCs and activated MYFs) and day 60 (SMCs and activated MYF descendants) were $tdTomato^+$ (93.2% and 92.5% respectively) (Fig. 21M), demonstrating that our lineage-tracing approach allowed to capture effectively the majority of $ACTA2^+$ cells.

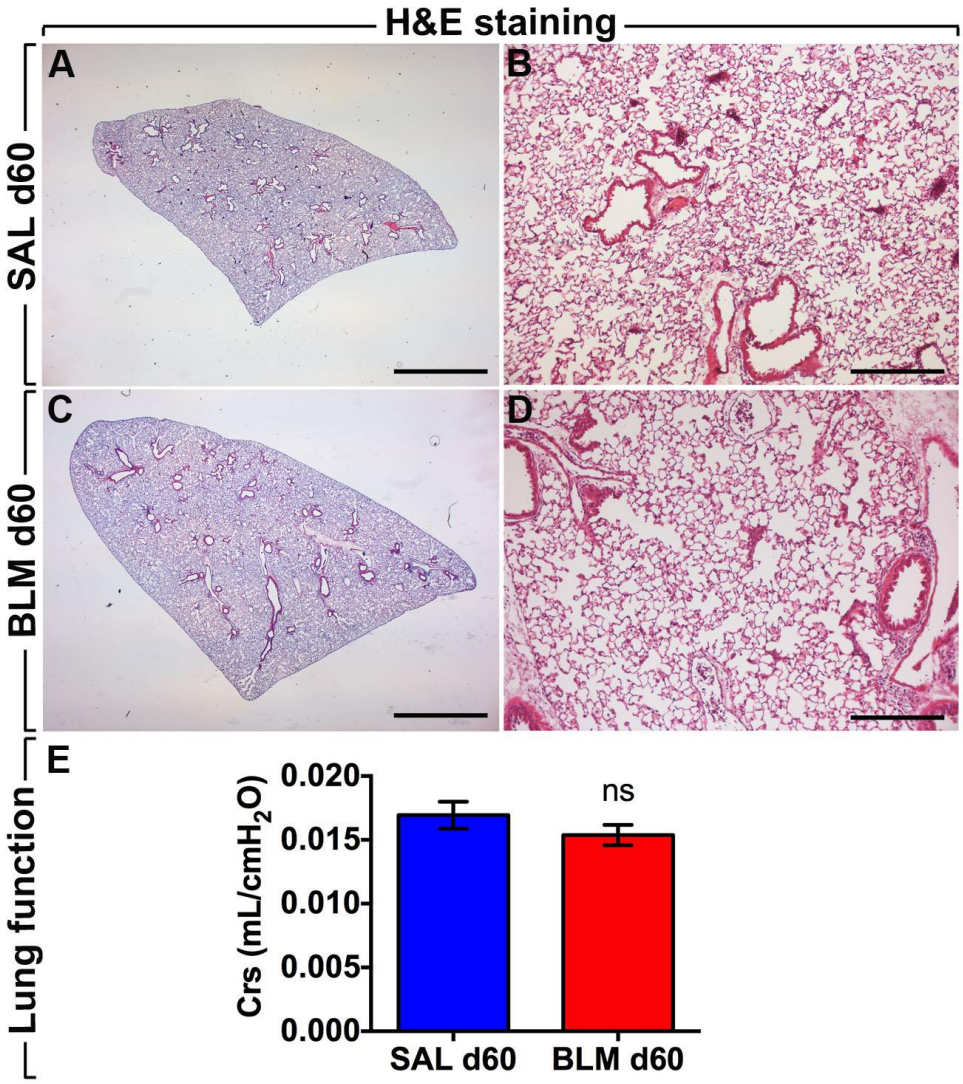

Figure 22: Fibrosis resolution validation in *Acta2-CreERT2; tdTomato^{flox}* mice at day 60 after saline or bleomycin treatment. (A) H&E staining of saline treated lungs at day 60 after the treatment. A higher magnification is show in (B). **(C)** H&E staining of bleomycin treated lungs at day 60 after the treatment. A higher magnification is show in (D). **(E)** Lung function measurement demonstrating no difference in compliance in bleomycin treated group in comparison to control group. BLM – bleomycin, SAL – saline, Crs - compliance. N = 3 for both groups. Scale bar: 2 mm in A and C, 200 µm in B and D. ** *P*<0.01. (El Agha et al., 2017)

4.2.3. Activated MYFs undergo a phenotypic switch after fibrosis resolution

To investigate whether activated MYF transition to lipofibroblast-like phenotype after fibrosis resolution, immunofluorescence for the lipofibroblast marker (ADRP) and AECII marker (SFTPC) was performed. Lineage labeled tdTomato^{+} cells were ADRP^{+} and were found adjacent to SFTPC^{+} cells at day 60 after bleomycin treatment

(Fig. 23A). According to quantification of immunofluorescence out of total tdTomato$^+$ cells 30.5% were ADRP$^+$ at day 60 compared to 15.8% at day 14 after bleomycin treatment (Fig. 23B). Immunofluorescence for collagen revealed the absence of collagen at day 60 compared to day 14 after bleomycin treatment (Fig. 23C,D). Furthermore, activated MYFs (day 14 after bleomycin treatment) and activated MYF descendants (day 60 after bleomycin treatment) were isolated by FACS and gene expression was analyzed by qPCR. The results showed a downregulation of *Acta2* (Fig. 23E) and a significant 4.1-fold upregulation of *Adrp* (Fig. 23F), confirming the histological observations. There was a trend towards increase (1.25-fold) in *Pparg* expression (a key regulator of lipogenesis and lipofibroblast formation), and a 1.75-fold increase in *Fgf10* expression (Fig. 23G,H). To support these observations, FACS-based quantification of the neutral lipid stain (LipidTOX) was performed (Fig. 23I-K). The results showed an increase in the number of LipidTOX$^+$ cells at day 60 (7.7%) compared to day 14 (3.2%) after bleomycin treatment (Fig. 23L). The proportion of lineage-labeled tdTomato$^+$ cells that were stained for LipidTOX was also increased at day 60 (13.3%) compared to day 14 (6.2%) after bleomycin treatment (Fig. 23M).

Additionally, immunofluorescent staining for ADRP revealed that only 1.5% of ASMCs and VSMCs were ADRP$^+$ in saline treated lungs (data not shown), indicating that under homeostatic conditions, SMCs and LIFs are distinct mesenchymal lineages. At day 14 after bleomycin treatment a considerable proportion of lineage-labeled activated MYFs were ADRP$^+$ and LipidTOX$^+$, indicating that LIFs might contribute to the accumulation of activated MYFs during fibrosis progression.

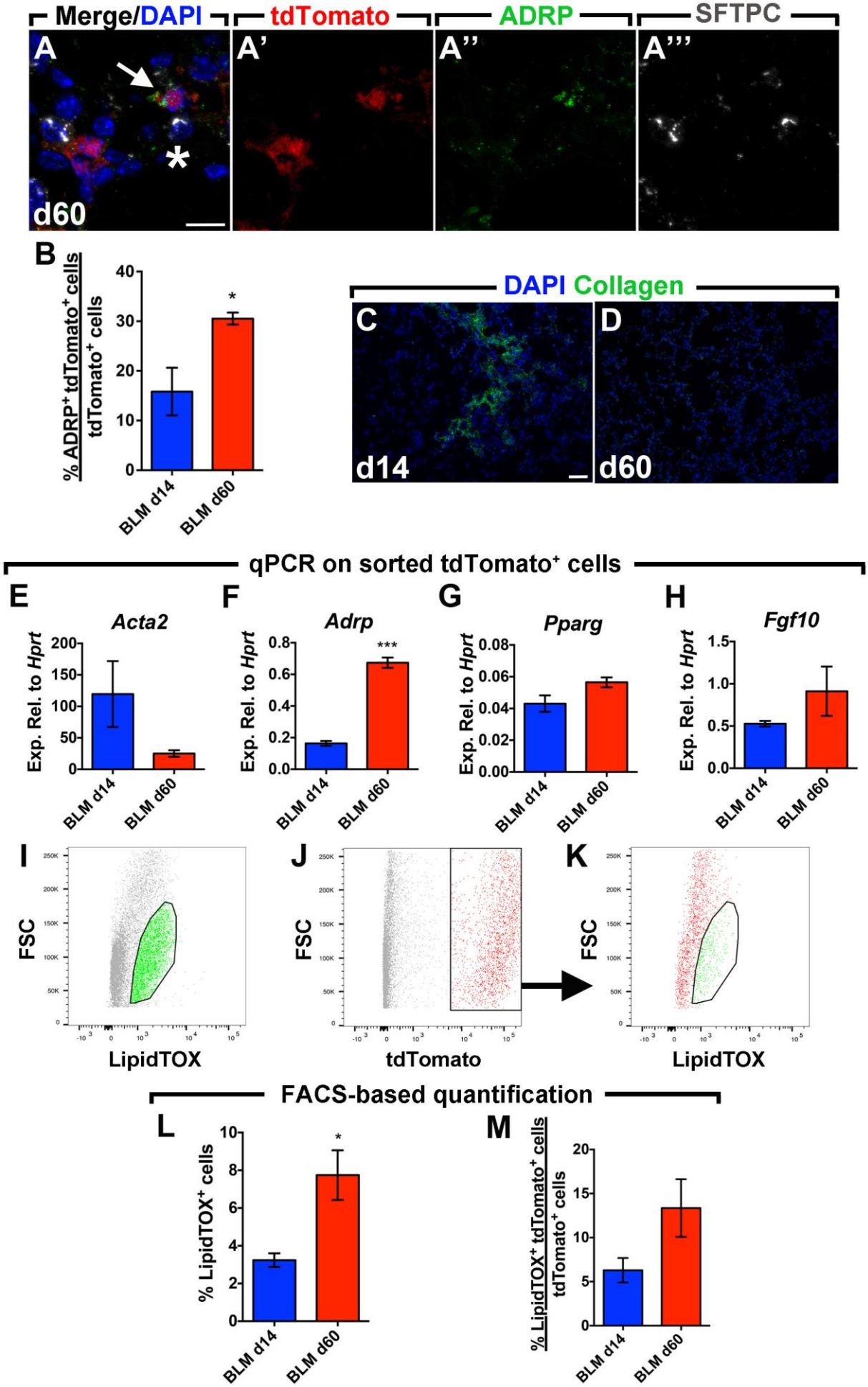
Merge/DAPI
tdTomato
ADRP
SFTPC
A
A'
A''
A'''
d60
B
% ADRP+ tdTomato+ cells / tdTomato+ cells
BLM d14
BLM d60
DAPI Collagen
C
D
d14
d60
qPCR on sorted tdTomato+ cells
E
Acta2
F
Adrp
G
Pparg
H
Fgf10
Exp. Rel. to Hprt
I
J
K
FSC
LipidTOX
tdTomato
FACS-based quantification
L
% LipidTOX+ cells
M
% LipidTOX+ tdTomato+ cells / tdTomato+ cells

Figure 23: Activated MYFs acquire lipofibroblasts characteristics during fibrosis resolution. (A) Immunofluorescence for ADRP and SFTPC in lungs at day 60 after bleomycin treatment. TdTomato, ADRP and SFTPC single channels are shown in addition to merge/DAPI image. The arrow points an ADRP$^+$tdTomato$^+$ cell adjacent to SFTPC$^+$ cell (asterisk). **(B)** Quantification of the immunofluorescence showing increase in ADRP expression in labeled cells at day 60 compared to day 14. **(C,D)** Immunofluorescence for Collagen type I at day 14 and 60 after bleomycin treatment. **(E-H)** qPCR for *Acta2*, *Adrp*, *Pparg* and *Fgf10* on labeled cells sorted from bleomycin treated lung at day 14 and 60 after treatment. **(I-K)** Gating strategy for FACS-based quantification of LipidTOX$^+$ and tdTomato$^+$ cell populations. **(L-M)** FACS-based quantification of LipidTOX$^+$ and tdTomato$^+$ cell populations in lung suspensions at day 14 and 60 after bleomycin treatment. BLM – bleomycin, FSC – forward scatter. N = 3-4 for BLM d14, N = 2-4 for BLM d60. Scale bar: 10 μm in A, 50 μm in C,D. *P<0.05, *** *P*<0.001. (El Agha et al., 2017)

4.2.4. Activated MYFs do not proliferate at peak of fibrosis and do not undergo apoptosis in fibrosis resolution

In order to investigate whether activated MYFs proliferate at day 14 after bleomycin treatment immunofluorescence for Ki67 was performed. There was no co-localization of lineage-traced tdTomato$^+$ cells and Ki67 staining observed, indicating that labeled activated MYFs do not proliferate (Fig. 24A-H).

To test whether activated MYF descendants undergo apoptosis at day 60 after bleomycin treatment TUNEL staining was carried out. There was no sign of co-localization observed between lineage-labeled tdTomato$^+$ activated MYF descendants and TUNEL$^+$ cells indicating the absence of apoptosis in activated MYF descendants.

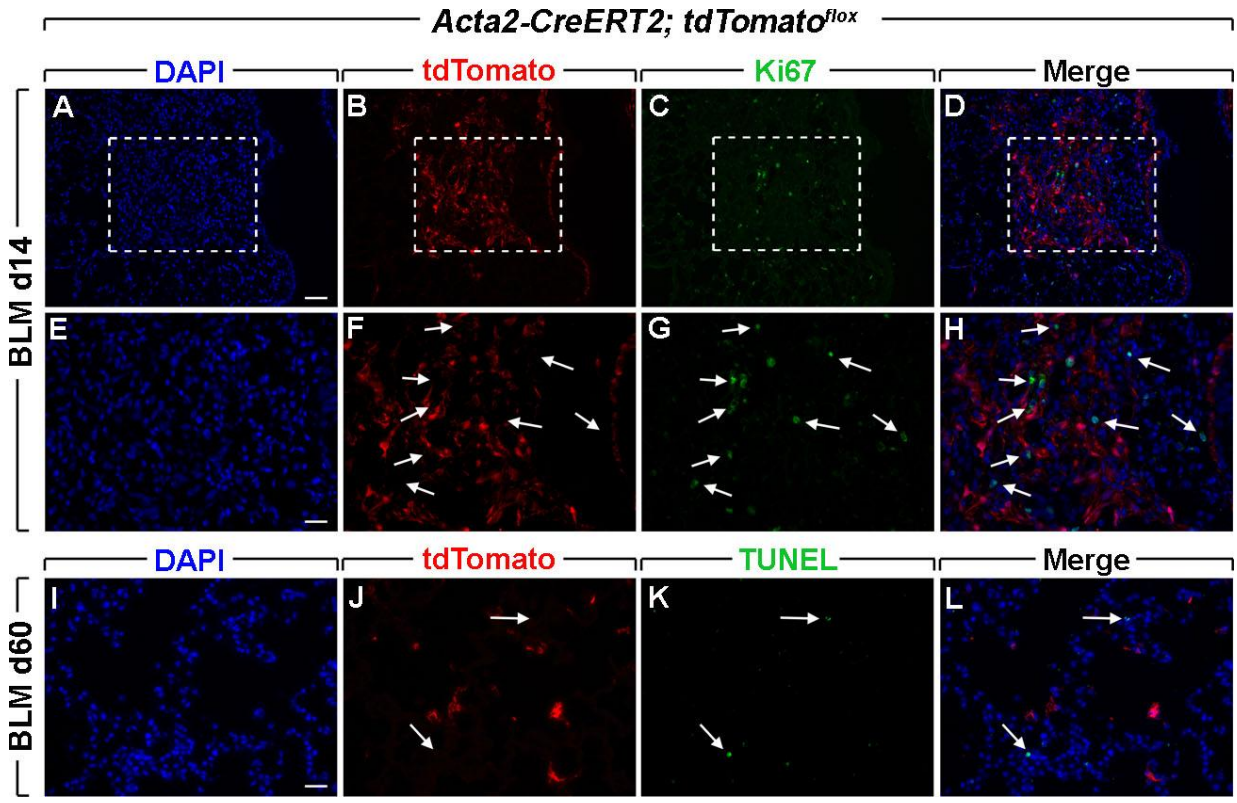

Figure 24: Proliferation and apoptosis in labeled cells of bleomycin treated *Acta2-CreERT2; tdTomato^{flox}* mice at the peak of fibrosis and during resolution phase. (A-D) Immunofluorescence for Ki67 of bleomycin treated lungs at day 14 after the treatment. Single channels DAPI, tdTomato and ACTA2 are shown in addition to merged image. Higher magnifications of images marked in boxes are shown in **(E-H).** White arrows point apoptotic cells. Note the absence of co-localization between tdTomato^{+} and Ki67^{+} cells. **(I-L)** TUNEL staining of bleomycin treated lungs at day 60 after the treatment. White arrows point apoptotic cells. Note the absence of co-localization between tdTomato^{+} and TUNEL^{+} cells. BLM – bleomycin. N = 3 for BLM d14, N = 2 for BLM d60. Scale bars: 50 µm in A-D, 25 µm in E-L. (El Agha et al., 2017)

5. Discussion

5.1. Origin of pulmonary SMCs and alveolar MYFs

Our detailed side-by-side analysis of various mesenchymal driver lines allowed labeling of mature SMCs and their progenitors. Using different driver lines the contribution of different mesenchymal lineages to SMC lineage was analyzed (Fig. 25). The minor contributors are mesothelial and sub-mesothelial-mesenchymal lineages, represented by $WT1^+$ and $FGF10^+$ cells. These two lines also show low specificity towards the SMC lineage. The major contributors are the $GLI1^+$ and $AXIN2^+$ lineages that are enriched in the sub-epithelial mesenchyme, where they are targets of epithelium-derived growth factors such as SHH and various WNT ligands. Nevertheless, the $GLI1^+$ and $AXIN2^+$ lineages also show low specificity towards the SMC lineage during embryonic development. However, the $GLI1^+$ lineage shows both high contribution and high specificity to the SMC lineage during the alveolar stage of postnatal lung development. In particular, our results confirm the previous finding that this driver line is useful to target alveolar MYFs at this stage (Li et al., 2015).

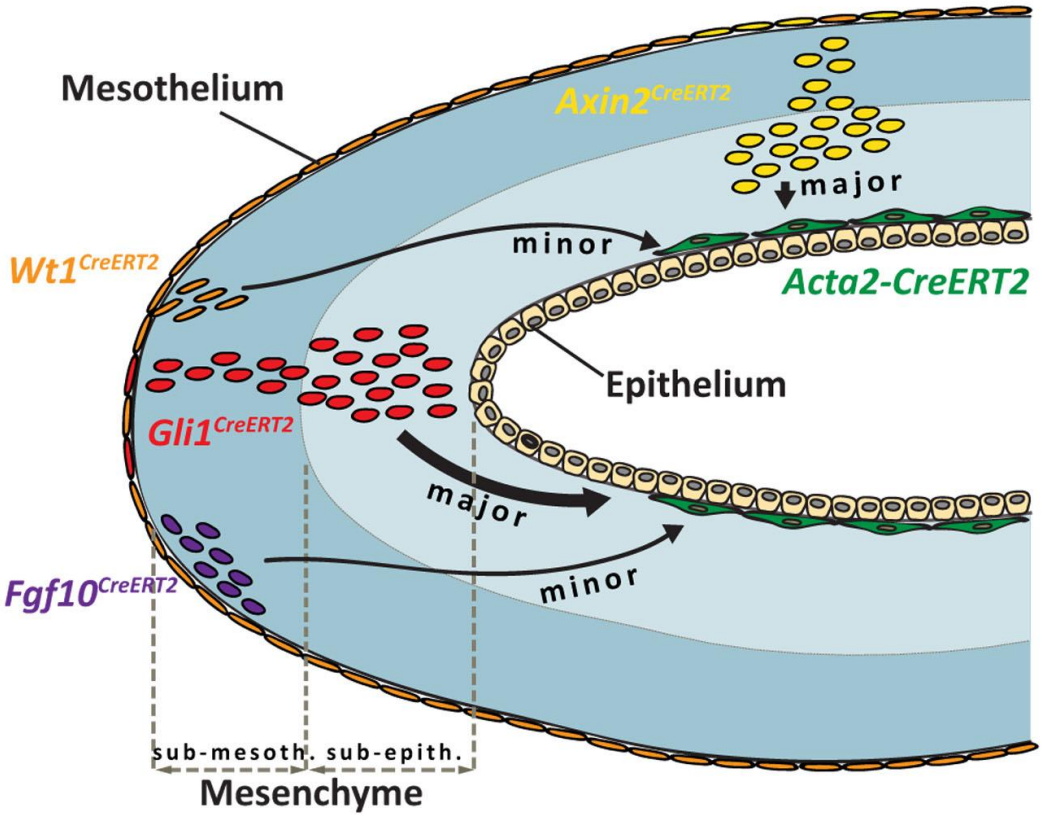

Figure 25: Model summarizing the impact of different progenitor populations on the SMC lineage. Mesothelial WT1$^+$ and FGF10$^+$ cells that can be labeled using *Wt1^{CreERT2}*, *Fgf10^{CreERT2}* contribute in a minor way to the SMC lineage, while GLI1$^+$ and AXIN2$^+$ cells that can be labeled using *Gli1^{CreERT2}* and *Axin2^{CreERT2}* contribute massively to the SMC lineage. Sub-mesoth. – sub-mesothelial, sub-epith. – sub-epithelial. (Moiseenko et al., 2017, Stem Cells, manuscript accepted for publication)

As expected, the *Acta2-CreERT2* line showed high specificity to the ASMC and VSMC lineages. A single IP injection of tamoxifen at E15.5 led to 91±5% labeling of all SMCs in the lung at E18.5 (Fig. 13N,O). This line also allows labeling the absolute majority of SMCs in the adult lung (El Agha et al., 2017). One of the questions that we tried to answer was whether pre-existing ACTA2$^+$ cells at early lung development serve as progenitors for future SMCs that progressively appear as the epithelial tubes undergo iterative branching. Our data revealed that E11.5 ACTA2$^+$ cells and their descendants settled in the proximal regions of the lung at E18.5, whereas E15.5 ACTA2$^+$ cells and their descendants populated both the proximal and distal regions at E18.5. Therefore, we conclude that the *Acta2-CreERT2* line mostly targets differentiated ASMCs and VSMCs, but not their progenitors. One of the novel findings of this work is that the *Acta2-CreERT2* line also labels ACTA2^{low} parenchymal cells at E18.5. In addition, we provide evidence that these cells are likely progenitors for ACTA2$^+$ ELN$^+$ alveolar MYFs that are located at the tips of secondary septa at PN14. No evidence for proliferation was observed in these cells at E18.5 or PN14 (Fig. 17). Moreover, when labeling at E15.5, we found similar numbers of tdTomato$^+$ cells in the lung parenchyma at E18.5 and PN14, demonstrating limited expansion and lack of proliferation in these cells. These results confirm that ACTA2 is a marker for differentiated smooth muscle cells as previously described (Fatigati and Murphy, 1984; Owens et al., 2004) and also demonstrate that late progenitors/early differentiated alveolar MYFs are generally ACTA2^{low} compared to *bona fide* SMCs.

The presence of ACTA2^{low} cells was also shown using 3D-reconstruction of a thick vibratome section of a wild type lung immunostained for ACTA2 (Fig. 26) The staining clearly showed the presence of ACTA2^{high} cells that are located at ASMC and VSMC regions and also ACTA2^{low} cells located in parenchyma. These ACTA2^{low} cells are likely progenitors for alveolar MYFs.

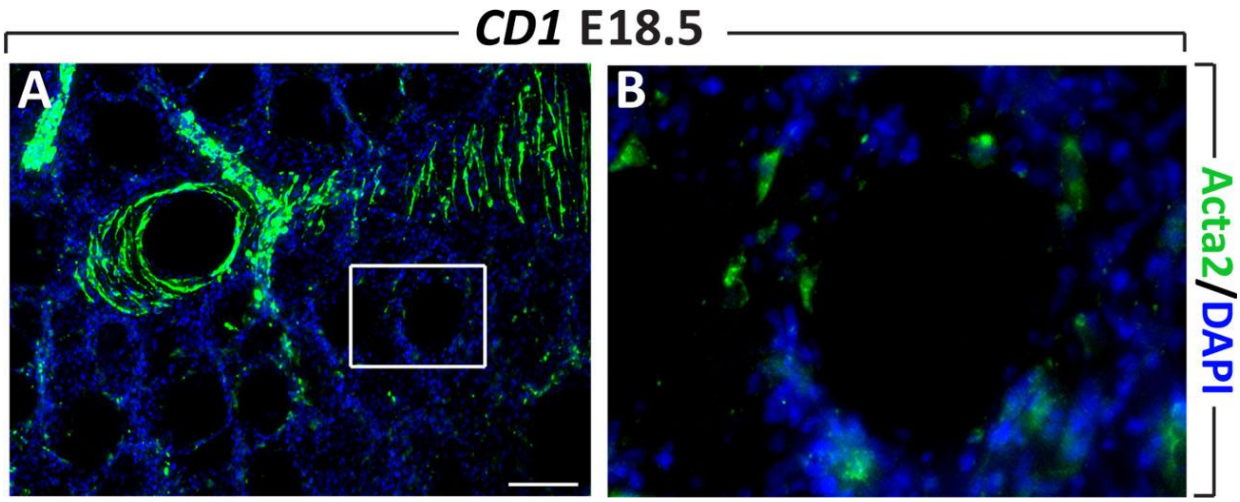

Figure 26: ACTA2^{high} and ACTA2^{low} populations in the wild type lung. (A-B) Immunofluorescence for ACTA2 of the thick (100 µm) sections of CD1 mouse lungs. Higher magnification of image marked in box is shown in **(B).** Note that intensity of ACTA2-signal is much higher in airway and vascular SMCs than in parenchymal cells. N = 3. Scale bars: 75 µm in A, 15 µm in B.

To analyze the gene array results, the “LungGENS” web tool was used. According to the “LungGENS” (Du et al., 2015), that compiles mRNA signatures of single cells isolated from the entire embryonic mouse lung at different stages, there are two types of fibroblasts observed at E18.5 – the Myofibroblast (MyoF) and the Matrix fibroblast (MFB). MyoFs were identified by the expression of genes involved in actin binding and smooth muscle contraction, and the signature genes included hedgehog-interacting protein *(Hhip)*, *Acta2*, gamma 2 smooth muscle actin (*Actg2)*, myosin heavy polypeptide 11 (*Myh11)* and transgelin (*Tagln)*. MFBs express genes associated with extracellular matrix and cell adhesion, and the signature genes included fibronectin (*Fn1)*, *Eln*, vascular cell adhesion molecule (*Vcam)* and *Fgf10*. Another powerful characteristic of LungGENS is that the expression level of a given gene can be assessed and compared among different cell types. We found that in our conditions, alveolar MYF progenitors resemble the MFB group, but with higher specificity - most of the signature genes for the MFB were even more enriched in alveolar MYF progenitors vs. SMCs. For example, *Eln* expression in MFBs is around 2.5 fold higher than in MyoFs (375 vs. 139), which is quite surprising for a gene that appears to be expressed specifically in alveolar MYFs. In our case, it was 400 fold higher in alveolar MYF progenitors than in SMCs according to qPCR data (Fig. 15B). *Pdgfra* is upregulated by 7 fold in MyoFs compared to MFBs (102 vs.15), while

according to our data, this gene was upregulated by 70 fold according to qPCR analysis and 93 fold according to gene arrays in alveolar MYF progenitors compared to SMCs. SMCs in our conditions resemble MyoF from LungGENS. Interestingly, some feature genes of MyoF, for example *Hhip*, were highly upregulated in alveolar MYF progenitors. This suggests that the cell type called “MyoF” in LungGENS likely contains different subpopulations, such as SMCs and alveolar MYF progenitors. These results underscore the difficulty to assign specific cell types to a given transcriptomic signature obtained from single cell experiments, especially when the single cell data were obtained by systematically analyzing all the cells, without introducing a specific filter such as lineage-labeled cells. In the future, single-cell transcriptomics with the *Acta2-CreERT2* line will be a powerful tool to distinguish between the different subpopulations of SMCs.

The role of SHH in the formation of SMCs has already been proposed. SHH knockout lungs fail to undergo normal branching morphogenesis (Pepicelli et al., 1998). Importantly, ACTA2+ cells are completely absent in SHH knockout lungs. ACTA2+ alveolar MYFs play a key role in alveolar formation. Interruption of alveologenesis is a hallmark of diseases like BPD in premature born infants and COPD in adult lungs. Both alveolar defects lead to high morbidity and mortality. Hyperoxia-induced lung injury, a model of BPD, causes up-regulation of SHH and it’s downstream target PTCH1 and thickening of alveolar walls (Dang et al., 2012), suggesting that SHH play a role in postnatal lung pathology. A recent study has shown that GLI1^{+} cells labeled at E10.5 give rise to alveolar MYFs at PN14 (Li et al., 2015). In our experimental conditions, we observed that HH activation also marks alveolar MYF progenitors, postnatally. The observation that the *Gli1*^{CreERT2} driver allows labeling more alveolar MYFs at PN14 when labeled between PN2-PN14 rather than between PN2-PN5, suggests that not all the alveolar MYF progenitors are GLI1^{+} at PN2-PN5. There is likely another pool of progenitors that gradually acquires *Gli1* expression later during alveologenesis. The data suggest that there is a progressive increase in hedgehog signaling as alveologenesis proceeds, and this correlates with increased alveolar MYFs formation. Interestingly, it has been shown that *Shh* is expressed much higher at E14.5 in comparison to E18.5 (Li et al., 2015). That means that there might be at least two time periods during lung development when SHH is activated – first during early lung development between E10.5-E14.5 and second postnatally during the onset of alveolarization at P0 till peak of

alveolarization P15 and is undetectable at P24 (end of alveolarization) (Miller et al., 2001).

WNT signaling is also involved in SMC formation during embryonic development. It plays a critical role in proliferation, migration and differentiation of SMC progenitor cells (Cohen et al., 2009; Kumar et al., 2014; Mailleux et al., 2005). In our study, overall WNT signaling was activated in alveolar MYF progenitors but not in differentiated SMCs. This again underlines the importance of WNT signaling for $ACTA2^+$ precursors, but not mature SMCs. It would be interesting to find the status of WNT signaling in mature differentiated $ACTA2^+$ MYF. *Axin2* was also upregulated in alveolar MYF progenitors, but not in SMCs. $AXIN2^+$ cells, labeled at E11.5, contributed to the ASMC and VSMC lineages. In differentiated SMCs, *Axin2* expression appears downregulated, suggesting downregulation of WNT signaling in differentiated vs. progenitor SMC. *Wnt5a* was one of the highest upregulated genes in alveolar MYF progenitors. It has already been shown that deletion of *Wnt5a* leads to increased proliferation of the mesenchyme and dysregulated lung maturation (Li et al., 2002). In the lungs of asthma and COPD patients, WNT5A, activated by TGFβ-signaling, promotes excessive SMC proliferation (Kumawat et al., 2013). Recently, it has been shown that in the lungs of COPD patients up-regulated *Wnt5a* attenuated alveolar epithelial cell wound healing and transdifferentiation. Overexpression of *Wnt5a* exacerbated airspace enlargement and inhibition of *Wnt5a* improved lung function and attenuated lung tissue destruction (Baarsma et al., 2017).

Using the *Acta2-CreERT2* line, we found that in addition to WNT and SHH signaling pathways, FGF signaling was also activated at E18.5 in alveolar MYF progenitors compared to SMCs. FGF signaling, particularly FGF10, is known to be important for alveolar MYF formation, and *Fgf10* hypomorphic lungs are characterized by the absence of alveolar MYFs (Ramasamy et al., 2007). Interestingly, alveolar MYFs have never been described as a potential source of FGF10 in the developing lung.

In the future, it will be important to analyze the transcriptome of $ACTA2^+$ cells labeled at E15.5 and examined at E18.5, PN14, PN30 and PN60. This approach should enable the identification of the genes and pathways important for alveolar MYF differentiation and dedifferentiation.

5.2. Origin and fate of activated MYFs in bleomycin-induced lung fibrosis

Currently there are only few treatments against IPF. The IPF patients are mostly at the end stage of fibrosis when being diagnosed, making the investigation of the mechanisms underlying the onset of disease and tissue remodeling difficult. Using mouse models of lung fibrosis, it is possible to understand better the processes of the initial formation of lung fibrosis, for example to identify possible sources of activated MYFs in IPF; as well as further investigate the resolution phase.

The main feature of IPF is the accumulation of ECM-secreting activated myofibroblasts, that accumulate in fibrotic regions and lead to tissue scarring. For a long time researchers have been trying to identify the cell types that give rise to activated MYFs in order to interfere with the process of their formation.

The hypothesis that activated MYFs can originate from pre-existing SMCs was based on a study where remodeled excessive VSMCs in hypoxia model of pulmonary hypertension (PH) in mice originated from pre-existing SMCs (Sheikh et al., 2014). However in our work lineage-labeled pre-existing SMCs were not found in the fibrotic areas and did not contribute to fibrosis. Thus, activated MYFs in lung fibrosis do not originate from pre-existing SMCs and rather have other ACTA2$^-$ sources.

One of the potential source for activated MYFs are Gli1$^+$ cells, since SHH has been shown to be involved in TGF-β1-induced MYF differentiation (Cigna et al., 2012) and Gli1$^+$ cells were already shown to give rise to activated MYFs (Kramann et al., 2015). In our work we also demonstrate that GLI1$^+$ cells give rise to different ACTA2$^+$ cell populations. Using *Gli1Cre*^{ERT2} line to target GLI1$^+$ cells would be a good instrumental approach to investigate the differentiation and de-differentiation of activated MYFs in bleomycin-induced lung fibrosis from the angle of SHH signaling.

The great advantage of bleomycin-induced mouse model of lung fibrosis is that fibrosis is reversible; mice recover completely, thus giving the opportunity to study regeneration process. Using this reversibility of fibrosis in mice, we aimed to investigate the fate of activated MYFs after fibrosis resolution. One of the observation of our work was that activated MYFs and their descendants are not cleared from the lung, they do not undergo apoptosis and do not disappear, they are still present in

the lung at day 60 after bleomycin injury, when fibrosis is resolved. These findings agree with previously published reports that activated MYFs are not cleared from the tissue during fibrosis resolution but rather de-differentiate (Kosla et al., 2013; Reddy et al., 2014). The de-differentiation of activated MYFs was also proposed in the study where it was shown that differentiation of MYFs is regulated by TGF-β1/ALK5/ MyoD and suppression and de-differentiation of MYFs is driven by mitogens/ERK-MAPK/CDKs (Hecker et al., 2011). Our gene arrays on sorted lineage-traced tdTomato^{+} cells show no significant upregulation of apoptotic markers at day 60 compared to day 14 after bleomycin administration (1.2, 1.6 and 1.3-fold downregulation of caspase 3 (*Casp3*), *Casp6* and *Casp7* respectively at day 60 compared to day 14). No apoptosis in activated MYF descendants at day 60 after bleomycin injury was observed in TUNEL staining of lung sections (Fig. 24).

Another observation was that a subset of these labeled activated MYFs undergoes transition to lipofibroblast-like phenotype after fibrosis resolution. LIFs are lipid-droplet-containing cells that take part in surfactant production by AECII and has been also shown to support AECII clonogenic growth in vitro (Barkauskas et al., 2013; Schultz et al., 2002). LIFs also contain retinoic acids that have been shown to be important for the alveolar septation postnatally (Simon and Mariani, 2007). During late lung development LIFs can be detected in rat lung starting from E16 increasing in number with the peak on the second postnatal week, when alveolarization is at it's peak (Tordet et al., 1981). PPAR pathway that is required for the maintenance of the LIF phenotype, is downstream of parathyroid hormone-related protein (*Pthrp*) signaling (Torday et al., 2003). It has been demonstrated that inactivation of the Pthrp pathway in vivo results in abnormal alveolarization and surfactant synthesis (Rubin et al., 2004). This suggests that LIFs are involved in alveologenesis and septation. During fibrosis resolution the damaged tissues undergo the so-called "de-novo" alveologenesis, where LIFs may play the same important role as during development. This can partly explain the de-differentiation of activated MYF to LIF program.

The transdifferentiation of cells from contractile SMC-like phenotype to adipocyte-like phenotype has already been shown by other investigators. Lipid accumulation in skeletal muscles has been reported in Dysferlin-deficient mice (Grounds et al., 2014). Under special culture conditions, permissive for adipogenesis, skeletal muscle can

transdifferentiate to mature adipocytes via PPAR pathway activation and upregulation of lipogenic markers Pparg and C/ebpa (Hu et al., 1995). Our gene arrays result showed activation of PPARγ signaling pathways in activated MYF descendants at day 60 after bleomycin injury compared to activated MYFs at day 14, indicating that this pathway is involved in the reversal of activated MYFs phenotype to LIF-like phenotype, activating the genes involved in lipogenesis, cholesterol metabolism and adipocyte differentiation (Fig. 27).

PPARγ is the major pathway that orchestrates lipogenic differentiation in adipocyte progenitors (preadipocytes) as well as LIF formation (Rehan and Torday, 2012). Additionally, PPARγ agonists were shown to be protective against fibrosis in mice (Fang et al., 2012; Genovese et al., 2005). A direct transcriptional target for PPARγ adiponectin showed a similar effect in primary culture of skin fibroblasts isolated from scleroderma patients (Fang et al., 2012). The potential use of PPARγ agonists to induce lipogenic differentiation in IPF would be a next important step to investigate.

Interestingly, there have been controversial opinions about whether lipid-containing cells exist in the human lung. A recent study claimed the absence of these cells in the lung (Tahedl et al., 2014), however another study using Oil Red O staining showed that these cells exist in both infant and adult human lungs (Rehan et al., 2006). The discrepancy between the findings can be related to the differences in detection methods (Ahlbrecht and McGowan, 2014).

Although dedifferentiation of MYFs is happening in mouse model of lung fibrosis, this process is not studied in human IPF lungs. It is not yet known whether activated MYFs can dedifferentiate to cell types other than LIFs, this has to be investigated. Generally there is lack of knowledge regarding cellular heterogeneity of human lung mesenchyme. Better understanding of the human mesenchymal cell types and identifying new fibroblastic populations can give rise to new opportunities for IPF treatment.

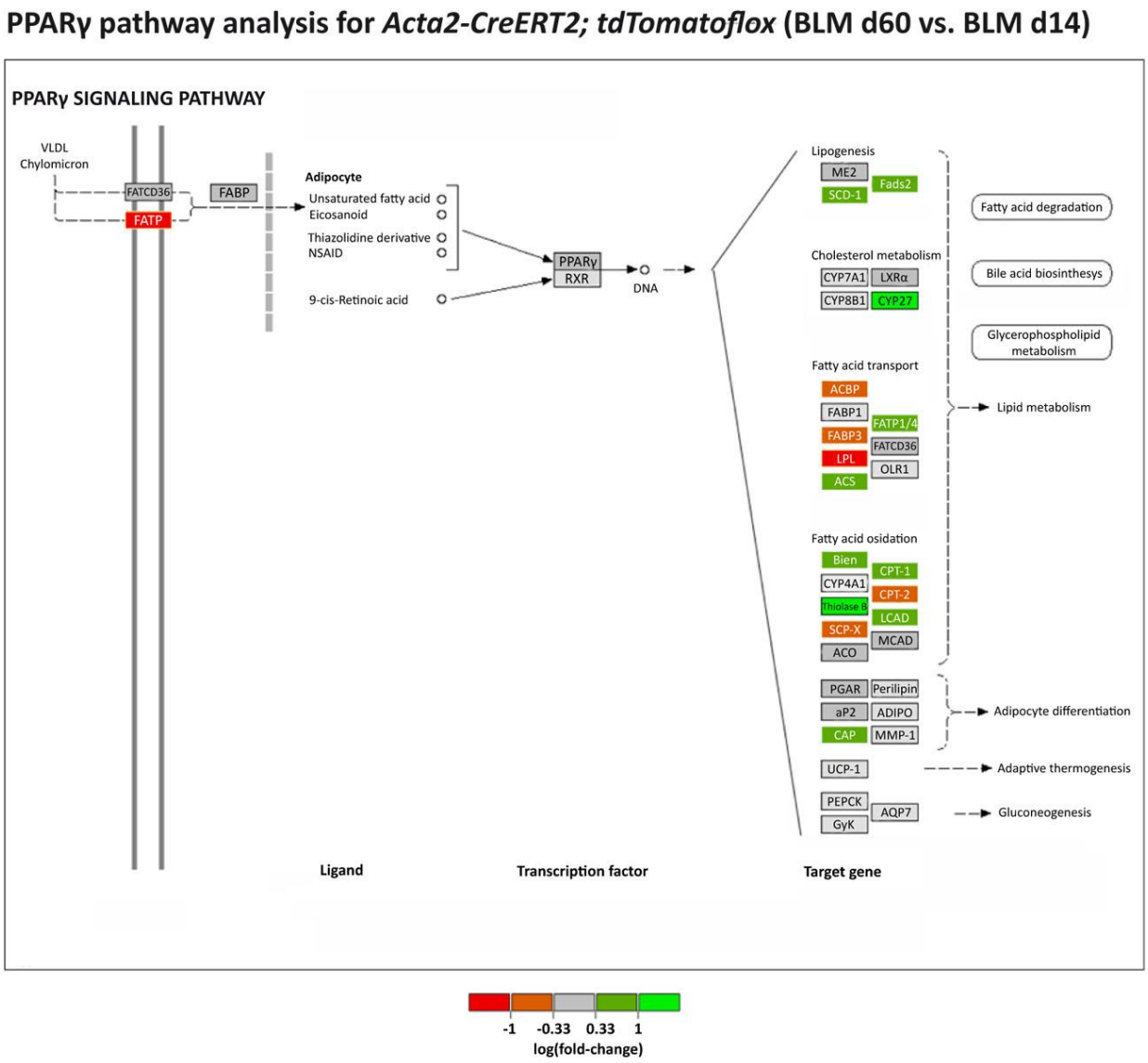

Figure 27: Analysis of PPARγ signaling pathway on lineage labeled cells isolated from *Acta2-CreERT2; tdTomato^{flox}* mice during peak of fibrosis and resolution phase. Gene array analysis performed on sorted tdTomato^{+} cells showing activation of the PPARγ pathway in activated MYF descendants during fibrosis resolution. Green indicates upregulation in BLM d60 group. BLM – bleomycin. N = 3 for BLM d14, N = 2 for BLM d60. (El Agha et al., 2017)

6. Conclusion

The study overall gives more insight into the mechanisms underlying ACTA2$^+$ precursor cells behavior and differentiation as well as offers extensive characterization of mature ACTA2$^+$ cells during lung development and lung injury.

In the first part of the study different progenitor lines were analyzed for their contribution to SMCs lineage. The major contributors were identified – GLI1$^+$ and AXIN2$^+$ cells give rise to majority of SMCs and alveolar MYFs in the embryonic lung, but these progenitor cells are not specific for only SMC lineage, they give rise to other mesenchymal cell types. Using *Acta2-CreERT2* FACS-based isolation of lineage-traced cells followed by gene arrays, we identified transcriptomic signatures for alveolar MYF progenitors versus ASMCs and VSMCs. This new knowledge will allow in the future discriminating between the different subpopulations of ACTA2$^+$ cells. Taken together, our results provide a more balanced view on the origin of the SMCs during embryonic lung development. Our side-by-side driver line analyses will be instrumental to design new experiments addressing the function of signaling pathways in various SMC and SMC-like subpopulations.

The second part of this study gives better understanding of the origin and fate of activated MYFs in lung fibrosis. It was shown that activated MYFs do not originate from pre-existing ACTA2$^+$ cells. In fibrosis resolution a phenotypic switch has been observed – activated MYFs acquire lipogenic program and become LIFs, and that process is dependent on PPARγ signaling. In future, PPARγ agonists should be considered as a potential treatment for IPF patients to switch myogenic phenotype in activated MYFs to lipogenic and induce fibrosis resolution.

7. Summary

Alpha smooth muscle actin (ACTA2)-expression identifies pulmonary airway and vascular SMCs as well as alveolar myofibroblasts (MYFs). These cells are important for normal respiratory function and their dysregulation is associated with disease. Mesenchymal progenitors expressing fibroblast growth factor 10 *(Fgf10)*, Wilm's tumor 1 *(Wt1)* or glioma-associated oncogene 1 *(Gli1)* contribute to SMC formation from early stages of lung development. However, their respective contribution and specificity to the SMC and alveolar MYF lineages remain controversial. In addition, the contribution of mesenchymal cells undergoing WNT signaling remains unknown. Using *Fgf10*^{CreERT2}, *Wt1*^{CreERT2}, *Gli1*^{CreERT2} and *Axin2*^{CreERT2} inducible driver lines in combination with a *tdTomato*^{flox} reporter line, the respective differentiation of each pool of labeled progenitor cells along the SMC and alveolar MYF lineages was quantified. The results revealed that while FGF10^{+} and WT1^{+} cells showed a minor contribution to the SMC lineage, GLI1^{+} and AXIN2^{+} cells significantly contributed to both the SMC and alveolar MYF lineages, but with very limited specificity. Lineage tracing using the *Acta2-CreERT2* transgenic line showed that differentiated airway and vascular SMCs labeled at E11.5 do not expand significantly to give rise to new SMCs at E18.5. However, ACTA2^{+} cells from E15.5 label almost all SMCs in the lung at E18.5, as well as alveolar MYF progenitors in the lung parenchyma. FACS-based isolation of different subpopulations of ACTA2^{+} lineage-traced cells followed by gene arrays, identified transcriptomic signatures for alveolar MYF progenitors versus airway and vascular SMCs at E18.5. Our results establish a new transcriptional landscape for further experiments addressing the function of signaling pathways in the formation of different subpopulations of ACTA2+ cells.

Contractile ACTA2^{+} cells called activated myofibroblasts (MYFs) are the main effector cells in idiopathic pulmonary fibrosis (IPF). IPF is characterized by excessive accumulation of activated MYFs and lung tissue scarring. Currently there is no effective treatment against IPF. Understanding the origin of the activated MYFs is of great interest. Using *Acta2-CreERT2* transgenic line to label pre-existing ACTA2^{+} showed that pre-existing ACTA2^{+} airway and vascular SMCs do not give rise to activated MYF. During resolution of fibrosis, we show that activated MYFs lose

ACTA2 expression and acquire lipofibroblast-like phenotype. Manipulating this phenotypic switch might offer new therapeutic opportunities for IPF patients.

8. Zusammenfassung

Glatte Muskelzellen der Atemwege und Blutgefäße der Lunge sowie Alveolarmyofibroblasten (MYFs) exprimieren Alpha-smooth-muscle-actin (ACTA2). Diese Zellen sind für die normale respiratorische Funktion von wichtiger Bedeutung, weswegen ihre Dysfunktion mit Erkrankungen assoziiert sind. Mesenchymale Progenitorzellen, die Fibroblastenwachstumsfaktor 10 (Fgf10), Wilm´s tumor 1 (Wt1) oder Glioma-assoziiertes Onkogen 1 (Gli1) exprimieren, sind an der Bildung von glatten Muskelzellen ab den frühen Stadien der Lungenentwicklung beteiligt. Allerdings ist diesbezüglich die Spezifität der Progenitorzellen und ihre anteilige Beteiligung an der Bildung der glatten Muskelzelllinien und der Alveolarmyofibroblastenzelllinie noch kontrovers. Weiterhin ist es ungeklärt, ob mesenchymale Zellen mit Einwirkung der WNT Signalwege an der Bildung der glatten Muskelzellen und der Alveolarmyofibroblasten beteiligt sind. Mit Hilfe der induzierbaren Driver-Mauslinien *Fgf10*^{CreERT2}, *Wt1*^{CreERT2}, *Gli1*^{CreERT2} und *Axin2*^{CreERT2} in Kombination mit der Reporter-Mauslinie tdTomatoflox wurde die Differenzierung der entsprechend markierten Progenitorzellpopulationen zu den glatten Muskelzelllinien und Alveolarmyofibroblastenzelllinie quantifiziert. Die Ergebnisse zeigten, dass FGF10^{+} und WT1^{+} Zellen nur geringfügig an der Bildung der glatten Muskelzelllinie beteiligt sind, während GLI1^{+} und AXIN2^{+} Zellen signifikant, jedoch mit einer niedrigen Spezifität, zur Bildung sowohl der glatten Muskelzelllinien als auch der Alveolarmyofibroblastenzelllinie beitragen. Eine zeitliche Verfolgung der Zelldifferenzierung (lineage tracing) mit Hilfe der *Acta2-CreERT2* transgenen Mauslinie ergab, dass an E11.5 markierte differenzierte glatte Muskelzellen der Atemwege und Blutgefäße nicht signifikant zur Bildung neuer glatter Muskelzellen an E18.5 beitragen. Andererseits sind an E15.5 ACTA2^{+} Zellen an der Bildung von nahezu allen glatten Muskelzellen und Progenitorzellen der Alveolarmyofibroblasten im Lungenparenchym an E18.5 beteiligt. Mittels einer FACS-basierten Isolation der verschiedenen ACTA2^{+} Subpopulationen mit anschließender Genarray-Analyse, identifizierten wir an E18.5 die Signaturen der Transkription für Progenitorzellen der Alveolarmyofibroblasten sowie für glatte Muskelzellen der Atemwege und Blutgefäße der Lunge. Unsere Ergebnisse etabliert eine neue Basis auf der Ebene der Transkription, um weitere Experimente zum Verständnis der Funktion der

verschiedenen Signalwege in der Bildung unterschiedlicher Subpopulationen $ACTA2^+$ Zellen darauf aufzubauen.

Als aktivierte Myofibroblasten (MYFs) genannte, kontraktile $ACTA2^+$ Zellen, sind die hauptsächlichen krankheits-assoziierten Zellen bei der idiopathischen Lungenfibrose (IPF). Die IPF ist durch exzessive Akkumulation von aktivierten Myofibroblasten und Vernarbung des Lungengewebes charakterisiert. Aktuell besteht keine kausale Therapie für die IPF. Das Verständnis über die Herkunft der aktivierten Myofibroblasten ist somit von größtem Interesse. Mit Hilfe der *Acta2-CreERT2* transgenen Mauslinie markierte prä-existente $ACTA2^+$ glatte Muskelzellen der Atemwege und Blutgefäße der Lunge zeigten, dass diese sich nicht zu aktivierten Myofibroblasten entwickeln. Während der Rückbildung der Fibrose, stellten wir fest, dass aktivierte Myofibroblasten ACTA2 Expression verlieren und einen Lipofibroblasten ähnlichen Phänotyp annehmen. Die Manipulation dieser phänotypischen Umwandlung stellt eine potentiell neue therapeutische Möglichkeit für Patienten mit IPF dar.

9. References

Ahlbrecht, K., McGowan, S.E., 2014. In search of the elusive lipofibroblast in human lungs. Am. J. Physiol. Lung Cell. Mol. Physiol. 307, L605-8. doi:10.1152/ajplung.00230.2014

Baarsma, H.A., Skronska-Wasek, W., Mutze, K., Ciolek, F., Wagner, D.E., John-Schuster, G., Heinzelmann, K., Günther, A., Bracke, K.R., Dagouassat, M., Boczkowski, J., Brusselle, G.G., Smits, R., Eickelberg, O., Yildirim, A.Ö., Königshoff, M., 2017. Noncanonical WNT-5A signaling impairs endogenous lung repair in COPD. J. Exp. Med. 214, 143–163. doi:10.1084/jem.20160675

Bai, C.B., Stephen, D., Joyner, A.L., 2004. All Mouse Ventral Spinal Cord Patterning by Hedgehog Is Gli Dependent and Involves an Activator Function of Gli3. Dev. Cell 6, 103–115. doi:10.1016/S1534-5807(03)00394-0

Barkauskas, C.E., Cronce, M.J., Rackley, C.R., Bowie, E.J., Keene, D.R., Stripp, B.R., Randell, S.H., Noble, P.W., Hogan, B.L.M., 2013. Type 2 alveolar cells are stem cells in adult lung. J. Clin. Invest. 123, 3025–36. doi:10.1172/JCI68782

Bellusci, S., Furuta, Y., Rush, M.G., Henderson, R., Winnier, G., Hogan, B.L., 1997a. Involvement of Sonic hedgehog (Shh) in mouse embryonic lung growth and morphogenesis. Development 124, 53–63.

Bellusci, S., Grindley, J., Emoto, H., Itoh, N., Hogan, B.L., 1997b. Fibroblast growth factor 10 (FGF10) and branching morphogenesis in the embryonic mouse lung. Development 124, 4867–78.

Bellusci, S., Henderson, R., Winnier, G., Oikawa, T., Hogan, B.L., 1996. Evidence from normal expression and targeted misexpression that bone morphogenetic protein (Bmp-4) plays a role in mouse embryonic lung morphogenesis. Development 122, 1693–702.

Bland, R.D., 2005. Neonatal chronic lung disease in the post-surfactant era. Biol. Neonate 88, 181–91. doi:10.1159/000087581

Boström, H., Gritli-Linde, A., Betsholtz, C., 2002. PDGF-A/PDGF alpha-receptor signaling is required for lung growth and the formation of alveoli but not for early lung branching morphogenesis. Dev. Dyn. 223, 155–62. doi:10.1002/dvdy.1225

Boström, H., Willetts, K., Pekny, M., Levéen, P., Lindahl, P., Hedstrand, H., Pekna, M., Hellström, M., Gebre-Medhin, S., Schalling, M., Nilsson, M., Kurland, S., Törnell, J., Heath, J.K., Betsholtz, C., 1996. PDGF-A signaling is a critical event

in lung alveolar myofibroblast development and alveogenesis. Cell 85, 863–73.

Branchfield, K., Li, R., Lungova, V., Verheyden, J.M., McCulley, D., Sun, X., 2016. A three-dimensional study of alveologenesis in mouse lung. Dev. Biol. 409, 429–41. doi:10.1016/j.ydbio.2015.11.017

Cardoso, W. V, Lu, J., 2006. Regulation of early lung morphogenesis: questions, facts and controversies. Development 133, 1611–1624. doi:10.1242/dev.02310

Chao, C.-M., Moiseenko, A., Zimmer, K.-P., Bellusci, S., 2016. Alveologenesis: key cellular players and fibroblast growth factor 10 signaling. Mol. Cell. Pediatr. 3, 17. doi:10.1186/s40348-016-0045-7

Chen, L., Acciani, T., Le Cras, T., Lutzko, C., Perl, A.-K.T., 2012. Dynamic regulation of platelet-derived growth factor receptor α expression in alveolar fibroblasts during realveolarization. Am. J. Respir. Cell Mol. Biol. 47, 517–27. doi:10.1165/rcmb.2012-0030OC

Cigna, N., Farrokhi Moshai, E., Brayer, S., Marchal-Somme, J., Wémeau-Stervinou, L., Fabre, A., Mal, H., Lesèche, G., Dehoux, M., Soler, P., Crestani, B., Mailleux, A.A., 2012. The Hedgehog System Machinery Controls Transforming Growth Factor-β–Dependent Myofibroblastic Differentiation in Humans. Am. J. Pathol. 181, 2126–2137. doi:10.1016/j.ajpath.2012.08.019

Cohen, E.D., Ihida-Stansbury, K., Lu, M.M., Panettieri, R.A., Jones, P.L., Morrisey, E.E., 2009. Wnt signaling regulates smooth muscle precursor development in the mouse lung via a tenascin C/PDGFR pathway. J. Clin. Invest. 119, 2538–49. doi:10.1172/JCI38079

Corvol, H., Flamein, F., Epaud, R., Clement, A., Guillot, L., 2009. Lung alveolar epithelium and interstitial lung disease. Int. J. Biochem. Cell Biol. 41, 1643–51. doi:10.1016/j.biocel.2009.02.009

Dang, H., Wang, S., Yang, L., Fang, F., Xu, F., 2012. Upregulation of Shh and Ptc1 in hyperoxia‐induced acute lung injury in neonatal rats. Mol. Med. Rep. 6, 297–302. doi:10.3892/mmr.2012.929

De Langhe, S.P., Carraro, G., Tefft, D., Li, C., Xu, X., Chai, Y., Minoo, P., Hajihosseini, M.K., Drouin, J., Kaartinen, V., Bellusci, S., 2008. Formation and differentiation of multiple mesenchymal lineages during lung development is regulated by beta-catenin signaling. PLoS One 3, e1516. doi:10.1371/journal.pone.0001516

De Langhe, S.P., Carraro, G., Warburton, D., Hajihosseini, M.K., Bellusci, S., 2006.

Levels of mesenchymal FGFR2 signaling modulate smooth muscle progenitor cell commitment in the lung. Dev. Biol. 299, 52–62. doi:10.1016/j.ydbio.2006.07.001

De Langhe, S.P., Sala, F.G., Del Moral, P.-M., Fairbanks, T.J., Yamada, K.M., Warburton, D., Burns, R.C., Bellusci, S., 2005. Dickkopf-1 (DKK1) reveals that fibronectin is a major target of Wnt signaling in branching morphogenesis of the mouse embryonic lung. Dev. Biol. 277, 316–31. doi:10.1016/j.ydbio.2004.09.023

Degryse, A.L., Lawson, W.E., 2011. Progress toward improving animal models for idiopathic pulmonary fibrosis. Am. J. Med. Sci. 341, 444–9. doi:10.1097/MAJ.0b013e31821aa000

Degryse, A.L., Tanjore, H., Xu, X.C., Polosukhin, V. V, Jones, B.R., McMahon, F.B., Gleaves, L.A., Blackwell, T.S., Lawson, W.E., 2010. Repetitive intratracheal bleomycin models several features of idiopathic pulmonary fibrosis. Am. J. Physiol. Lung Cell. Mol. Physiol. 299, L442-52. doi:10.1152/ajplung.00026.2010

del Moral, P.-M., De Langhe, S.P., Sala, F.G., Veltmaat, J.M., Tefft, D., Wang, K., Warburton, D., Bellusci, S., 2006. Differential role of FGF9 on epithelium and mesenchyme in mouse embryonic lung. Dev. Biol. 293, 77–89. doi:10.1016/j.ydbio.2006.01.020

Dickie, R., Wang, Y.T., Butler, J.P., Schulz, H., Tsuda, A., 2008. Distribution and quantity of contractile tissue in postnatal development of rat alveolar interstitium. Anat. Rec. (Hoboken). 291, 83–93. doi:10.1002/ar.20622

Dixit, R., Ai, X., Fine, A., 2013. Derivation of lung mesenchymal lineages from the fetal mesothelium requires hedgehog signaling for mesothelial cell entry. Development 140, 4398–4406. doi:10.1242/dev.098079

Du, Y., Guo, M., Whitsett, J.A., Xu, Y., 2015. “LungGENS”: a web-based tool for mapping single-cell gene expression in the developing lung. Thorax 70, 1092–4. doi:10.1136/thoraxjnl-2015-207035

du Bois, R.M., Weycker, D., Albera, C., Bradford, W.Z., Costabel, U., Kartashov, A., Lancaster, L., Noble, P.W., Sahn, S.A., Szwarcberg, J., Thomeer, M., Valeyre, D., King, T.E., 2011. Six-minute-walk test in idiopathic pulmonary fibrosis: test validation and minimal clinically important difference. Am. J. Respir. Crit. Care Med. 183, 1231–7. doi:10.1164/rccm.201007-1179OC

El Agha, E., Al Alam, D., Carraro, G., MacKenzie, B., Goth, K., De Langhe, S.P., Voswinckel, R., Hajihosseini, M.K., Rehan, V.K., Bellusci, S., 2012.

Characterization of a novel fibroblast growth factor 10 (Fgf10) knock-in mouse line to target mesenchymal progenitors during embryonic development. PLoS One 7, e38452. doi:10.1371/journal.pone.0038452

El Agha, E., Herold, S., Al Alam, D., Quantius, J., MacKenzie, B., Carraro, G., Moiseenko, A., Chao, C.-M., Minoo, P., Seeger, W., Bellusci, S., 2014. Fgf10-positive cells represent a progenitor cell population during lung development and postnatally. Development 141, 296–306. doi:10.1242/dev.099747

El Agha, E., Moiseenko, A., Kheirollahi, V., De Langhe, S., Crnkovic, S., Kwapiszewska, G., Kosanovic, D., Schwind, F., Schermuly, R.T., Henneke, I., MacKenzie, B., Quantius, J., Herold, S., Ntokou, A., Ahlbrecht, K., Morty, R.E., Günther, A., Seeger, W., Bellusci, S., 2017. Two-Way Conversion between Lipogenic and Myogenic Fibroblastic Phenotypes Marks the Progression and Resolution of Lung Fibrosis. Cell Stem Cell 20, 261–273.e3. doi:10.1016/j.stem.2016.10.004

Fang, F., Liu, L., Yang, Y., Tamaki, Z., Wei, J., Marangoni, R.G., Bhattacharyya, S., Summer, R.S., Ye, B., Varga, J., 2012. The adipokine adiponectin has potent anti-fibrotic effects mediated via adenosine monophosphate-activated protein kinase: novel target for fibrosis therapy. Arthritis Res. Ther. 14, R229. doi:10.1186/ar4070

Fatigati, V., Murphy, R.A., 1984. Actin and tropomyosin variants in smooth muscles. Dependence on tissue type. J. Biol. Chem. 259, 14383–8.

Felton, V.M., Borok, Z., Willis, B.C., 2009. N-acetylcysteine inhibits alveolar epithelial-mesenchymal transition. Am. J. Physiol. Lung Cell. Mol. Physiol. 297, L805-12. doi:10.1152/ajplung.00009.2009

Genovese, T., Cuzzocrea, S., Di Paola, R., Mazzon, E., Mastruzzo, C., Catalano, P., Sortino, M., Crimi, N., Caputi, A.P., Thiemermann, C., Vancheri, C., 2005. Effect of rosiglitazone and 15-deoxy-Delta12,14-prostaglandin J2 on bleomycin-induced lung injury. Eur. Respir. J. 25, 225–34. doi:10.1183/09031936.05.00049704

Gentleman, R.C., Carey, V.J., Bates, D.M., Bolstad, B., Dettling, M., Dudoit, S., Ellis, B., Gautier, L., Ge, Y., Gentry, J., Hornik, K., Hothorn, T., Huber, W., Iacus, S., Irizarry, R., Leisch, F., Li, C., Maechler, M., Rossini, A.J., Sawitzki, G., Smith, C., Smyth, G., Tierney, L., Yang, J.Y.H., Zhang, J., 2004. Bioconductor: open software development for computational biology and bioinformatics. Genome

Biol. 5, R80. doi:10.1186/gb-2004-5-10-r80

Greif, D.M., Kumar, M., Lighthouse, J.K., Hum, J., An, A., Ding, L., Red-Horse, K., Espinoza, F.H., Olson, L., Offermanns, S., Krasnow, M.A., 2012. Radial construction of an arterial wall. Dev. Cell 23, 482–93. doi:10.1016/j.devcel.2012.07.009

Grindley, J.C., Bellusci, S., Perkins, D., Hogan, B.L., 1997. Evidence for the involvement of the Gli gene family in embryonic mouse lung development. Dev. Biol. 188, 337–48. doi:10.1006/dbio.1997.8644

Grounds, M.D., Terrill, J.R., Radley-Crabb, H.G., Robertson, T., Papadimitriou, J., Spuler, S., Shavlakadze, T., 2014. Lipid accumulation in dysferlin-deficient muscles. Am. J. Pathol. 184, 1668–76. doi:10.1016/j.ajpath.2014.02.005

Günther, A., Korfei, M., Mahavadi, P., von der Beck, D., Ruppert, C., Markart, P., 2012. Unravelling the progressive pathophysiology of idiopathic pulmonary fibrosis. Eur. Respir. Rev. 21, 152–60. doi:10.1183/09059180.00001012

Halayko, A.J., Stephens, N.L., 1994. Potential role for phenotypic modulation of bronchial smooth muscle cells in chronic asthma. Can. J. Physiol. Pharmacol. 72, 1448–57.

Hashimoto, N., Jin, H., Liu, T., Chensue, S.W., Phan, S.H., 2004. Bone marrow-derived progenitor cells in pulmonary fibrosis. J. Clin. Invest. 113, 243–52. doi:10.1172/JCI18847

Hecker, L., Jagirdar, R., Jin, T., Thannickal, V.J., 2011. Reversible differentiation of myofibroblasts by MyoD. Exp. Cell Res. 317, 1914–21. doi:10.1016/j.yexcr.2011.03.016

Hinz, B., Phan, S.H., Thannickal, V.J., Galli, A., Bochaton-Piallat, M.-L., Gabbiani, G., 2007. The myofibroblast: one function, multiple origins. Am. J. Pathol. 170, 1807–16. doi:10.2353/ajpath.2007.070112

Hoyles, R.K., Derrett-Smith, E.C., Khan, K., Shiwen, X., Howat, S.L., Wells, A.U., Abraham, D.J., Denton, C.P., 2011. An essential role for resident fibroblasts in experimental lung fibrosis is defined by lineage-specific deletion of high-affinity type II transforming growth factor β receptor. Am. J. Respir. Crit. Care Med. 183, 249–61. doi:10.1164/rccm.201002-0279OC

Hu, E., Tontonoz, P., Spiegelman, B.M., 1995. Transdifferentiation of myoblasts by the adipogenic transcription factors PPAR gamma and C/EBP alpha. Proc. Natl. Acad. Sci. U. S. A. 92, 9856–60.

Hung, C., Linn, G., Chow, Y.-H., Kobayashi, A., Mittelsteadt, K., Altemeier, W.A., Gharib, S.A., Schnapp, L.M., Duffield, J.S., 2013. Role of lung pericytes and resident fibroblasts in the pathogenesis of pulmonary fibrosis. Am. J. Respir. Crit. Care Med. 188, 820–30. doi:10.1164/rccm.201212-2297OC

Hynes, M., Stone, D.M., Dowd, M., Pitts-Meek, S., Goddard, A., Gurney, A., Rosenthal, A., 1997. Control of Cell Pattern in the Neural Tube by the Zinc Finger Transcription Factor and Oncogene Gli-1. Neuron 19, 15–26. doi:10.1016/S0896-6273(00)80344-X

Issa, R., Williams, E., Trim, N., Kendall, T., Arthur, M.J., Reichen, J., Benyon, R.C., Iredale, J.P., 2001. Apoptosis of hepatic stellate cells: involvement in resolution of biliary fibrosis and regulation by soluble growth factors. Gut 48, 548–57.

Jeffery, P.K., 2004. Remodeling and inflammation of bronchi in asthma and chronic obstructive pulmonary disease. Proc. Am. Thorac. Soc. 1, 176–83. doi:10.1513/pats.200402-009MS

Kapanci, Y., Desmouliere, A., Pache, J.C., Redard, M., Gabbiani, G., 1995. Cytoskeletal protein modulation in pulmonary alveolar myofibroblasts during idiopathic pulmonary fibrosis. Possible role of transforming growth factor beta and tumor necrosis factor alpha. Am. J. Respir. Crit. Care Med. 152, 2163–9. doi:10.1164/ajrccm.152.6.8520791

Kelly, R., Brown, N., Buckingham, M., 2001. The Arterial Pole of the Mouse Heart Forms from Fgf10-Expressing Cells in Pharyngeal Mesoderm. Dev. Cell 1, 435–440. doi:10.1016/S1534-5807(01)00040-5

Kim, H.Y., Pang, M.-F., Varner, V.D., Kojima, L., Miller, E., Radisky, D.C., Nelson, C.M., 2015. Localized Smooth Muscle Differentiation Is Essential for Epithelial Bifurcation during Branching Morphogenesis of the Mammalian Lung. Dev. Cell 34, 719–26. doi:10.1016/j.devcel.2015.08.012

Kosla, J., Dvorakova, M., Dvorak, M., Cermak, V., 2013. Effective myofibroblast dedifferentiation by concomitant inhibition of TGF-β signaling and perturbation of MAPK signaling. Eur. J. Cell Biol. 92, 363–373. doi:10.1016/j.ejcb.2013.10.013

Kramann, R., Schneider, R.K., DiRocco, D.P., Machado, F., Fleig, S., Bondzie, P.A., Henderson, J.M., Ebert, B.L., Humphreys, B.D., 2015. Perivascular Gli1+ Progenitors Are Key Contributors to Injury-Induced Organ Fibrosis. Cell Stem Cell 16, 51–66. doi:10.1016/j.stem.2014.11.004

Kumar, M.E., Bogard, P.E., Espinoza, F.H., Menke, D.B., Kingsley, D.M., Krasnow,

M.A., 2014. Defining a mesenchymal progenitor niche at single-cell resolution. Science (80-.). 346, 1258810–1258810. doi:10.1126/science.1258810

Kumawat, K., Menzen, M.H., Bos, I.S.T., Baarsma, H.A., Borger, P., Roth, M., Tamm, M., Halayko, A.J., Simoons, M., Prins, A., Postma, D.S., Schmidt, M., Gosens, R., 2013. Noncanonical WNT-5A signaling regulates TGF-β-induced extracellular matrix production by airway smooth muscle cells. FASEB J. 27, 1631–43. doi:10.1096/fj.12-217539

Lee, J., Platt, K.A., Censullo, P., Ruiz i Altaba, A., 1997. Gli1 is a target of Sonic hedgehog that induces ventral neural tube development. Development 124, 2537–52.

Li, C., Li, M., Li, S., Xing, Y., Yang, C.-Y., Li, A., Borok, Z., De Langhe, S., Minoo, P., 2015. Progenitors of secondary crest myofibroblasts are developmentally committed in early lung mesoderm. Stem Cells 33, 999–1012. doi:10.1002/stem.1911

Li, C., Xiao, J., Hormi, K., Borok, Z., Minoo, P., 2002. Wnt5a participates in distal lung morphogenesis. Dev. Biol. 248, 68–81.

Li, L., Miano, J.M., Cserjesi, P., Olson, E.N., 1996. SM22 alpha, a marker of adult smooth muscle, is expressed in multiple myogenic lineages during embryogenesis. Circ. Res. 78, 188–95.

Lindahl, P., Karlsson, L., Hellström, M., Gebre-Medhin, S., Willetts, K., Heath, J.K., Betsholtz, C., 1997. Alveogenesis failure in PDGF-A-deficient mice is coupled to lack of distal spreading of alveolar smooth muscle cell progenitors during lung development. Development 124, 3943–53.

Lü, J., Izvolsky, K.I., Qian, J., Cardoso, W. V, 2005. Identification of FGF10 targets in the embryonic lung epithelium during bud morphogenesis. J. Biol. Chem. 280, 4834–41. doi:10.1074/jbc.M410714200

Mailleux, A.A., Kelly, R., Veltmaat, J.M., De Langhe, S.P., Zaffran, S., Thiery, J.P., Bellusci, S., 2005. Fgf10 expression identifies parabronchial smooth muscle cell progenitors and is required for their entry into the smooth muscle cell lineage. Development 132, 2157–66. doi:10.1242/dev.01795

McGowan, S.E., Grossmann, R.E., Kimani, P.W., Holmes, A.J., 2008. Platelet-derived growth factor receptor-alpha-expressing cells localize to the alveolar entry ring and have characteristics of myofibroblasts during pulmonary alveolar septal formation. Anat. Rec. (Hoboken). 291, 1649–61. doi:10.1002/ar.20764

McGowan, S.E., McCoy, D.M., 2014. Regulation of fibroblast lipid storage and myofibroblast phenotypes during alveolar septation in mice. Am. J. Physiol. Lung Cell. Mol. Physiol. 307, L618-31. doi:10.1152/ajplung.00144.2014

McGowan, S.E., McCoy, D.M., 2013a. Platelet-derived growth factor-A regulates lung fibroblast S-phase entry through p27(kip1) and FoxO3a. Respir. Res. 14, 68. doi:10.1186/1465-9921-14-68

McGowan, S.E., McCoy, D.M., 2013b. Platelet-derived growth factor-A and sonic hedgehog signaling direct lung fibroblast precursors during alveolar septal formation. Am. J. Physiol. Lung Cell. Mol. Physiol. 305, L229-39. doi:10.1152/ajplung.00011.2013

McHugh, K.M., 1995. Molecular analysis of smooth muscle development in the mouse. Dev. Dyn. 204, 278–90. doi:10.1002/aja.1002040306

McMahon, A.P., 2000. More surprises in the Hedgehog signaling pathway. Cell 100, 185–8.

McQualter, J.L., McCarty, R.C., Van der Velden, J., O'Donoghue, R.J.J., Asselin-Labat, M.-L., Bozinovski, S., Bertoncello, I., 2013. TGF-β signaling in stromal cells acts upstream of FGF-10 to regulate epithelial stem cell growth in the adult lung. Stem Cell Res. 11, 1222–33. doi:10.1016/j.scr.2013.08.007

Méthot, N., Basler, K., 2001. An absolute requirement for Cubitus interruptus in Hedgehog signaling. Development 128, 733–42.

Miller, L.-A.D., Wert, S.E., Clark, J.C., Xu, Y., Perl, A.-K.T., Whitsett, J.A., 2004. Role ofSonic hedgehog in patterning of tracheal-bronchial cartilage and the peripheral lung. Dev. Dyn. 231, 57–71. doi:10.1002/dvdy.20105

Miller, L.A., Wert, S.E., Whitsett, J.A., 2001. Immunolocalization of sonic hedgehog (Shh) in developing mouse lung. J. Histochem. Cytochem. 49, 1593–604.

Morrisey, E.E., Hogan, B.L.M., 2010. Preparing for the first breath: genetic and cellular mechanisms in lung development. Dev. Cell 18, 8–23. doi:10.1016/j.devcel.2009.12.010

Owens, G.K., Kumar, M.S., Wamhoff, B.R., 2004. Molecular regulation of vascular smooth muscle cell differentiation in development and disease. Physiol. Rev. 84, 767–801. doi:10.1152/physrev.00041.2003

Park, W.Y., Miranda, B., Lebeche, D., Hashimoto, G., Cardoso, W. V, 1998. FGF-10 is a chemotactic factor for distal epithelial buds during lung development. Dev. Biol. 201, 125–34. doi:10.1006/dbio.1998.8994

Peng, T., Tian, Y., Boogerd, C.J., Lu, M.M., Kadzik, R.S., Stewart, K.M., Evans, S.M., Morrisey, E.E., 2013. Coordination of heart and lung co-development by a multipotent cardiopulmonary progenitor. Nature advance on. doi:10.1038/nature12358

Pepicelli, C. V., Lewis, P.M., McMahon, A.P., 1998. Sonic hedgehog regulates branching morphogenesis in the mammalian lung. Curr. Biol. 8, 1083–1086. doi:10.1016/S0960-9822(98)70446-4

Perl, A.-K.T., Gale, E., 2009. FGF signaling is required for myofibroblast differentiation during alveolar regeneration. Am. J. Physiol. Lung Cell. Mol. Physiol. 297, L299-308. doi:10.1152/ajplung.00008.2009

Peters, K., Werner, S., Liao, X., Wert, S., Whitsett, J., Williams, L., 1994. Targeted expression of a dominant negative FGF receptor blocks branching morphogenesis and epithelial differentiation of the mouse lung. EMBO J. 13, 3296–301.

Phillips, R.J., Burdick, M.D., Hong, K., Lutz, M.A., Murray, L.A., Xue, Y.Y., Belperio, J.A., Keane, M.P., Strieter, R.M., 2004. Circulating fibrocytes traffic to the lungs in response to CXCL12 and mediate fibrosis. J. Clin. Invest. 114, 438–46. doi:10.1172/JCI20997

Que, J., Wilm, B., Hasegawa, H., Wang, F., Bader, D., Hogan, B.L.M., 2008. Mesothelium contributes to vascular smooth muscle and mesenchyme during lung development. Proc. Natl. Acad. Sci. U. S. A. 105, 16626–30. doi:10.1073/pnas.0808649105

R Development Core Team (2007). R: A language and environment for statistical computing. R Foundation for Statistical Computing, Vienna, Austria. Available at: http://www.R-project.org.

Ramasamy, S.K., Mailleux, A.A., Gupte, V. V, Mata, F., Sala, F.G., Veltmaat, J.M., Del Moral, P.M., De Langhe, S., Parsa, S., Kelly, L.K., Kelly, R., Shia, W., Keshet, E., Minoo, P., Warburton, D., Bellusci, S., 2007. Fgf10 dosage is critical for the amplification of epithelial cell progenitors and for the formation of multiple mesenchymal lineages during lung development. Dev. Biol. 307, 237–47. doi:10.1016/j.ydbio.2007.04.033

Reddy, A.T., Lakshmi, S.P., Zhang, Y., Reddy, R.C., 2014. Nitrated fatty acids reverse pulmonary fibrosis by dedifferentiating myofibroblasts and promoting collagen uptake by alveolar macrophages. FASEB J. 28, 5299–5310.

doi:10.1096/fj.14-256263

Rehan, V.K., Sugano, S., Wang, Y., Santos, J., Romero, S., Dasgupta, C., Keane, M.P., Stahlman, M.T., Torday, J.S., 2006. Evidence for the presence of lipofibroblasts in human lung. Exp. Lung Res. 32, 379–93. doi:10.1080/01902140600880257

Rehan, V.K., Torday, J.S., 2014. The lung alveolar lipofibroblast: an evolutionary strategy against neonatal hyperoxic lung injury. Antioxid. Redox Signal. 21, 1893–904. doi:10.1089/ars.2013.5793

Rehan, V.K., Torday, J.S., 2012. PPARγ Signaling Mediates the Evolution, Development, Homeostasis, and Repair of the Lung. PPAR Res. 2012, 289867. doi:10.1155/2012/289867

Rock, J.R., Barkauskas, C.E., Cronce, M.J., Xue, Y., Harris, J.R., Liang, J., Noble, P.W., Hogan, B.L.M., 2011. Multiple stromal populations contribute to pulmonary fibrosis without evidence for epithelial to mesenchymal transition. Proc. Natl. Acad. Sci. U. S. A. 108, E1475-83. doi:10.1073/pnas.1117988108

Rubin, L.P., Kovacs, C.S., De Paepe, M.E., Tsai, S.-W., Torday, J.S., Kronenberg, H.M., 2004. Arrested pulmonary alveolar cytodifferentiation and defective surfactant synthesis in mice missing the gene for parathyroid hormone-related protein. Dev. Dyn. 230, 278–89. doi:10.1002/dvdy.20058

Schultz, C.J., Torres, E., Londos, C., Torday, J.S., 2002. Role of adipocyte differentiation-related protein in surfactant phospholipid synthesis by type II cells. Am. J. Physiol. Lung Cell. Mol. Physiol. 283, L288-96. doi:10.1152/ajplung.00204.2001

Sekine, K., Ohuchi, H., Fujiwara, M., Yamasaki, M., Yoshizawa, T., Sato, T., Yagishita, N., Matsui, D., Koga, Y., Itoh, N., Kato, S., 1999. Fgf10 is essential for limb and lung formation. Nat. Genet. 21, 138–41. doi:10.1038/5096

Shan, L., Subramaniam, M., Emanuel, R.L., Degan, S., Johnston, P., Tefft, D., Warburton, D., Sunday, M.E., 2008. Centrifugal migration of mesenchymal cells in embryonic lung. Dev. Dyn. 237, 750–7. doi:10.1002/dvdy.21462

Sheikh, A.Q., Lighthouse, J.K., Greif, D.M., 2014. Recapitulation of Developing Artery Muscularization in Pulmonary Hypertension. Cell Rep. 6, 809–817. doi:10.1016/j.celrep.2014.01.042

Shu, W., Jiang, Y.Q., Lu, M.M., Morrisey, E.E., 2002. Wnt7b regulates mesenchymal proliferation and vascular development in the lung. Development 129, 4831–42.

Simon, D.M., Mariani, T.J., 2007. Role of PPARs and Retinoid X Receptors in the Regulation of Lung Maturation and Development. PPAR Res. 2007, 91240. doi:10.1155/2007/91240

Smyth, G.K., 2005. limma: Linear Models for Microarray Data, in: Bioinformatics and Computational Biology Solutions Using R and Bioconductor. Springer-Verlag, New York, pp. 397–420. doi:10.1007/0-387-29362-0_23

Smyth, G.K., 2004. Linear models and empirical bayes methods for assessing differential expression in microarray experiments. Stat. Appl. Genet. Mol. Biol. 3, Article3. doi:10.2202/1544-6115.1027

Smyth, G.K., Speed, T., 2003. Normalization of cDNA microarray data. Methods 31, 265–73.

Tahedl, D., Wirkes, A., Tschanz, S.A., Ochs, M., Mühlfeld, C., 2014. How common is the lipid body-containing interstitial cell in the mammalian lung? Am. J. Physiol. Lung Cell. Mol. Physiol. 307, L386-94. doi:10.1152/ajplung.00131.2014

Tanjore, H., Cheng, D.-S., Degryse, A.L., Zoz, D.F., Abdolrasulnia, R., Lawson, W.E., Blackwell, T.S., 2011. Alveolar epithelial cells undergo epithelial-to-mesenchymal transition in response to endoplasmic reticulum stress. J. Biol. Chem. 286, 30972–80. doi:10.1074/jbc.M110.181164

Thannickal, V.J., Toews, G.B., White, E.S., Lynch, J.P., Martinez, F.J., 2004. Mechanisms of pulmonary fibrosis. Annu. Rev. Med. 55, 395–417. doi:10.1146/annurev.med.55.091902.103810

Torday, J.S., Torres, E., Rehan, V.K., 2003. The role of fibroblast transdifferentiation in lung epithelial cell proliferation, differentiation, and repair in vitro. Pediatr. Pathol. Mol. Med. 22, 189–207.

Tordet, C., Marin, L., Dameron, F., 1981. Pulmonary di-and-triacylglycerols during the perinatal development of the rat. Experientia 37, 333–334. doi:10.1007/BF01959845

Tuder, R.M., 2016. Pulmonary vascular remodeling in pulmonary hypertension. Cell Tissue Res. doi:10.1007/s00441-016-2539-y

Volckaert, T., Dill, E., Campbell, A., Tiozzo, C., Majka, S., Bellusci, S., De Langhe, S.P., 2011. Parabronchial smooth muscle constitutes an airway epithelial stem cell niche in the mouse lung after injury. J. Clin. Invest. 121, 4409–19. doi:10.1172/JCI58097

Wang, Z., Shu, W., Lu, M.M., Morrisey, E.E., 2005. Wnt7b activates canonical

signaling in epithelial and vascular smooth muscle cells through interactions with Fzd1, Fzd10, and LRP5. Mol. Cell. Biol. 25, 5022–30. doi:10.1128/MCB.25.12.5022-5030.2005

Weaver, M., Dunn, N.R., Hogan, B.L., 2000. Bmp4 and Fgf10 play opposing roles during lung bud morphogenesis. Development 127, 2695–704.

Wendel, D.P., Taylor, D.G., Albertine, K.H., Keating, M.T., Li, D.Y., 2000. Impaired distal airway development in mice lacking elastin. Am. J. Respir. Cell Mol. Biol. 23, 320–6. doi:10.1165/ajrcmb.23.3.3906

Wendling, O., Bornert, J.-M., Chambon, P., Metzger, D., 2009. Efficient temporally-controlled targeted mutagenesis in smooth muscle cells of the adult mouse. Genesis 47, 14–8. doi:10.1002/dvg.20448

Willis, B.C., duBois, R.M., Borok, Z., 2006. Epithelial origin of myofibroblasts during fibrosis in the lung. Proc. Am. Thorac. Soc. 3, 377–82. doi:10.1513/pats.200601-004TK

Wong, S.-P., Rowley, J.E., Redpath, A.N., Tilman, J.D., Fellous, T.G., Johnson, J.R., 2015. Pericytes, mesenchymal stem cells and their contributions to tissue repair. Pharmacol. Ther. 151, 107–20. doi:10.1016/j.pharmthera.2015.03.006

Yamada, M., Kurihara, H., Kinoshita, K., Sakai, T., 2005. Temporal expression of alpha-smooth muscle actin and drebrin in septal interstitial cells during alveolar maturation. J. Histochem. Cytochem. 53, 735–44. doi:10.1369/jhc.4A6483.2005

Zhang, H.Y., Gharaee-Kermani, M., Zhang, K., Karmiol, S., Phan, S.H., 1996. Lung fibroblast alpha-smooth muscle actin expression and contractile phenotype in bleomycin-induced pulmonary fibrosis. Am. J. Pathol. 148, 527–37.

10. Supplementary material

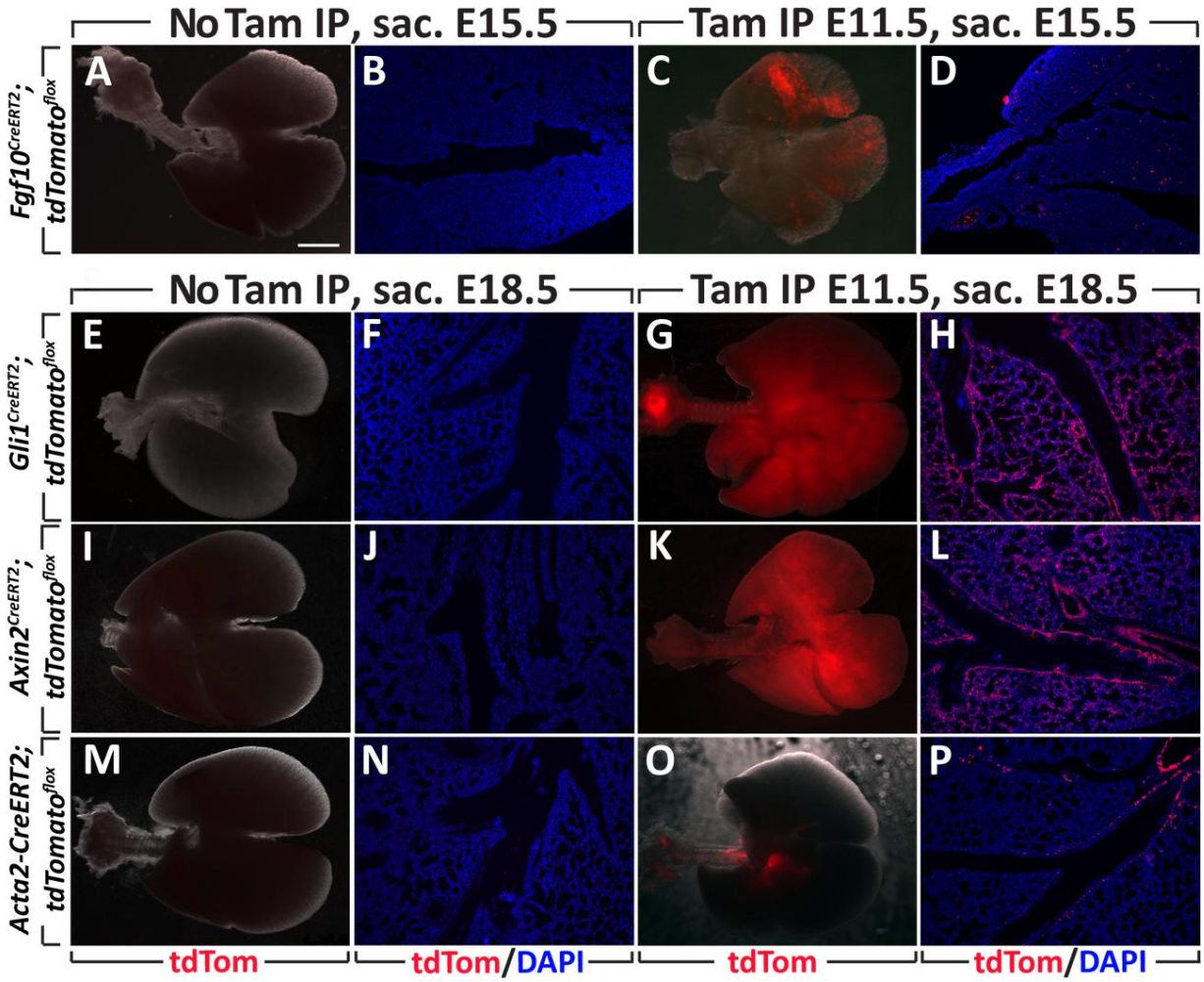

Supplementary Figure 1: Lack of leakiness in the mouse lines used. (A, C, E, G, I, K, M, O) Whole-mount images of the lungs in the presence or absence of tamoxifen induction. **(B, D, F, H, J, L, N, P)** Corresponding lung sections stained with DAPI. Note the absence of tdTomato signal in lungs that were not treated with tamoxifen. N = 3. Scale bar: 2.5 mm in E, G, I, M; 1.5 mm in K, O; 600 µm in C; 500 µm in A; 200 µm in B, D, F, H, L, N, P; 100 µm in J. (Moiseenko et al., 2017, Stem Cells, manuscript resubmitted)

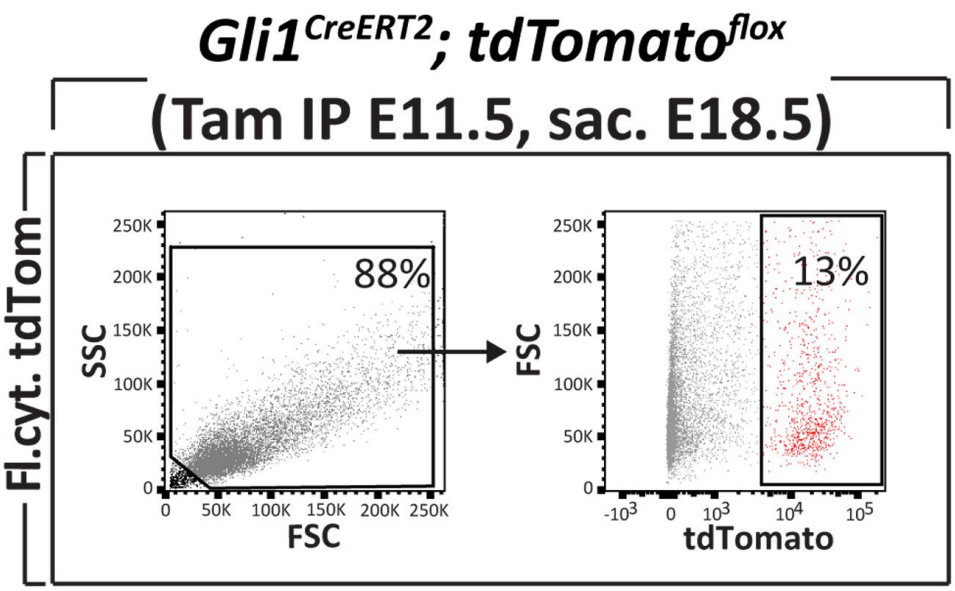

Supplementary Figure 2: Gating strategy for flow cytometry experiments. Initial gating for flow cytometry analysis of E18.5 *Gli1*^{CreERT2}*; tdTomato*^{flox} lungs labeled at E11.5. Live cells were selected based on forward/side scatter profiles. SSC – side scatter, FSC – forward scatter. N = 3. (Moiseenko et al., 2017, Stem Cells, manuscript resubmitted)

Supplementary Table 1: Transcriptomic signatures enriched in alveolar MYF progenitors vs. ASMCs and VSMCs.

Genes enriched in alveolar myofibroblasts
Gpr64 (G protein-coupled receptor 64) FC=541.19, p<0.001
Col6a4 (collagen, type VI, alpha 4) FC=352.14, p<0.001
Wif1 (Wnt inhibitory factor 1) FC=235.57, p<0.0001
Nrxn3 (neurexin III) FC=216.77, p<0.001
Egfem1 (EGF-like and EMI domain containing 1) FC=209.38, p<0.0001
Pcdh20 (protocadherin 20) FC=156.5, p<0.001
Cyp2e1 (cytochrome P450, family 2, subfamily e, polypeptide 1) FC=114.56, p<0.0001
Penk (preproenkephalin) FC=100.43, p<0.0001
P*dgfra* (platelet derived growth factor receptor, alpha polypeptide) FC=93.05, p<0.0001
Greb1 (gene regulated by estrogen in breast cancer protein) FC=81.57, p<0.0001
Col22a1 (collagen, type XXII, alpha 1) FC=76.11, p<0.0001
Ccdc3 (coiled-coil domain containing 3) FC=73.52, p<0.0001
Esr1 (estrogen receptor 1 (alpha)) FC=65.34, p<0.0001
Fmo4 (flavin containing monooxygenase 4) FC=64, p<0.0001
Adgrl3 (adhesion G protein-coupled receptor L3) FC=61.82, p<0.0001
Mkx (mohawk homeobox) FC=56.88, p<0.01
Zfp536 (zinc finger protein 536) FC=54.95, p<0.0001
Gria3 (glutamate receptor, ionotropic, AMPA3 (alpha 3) FC=53.82, p<0.0001
Dnm3os (dynamin 3, opposite strand) FC=52.34, p<0.0001
Scara5 (scavenger receptor class A, member 5 (putative)) FC=52.34, p<0.0001
Lgr5 (leucine rich repeat containing G protein coupled receptor 5) FC=51.62, p<0.0001
Aldh1a3 (aldehyde dehydrogenase family 1, subfamily A3) FC=49.52, p<0.001
Lamc3 (laminin gamma 3) FC=49.52, p<0.0001
Rerg (RAS-like, estrogen-regulated, growth-inhibitor) FC=47.18, p<0.01
Slc28a3 (solute carrier family 28 (sodium-coupled nucleoside transporter), member 3) FC=44.32, p<0.001

Kiss1 (KiSS-1 metastasis-suppressor) FC=41.07, p<0.0001
Fmo2 (flavin containing monooxygenase 2) FC=37.53, p<0.0001
Enpp2 (ectonucleotide pyrophosphatase/phosphodiesterase 2) FC=37.27, p<0.0001
Snai1 (snail family zinc finger 1) FC=35.5, p<0.0001
Frem1 (*Fras1* related extracellular matrix protein 1) FC=33.82, p<0.0001
Lef1 (lymphoid enhancer binding factor 1) FC=32, p<0.0001
Gdf10 (growth differentiation factor 10) FC=32, p<0.0001
Cacna1e (calcium channel, voltage-dependent, R type, alpha 1E subunit) FC=29.65, p<0.01
Tcf7 (transcription factor 7, T cell specific) FC=26.54, p<0.0001
Trim67 (tripartite motif-containing 67) FC=26.54, p<0.0001
Reck (reversion-inducing-cysteine-rich protein with kazal motifs) FC=26.17, p<0.0001
Vstm2b (V-set and transmembrane domain containing 2B) FC=25.99, p<0.001
Adamts14 (a disintegrin-like and metallopeptidase (reprolysin type) with thrombospondin type 1 motif, 14) FC=25.11, p<0.0001
Agt (angiotensinogen (serpin peptidase inhibitor, clade A, member 8)) FC=24.76, p<0.01
Glrp1 (glutamine repeat protein 1) FC=22.78, p<0.01
Negr1 (neuronal growth regulator 1) FC=21.11, p<0.01
Foxf2 (forkhead box F2) FC=20.82, p<0.0001
Jph1 (junctophilin 1) FC=18.89, p<0.05
Slco1a4 (solute carrier organic anion transporter family, member 1a4) FC=18.51, p<0.001
Mmp2 (matrix metallopeptidase 2) FC=18.25, p<0.0001
Entpd1 (ectonucleoside triphosphate diphosphohydrolase 1) FC=16.11, p<0.0001
Sncaip (synuclein, alpha interacting protein (synphilin)) FC=15.56, p<0.0001
Kcns3 (potassium voltage-gated channel, delayed-rectifier, subfamily S, member 3) FC=14.82, p<0.001
Zfp385b (zinc finger protein 385B) FC=14.22, p<0.01
Igfbp3 (insulin-like growth factor binding protein 3) FC=12.55, p<0.001
Megf10 (multiple EGF-like-domains 10) FC=12.38, p<0.01
Pappa2 (pappalysin 2) FC=11.79, p<0.0001

Fndc1 (fibronectin type III domain containing 1) FC=11.71, p<0.001
Wnt5a (wingless-type MMTV integration site family, member 5A) FC=11.48, p<0.0001
Megf10 (multiple EGF-like-domains 10) FC=12.38, p<0.01
Tgfbr3 (transforming growth factor, beta receptor III) FC=10.48, p<0.0001
Cdh10 (cadherin 10) FC=9.99, p<0.001

Supplementary Table 2: Transcriptomic signatures enriched in ASMCs and VSMCs vs. alveolar MYF progenitors.

Genes enriched in smooth muscle cells
C1qc (complement component 1, q subcomponent, C chain) FC=439.58, p<0.0001
Csrp3 (cysteine and glycine-rich protein 3) FC=424.61, p<0.0001
Sln (sarcolipin) FC=296.11, p<0.0001
Cox8b (cytochrome c oxidase subunit VIIIb) FC=203.66, p<0.0001
Myl4 (myosin, light polypeptide 4) FC=198.09, p<0.0001
Actn2 (actinin alpha 2) FC=178.53, p<0.0001
Chrm2 (cholinergic receptor, muscarinic 2, cardiac) FC=159.79, p<0.0001
Hspb7 (heat shock protein family, member 7 (cardiovascular)) FC=134.37, p<0.0001
Myl2 (myosin, light polypeptide 2, regulatory, cardiac, slow) FC=129.79, p<0.0001
Ccl12 (chemokine (C-C motif) ligand 12) FC=116.97, p<0.0001
Slc22a1 (solute carrier family 22 (organic cation transporter), member 1) FC=101.83, p<0.0001
Cd163 (CD163 antigen) FC=82.71, p<0.0001
Tmem182 (transmembrane protein 182) FC=58.89, p<0.0001
Nkx2-5 (NK2 homeobox 5) FC=49.18, p<0.0001
Ankrd1 (ankyrin repeat domain 1 (cardiac muscle)) FC=47.18, p<0.0001
Nrap (nebulin-related anchoring protein) FC=39.4, p<0.0001
Myl3 (myosin, light polypeptide 3) FC=37.79, p<0.0001
Fabp3 (fatty acid binding protein 3, muscle and heart) FC=36.76, p<0.0001
Ms4a6b (membrane-spanning 4-domains, subfamily A, member 6B) FC=33.13, p<0.0001
Tcap (titin-cap) FC=32, p<0.0001
Tbx20 (T-box 20) FC=28.64, p<0.0001
Tenm2 (teneurin transmembrane protein 2) FC=20.53, p<0.0001
Ldb3 (LIM domain binding 3) FC=19.56, p<0.001
Hfe2 (hemochromatosis type 2 (juvenile) (human homolog)) FC=17.39, p<0.0001
Klhl30 (kelch-like 30) FC=14.62, p<0.001
Syn2 (synapsin II) FC=13.74, p<0.01

Tnnt3 (troponin T3, skeletal, fast) FC=11.88, p<0.001
Dpf3 (D4, zinc and double PHD fingers, family 3) FC=11.55, p<0.001
Habp2 (hyaluronic acid binding protein 2) FC=10.63, p<0.001